

BRANCH OFFICE

194 NASSAU STREET
PRINCETON, NEW JERSEY 08540
PHONE 924-4228

SYSTEMS TECHNOLOGY, INC.



13766 SOUTH HAWTHORNE BOULEVARD • HAWTHORNE, CALIFORNIA 90250

Technical Memorandum 163-A



A REEXAMINATION OF EYE MOVEMENT DATA

Warren F. Clement
Dunstan Graham
John J. Best

28 February 1967

DDC
RECEIVED
APR 23 1968
RELEASE

LB^B

This document has been approved
for public release and sale; its
distribution is unlimited

Office of Naval Research
Contract N00014-66-C0072

Joint Army Navy Aircraft Instrumentation Research
JANAIR

Reproduced by the
CLEARINGHOUSE
for Federal Scientific & Technical
Information Springfield Va 22151

AD 667768

CONTENTS

	<u>Page</u>
I. INTRODUCTION.	1
II. REVIEW AND DISTILLATION OF COCKPIT INSTRUMENT SCANNING DATA.	3
A. Fixation-Frequency Loop Cross-Over Frequency Relationship.	4
B. Fixation Frequency-Maneuver Relationship.	10
C. Fixation Frequency-Instrument Arrangement Relationship.	13
D. Fixation Frequency-Instrument Co-relationship	14
E. Summary and Conclusions for Fixation Frequency. . . .	14
F. Fixation (dwell) Time Relationships	15
G. Summary and Conclusions for Dwell Time.	19
H. Display Fixation Link Values.	21
I. Display Arrangement	23
III. EXPERIMENTS PROPOSED TO RESOLVE QUESTIONS, VALIDATE MODELS OR FILL VOIDS IN EXISTING RESULTS.	24
BIBLIOGRAPHY	30
APPENDIX A. ANALYSIS OF DISPLAY-CONTROL LOOP DYNAMICS FOR C-45	
APPENDIX B. CALCULATIONS FOR FIXATION LINK VALUES	
APPENDIX C. CALCULATION OF EYE MOVEMENT LINK VALUES FOR C-45 INSTRUMENT LOW APPROACH BASED ON PRELIMINARY SCANNING MODEL HYPOTHESES	
APPENDIX D. CALCULATION OF EYE MOVEMENT LINK VALUES FOR C-45 INSTRUMENT LOW APPROACH BASED ON MODIFIED AIRSPEED AND DIRECTIONAL GYRO HYPOTHESES	

ILLUSTRATIONS

Figure

- 1 Cockpit Instrument Arrangements
- 2 Pilots' Eye Fixation Frequency as a Function of C-45 Aircraft Display-Control Loop Frequency Bandwidth in:
 - 2 Straight and Level IFR with Standard Air Force Panel
 - 3 Routine IFR with Standard Air Force Panel
 - 4 Instrument Low Approach with Standard Panel
 - 5 Straight and Level IFR with New Experimental Panel
 - 6 Routine IFR with New Experimental Panel
 - 7 Instrument Low Approach with New Experimental Panel
- 8 Pilot's Eye Fixation Frequency as a Function of Display-Control Loop Frequency Bandwidth in an AVRO 652A "Anson" Mk1 Aircraft on IFR Adcock Standard Beam Approach with Standard Royal Air Force Blind Flying Panel
- 9 Pilots' Eye Fixation (Dwell) Time on Flight Instruments in:
 - 9 Howard NH-1 Aircraft; IFR (4 minutes)
 - 10 Avro 652A "Anson" Mk1 Aircraft; Adcock Standard Beam Approach on IFR
 - 11 C-45 Aircraft; Routine IFR with Standard Air Force Panel
 - 12 C-45 Aircraft; Routine IFR with New Experimental Panel
 - 13 C-45 Aircraft; Instrument Low Approach
- 14 Eye Movement Link Values Between Aircraft Instruments; C-45 Instrument Low Approach with Standard Panel
- 15 Calculated Probabilities of Eye Fixation on Each Aircraft Instrument for C-45 Instrument Low Approach:
 - 15 Based on preliminary scanning model hypotheses
 - 16 With modified airspeed and directional gyro hypotheses

Figure

Calculated Eye Movement Link Values Between Aircraft Instruments
for C-45 Instrument Low Approach:

- 17 Based on preliminary scanning model hypotheses
- 18 With modified airspeed and directional gyro hypotheses
- 19 C-45 Display Arrangement based on Calculated Probabilities of Fixation
and Link Values for Instrument low approach

APPENDIX A
FIGURES

- A-1. Continuous Equivalent Parallel Loop Closures for Elevator Longitudinal Control
- A-2. C-45 IIA; Bode and Siggy Plots for $u \rightarrow \delta_e$
- A-3. C-45 IIA; Root Loci for $u \rightarrow \delta_e$ with $1/T_{Lu} = 0.1, 0.29$
- A-4. C-45 Cruise; Bode, Siggy, and Root Locus for $\theta \rightarrow \delta_e$
- A-5. C-45 IIA; Bode, Siggy and Root Locus for $\theta \rightarrow \delta_e$
- A-6. C-45 Cruise; Bode, Siggy and Root Locus for $\dot{h} \rightarrow \delta_e$
- A-7. C-45 IIA; Bode, Siggy and Root Locus for $\dot{h} \rightarrow \delta_e$
- A-8. Continuous Equivalent Parallel Loop Closures for Aileron Lateral-Directional Control
- A-9. C-45 Cruise; Bode and Siggy Plots for $\varphi \rightarrow \delta_a$
- A-10. C-45 Cruise; Root Locus for $\varphi \rightarrow \delta_a$
- A-11. C-45 Cruise; Bode and Siggy Plots for $\dot{\psi} \rightarrow \delta_a$
- A-12. C-45 Cruise; Root Locus for $\dot{\psi} \rightarrow \delta_a$
- A-13. Continuous Equivalent Parallel Loop Closures for Aileron Lateral-Directional Control in Instrument Low Approach
- A-14. C-45 IIA; Approximate Locus for $r \rightarrow \delta_r$
- A-15. C-45 IIA; Bode and Siggy Plots for $\dot{\varphi} \rightarrow \delta_a$
- A-16. C-45 IIA; Root Locus for $\dot{\varphi} \rightarrow \delta_a$
- A-17. C-45 IIA; Bode and Siggy Plots for $\ddot{\psi} \rightarrow \delta_a$
- A-18. C-45 IIA; Root Locus for $\ddot{\psi} \rightarrow \delta_a$
- A-19. C-45 IIA; Bode and Siggy Plots for $\ddot{y} \rightarrow \delta_a$
- A-20. C-45 IIA; Root Locus for $\ddot{y} \rightarrow \delta_a$
- A-21. Single-Loop Crossover Model Illustrating Air Turbulence Disturbance Suppression
- A-22. Single-Loop Crossover Model Illustrating Rolling Turbulence Disturbance Suppression Bandwidth
- A-23. Single-Loop Crossover Model Illustrating ILS Radio Disturbance Suppression Bandwidth
- A-24a. C-45 IIA; Approximate Closed-Loop ILS Error Bandpass Functions
- A-24b. C-45 IIA; Approximate Closed-Loop ILS Error Bandpass Functions

TABLE OF INSTRUMENT ABBREVIATIONS

XPT	Cross Pointer	(Localizer and Glideslope Deviation)
AS	Airspeed	(Indicated)
DG	Directional Gyro	(Heading)
GH	Gyro Horizon	(Roll and Pitch Attitude)
ALT	Altimeter	(Pressure Altitude)
VS	Vertical Speed	
TB	Turn and Bank (or Needle and Ball)	(Yaw Rate and Lateral Acceleration)
ENG	Engine Group	
CLK	Clock	
MISC	Miscellaneous	

SECTION I

INTRODUCTION

This technical memorandum contains an analysis of aircraft pilot eye movement data obtained by other investigators from flight tests. This reconsideration of experimental evidence, some of which is more than twenty years old, is motivated by a desire to formulate a mathematical model of pilot eye movements in instrument flight which would be capable of predicting results obtainable with experimental cockpit display arrangements. The memo does not present such a model in finished form. That is left for the hopefully near future. What the memo does present is a comprehensive account and reanalysis of the data contained in several reports, by different investigators. This suggests some features of a useful model which should be compatible with (i.e. "explain") all, or nearly all, of these data.

The second Section of the memo presents a review of key contributions to the literature. An attempt is made to interpret the results primarily of Fitts' and Senders' work, and to suggest possible scanning models for the pilot which explain the observations.

Pilots' eye fixation frequency measurements are first discussed with respect to four possible variables on which they may depend.

- (1) display-control loop bandwidth or cross-over frequency,
- (2) pilot-initiated flight maneuvers,
- (3) instrument arrangement,
- (4) the possible redundancy of information on the several instruments.

Pilots' eye fixation dwel times are then discussed with respect to:

- (1) a possible refractory threshold time interval which appears in certain experiments and
- (2) the purpose for and type of sampled signal reconstruction which may be performed by the pilot.

Finally, an approximate method suggested by Senders for calculating paired-display fixation link values is applied to an instrument low approach condition not previously examined by Senders.

The third Section suggests some experiments to resolve questions, validate models and fill voids in existing results.

Appendix A presents the pilot-vehicle analyses which were used for estimates of the "bandwidth" of the displayed information and which are an essential feature of the discussion in Section II.

Appendix B shows the calculations for the "link values" which are also discussed in Section II.

Appendices C and D present calculations for the "link values" based on preliminary scanning hypotheses discussed in Section II.

SECTION II

REVIEW AND DISTILLATION OF COCKPIT INSTRUMENT SCANNING DATA

In a series of outstanding experiments conducted from 1949 through 1954, Paul Fitts, John Milton, and other members of the Aero Medical Laboratory at Wright Field measured pilots' eye fixation frequencies and fixation (dwell) times under several instrument flight conditions in a C-45 aircraft, (Ref. 16, 17, 18, 19, 20, 36, 37.) A standard Air Force instrument panel arrangement and an experimental rearrangement of instruments were studied. Figure 1 shows the two instrument arrangements. All instruments had moving pointers except the directional gyro, which had a moving scale. Fixation frequencies and dwell times were recorded individually for the following instruments: cross-pointer, airspeed, directional gyro, gyro horizon, altimeter, vertical speed, and turn and bank. The array of nine engine instruments was treated as a group. Therefore, no records are available for the individual members of the engine group. Attention to the wet compass was never recorded, and attention to the clock was recorded only in some of the later experiments by Milton with 180° timed turns.

The Air Force experiments recorded measurements during the following maneuvers on instruments: instrument low approach, straight and level, level turn, climbing and descending turns, straight climb and dive. Further results (Ref. 16, 18) with the ground voice-controlled approach and the 180° timed turn have not been included in the present analysis, because these maneuvers were peculiar to an earlier era and the instrument scanning data seems to reflect the special training required for these maneuvers.

Some still earlier measurements of eye fixations were made by McGehee in 1944 with Navy pilots. Limited results were presented together with Fitts' first report (Ref. 17). McGehee's results have been included in the present analysis.

Finally we have included more recent (1955) small sample eye fixation frequency and duration measurements by Watts and Wiltshire in Adcock Standard Beam Approaches with a single subject pilot using a Royal Air Force standard

blind flying instrument panel.

We shall now discuss some of the trends in fixation frequency, and fixation time, which have been gleaned from Fitts', Watts' and McGehee's data.

A. Fixation-Frequency Loop Cross-Over Frequency Relationship

In order to appreciate that anything new may be accomplished with respect to the rather hoary data which is reexamined here, it is necessary to take two relatively recent suggestions into account. The first of these is derived from information theory and is that the fixation frequency (sampling rate) must be at least twice the "bandwidth" of the signal presented on the face of the instrument. (Ref. 1, 57, 63) The second suggestion is that the "bandwidth" of the signal displayed and useful to or used by the pilot might be estimated by means of pilot-vehicle system analysis. (Ref. 1, 55, 56)

Furthermore, it is necessary to recognize that what is attempted here depends pivotally on theories for and measurements of disturbances in the flight environment, all of which postdate the original eye fixation measurements re-examined herein. Thus, not only is the characterization of the human pilot founded on Norbert Wiener's cardinal classic on stationary time series in 1949, but also so is the theory of atmospheric turbulence and the characterization of the instrument landing system (ILS) radio noise-like components caused by irregularities in the radiation "beam" pattern.

As has already been mentioned, Appendix A (below) documents the pilot-vehicle analyses which were made so as to estimate the bandwidths of the signals on the several instruments. These analyses, however, were somewhat in the nature of bootstrap operations since estimates of fixation frequency and dwell time were required in the calculations. It is for this reason that the existing data are reviewed first.

Replotted in Fig. 2 are Fitts' data on eye fixation frequency for each instrument on the "standard" C-45 panel when the task was to maintain straight and level flight. The ordinate is the observed fixation frequency, ω_f ; while the abscissa is the estimated display-control loop-pass frequency "bandwidth."

Since Fitts, et al., published no record of speeds and altitudes in their statements of experimental procedure, we have indicated two abscissae which determine a range of possible longitudinal control bandwidth frequencies in cruising flight, depending on the altitude at which the C-45 was flown. All the instruments used in longitudinal flight control (gyro horizon [pitch], altimeter, airspeed, and vertical speed) are plotted at the same value of (longitudinal) frequency bandwidth; while the instruments used in lateral flight control (directional gyro, gyro horizon [roll], and turn and bank indicator) are all plotted at the same value of (lateral) frequency bandwidth which is, however, different from the one for longitudinal control. (See Appendix A.)

By analogy to an autopilot designed to fly straight and level we might imagine that the human pilot could do a competent job by consulting only the gyro horizon, the altimeter and the directional gyro. It is, therefore, interesting to note in Fig. 2 that the observed fixation frequencies for these three instruments are clustered in the vicinity of three or four times the calculated loop bandwidth frequencies. (It is, of course, impossible to distinguish the fixations on the gyro horizon for the purpose of obtaining pitch information from fixations for obtaining roll information. If pitch and roll were presented on different instruments, as in some very early German panel arrangements, it would appear highly likely that the pitch gyro horizon data point would then be superposed on the altimeter data point.)

In this case, and in others considered in Appendix A, the longitudinal characteristic frequency bandwidth, ω_b , is almost exactly half the phase crossover frequency $\omega_{\phi_m} = 0$ so that $4\omega_b \doteq 2\omega_{\phi_m} = 0$ and the latter number might be taken as an absolute upper limit to the bandwidth of any signal that the pilot would be interested in. The lateral characteristic frequency bandwidth, on the other hand, nearly matches its loop phase crossover frequency, so that $\omega_b \doteq \omega_{\phi_m} = 0$.

Note in Fig. 2 the lower sampling rates for the airspeed and vertical speed instruments, and the very low rate for the turn and bank indicator.

The implication is that these instruments are not required for flight control in straight and level flight with a "full panel" and are checked only occasionally. Much the same thing is true of the engine instruments, while, in this instance, the cross-pointer is not checked at all, which is as it should be.

The data for all routine instrument flight maneuvers including straight and level flight, has been plotted in Fig. 3 A and B. The data for instrument low approach appears in Fig. 4. Corresponding graphs of fixation frequency on the experimental panel appear in Fig. 5, 6 A and B, and 7. The straight and level data is emphasized in Fig. 2 and 5, because it serves as a norm, based on a simple compensatory flight condition, for interpreting trends in other flight conditions.

The abscissa in Fig. 4 and 7, the characteristic frequency bandwidth, ω_b , requires some qualification in the case of the cross-pointer (XPT) instrument, because the display-control loop has a bandpass character with respect to radio noise-like disturbances caused by irregularities in the antenna radiation pattern. The lower range of XPT abscissae represents the dominant or center frequency of the loop passband, whereas the higher range of abscissae is the loop pass bandwidth for an "average" conventional localizer. (Ref. 52.) Some justification for this manner of plotting is suggested by the need for smoothed signal reconstruction or filtering, which the pilot may be performing in the case of these instruments. Since Fitts, et al, published no record of the ILS facility, we have employed average conventional localizer characteristics because the directional waveguide localizer did not exist in 1949.

Because the roll and pitch presentations on the gyro horizon are inseparable in Fitts' data, the abscissae for both pitch and roll loop bandwidth frequencies have been plotted, based on the analysis in Appendix A.

Another set of instruments requiring special treatment is the engine group. Pilots are perhaps accustomed to scanning engine instruments with conscious application of a threshold-exceedence criterion, and with an equality-matching criterion in the case of multi-engine aircraft. We have suggested in Fig. 2, 3 and 4 that the engine group should be plotted against a threshold exceedence

frequency. An example of the calculation of such a frequency was given in Ref. 2 on p. 18. Without a history of engine experience on the C-45, it is difficult to choose any values for the abscissa coordinate here. However, some experimental studies by Senders and Mackworth may be related to engine instrument monitoring.

Subject to the revision in Ref. 2, p. 17, Senders' fixation frequency data appears directly applicable to engine, accelerometer, and angle of attack-apexer (USN), in a threshold exceedence sense. However, Fitts and Milton did not record fixation frequency and dwell time data individually on engine instruments, so we cannot verify a threshold exceedence theory quantitatively.

Mackworth, Kaplan and Metlay, Ref. 32 report eye movements recorded during vigilance in the laboratory. The task required only discrete signal detection. Six subjects watched for 0.5-second duration aperiodic pauses in the slow rotation of a pointer during 3.5 minutes of exposure. Pauses were programmed to appear at irregular intervals at two average rates: 7.6/minute for frequent signals and 1.8/minute for infrequent signals. Average fixation frequencies of subjects were between four and nine times the higher of the two average signal interruption frequencies. There was a correlation of 0.83 between average fixation frequency and average signal detection frequency.

There is no obviously unique correlation between fixation frequency and loop characteristic frequency bandwidth, in Fig. 2 through 7. One is more inclined to assign a constant fixation frequency of about 2.5 radians per second to both gyro horizon and directional gyro, from Fig. 3 A and 6 A. The lateral closures for the C-45 in Appendix A show that the gyro horizon and directional gyro may be plotted near the abscissa of one radian per second in Cruise and one-half in approach. The mean fixation frequency for both instruments is nearly three times the lateral characteristic frequency bandwidth in Cruise. GH mean fixation frequency is over four times the longitudinal frequency bandwidth in Cruise.

In the case of the instrument low approach, Fig. 4 and 7, the sampling frequency of the gyro horizon is lower, yet between three and four times its characteristic bandwidth. However, since the cross-pointer is known to be

sampled most frequently and longest during the approach, the gyro horizon may be lower because attention must be given to the cross-pointer and air-speed indicator to satisfy the precision approach guidance and control requirements. The "average" pilot's attention may be saturated by the signal reconstruction demands from the multiplicity of instruments, so that he just can't get around the cockpit. The high fixation frequency on the DG in the instrument low approach, about five times the loop bandwidth, may include some transfer of training from ground-voice-controlled approach procedure in which the same pilots were known to be skilled. (Ref. 20.) Indeed, cross reference to Fig. 8, for an Adcock Standard Beam Approach (SBA) in an Avro 652A "Anson" Mk1 with RAF instrument panel shows a markedly lower mean fixation frequency on the DG, about three times loop bandwidth. Although the aircraft is quite similar to the C-45, the lateral deviation was obtained aurally in Morse (A or N) Code and letdown guidance was by pressure altimetry between outer and inner marker beacons. Note also that in the British tests (Fig. 8) the altimeter was sampled much more frequently than in the C-45 tests, obviously, because it was the source of vertical guidance information.

Consider next the airspeed indicator for the straight and level case, Fig. 2 and 5. In straight and level flight, the airspeed display-control loop is probably purely compensatory. Notice that in both Fig. 2 and 5 the airspeed fixation frequency is between one and two times the loop frequency bandwidth calculated in Appendix A. In the case of the instrument low approach the airspeed sampling frequency is more than doubled with the standard panel in Fig. 4, over three times the loop frequency bandwidth. The increase during approach may be associated with a change in the role of airspeed control to that of major loop status; or the increase in airspeed sampling accompanied by the slight decrease in gyro horizon sampling frequency may show a reversion to the "needle-ball-and-airspeed" training for IFR flight of a slightly earlier era. The "needle-ball-and-airspeed" rationale is reinforced by the airspeed and gyro horizon sampling frequency data for the experimental panel in Fig. 7. The experimental panel data was obtained two years later (and possibly with a newer generation of pilots) with the airspeed

indicator and gyro horizon locations unaltered (Fig. 1). Notice that both instruments in Fig. 7 exhibit approach fixation frequencies nearly identical to those measured in straight and level flight, Fig. 5. Thus we may treat Fig. 4 as exceptional and conclude that airspeed is typically sampled at about two times its loop frequency bandwidth in compensatory cases, except when airspeed control has major loop status as in approaches.

The exceptional character of Fig. 4 approach airspeed fixation frequency appears even more dramatically in Fig. 8 for an RAF Adcock Standard Beam Approach in an Avro 652A "Anson" Mk1, which is similar to the C-45. The longitudinal closure analysis in Appendix A shows for the C-45 that airspeed sampling requires pilot phase lead (or acceleration sampling) at extraordinarily low frequencies — lower than that of the open loop phugoid — to offset the lag of the average sampling delay. Yet the increase in phugoid damping ratio and bandwidth are very slight when compared with the concentration required to generate low frequency lead at the average airspeed sampling rate. Clearly the improvement in phugoid damping ratio and bandwidth for the pilot effort is not commensurate with that achievable by gyro horizon (pitch attitude) sampling at comparable average sampling rates. We suggest that the pilot population represented in Fig. 4 and the single pilot in Fig. 8 may be using an airspeed loop closure as a redundant technique for damping the phugoid and increasing phugoid bandwidth. The very high airspeed fixation frequency in Fig. 8 is possible because cross-pointer instrument guidance was absent, and lateral deviation was received aurally in Morse (A or N) code.

Consider next the altimeter for straight and level flight and level turns, Fig. 2, 3, 5, and 6. The altimeter is sampled much more frequently than the airspeed indicator even though both instruments operate in loops with about the same frequency bandwidth. Although we propose a rationale for the decrease in altimeter sampling frequency with maneuvers in a following section, the high altimeter sampling frequency norm is difficult to explain.

Penultimately take the vertical speed indicator for straight and level flight and level turns. In the standard Air Force panel in Fig. 2 and 3B, the vertical speed indicator is sampled at over one and two times the altitude loop frequency bandwidth, respectively. In the new experimental panel

in Fig. 5 and 6B, the vertical speed indicator in straight and level flight, and in level turns is sampled at a much higher frequency, between 2 and 2.5 radians per second, over four and five times the characteristic bandwidth. Vertical speed is sampled at nearly the frequency of the gyro horizon and directional gyro. This may simply be because the vertical speed is nearly between the gyro horizon and directional gyro, as Fig. 1X shows.

Finally consider the turn and bank (needle and ball) indicator. In straight and level flight and in straight diving and climbing flight with the standard panel, Fig. 2 and 3A, the turn and bank indicator is sampled at between 0.45 and 0.85 radian per second near half the turning loop cross-over frequency. However on the new panel in Fig. 5 and 6A it is sampled at less than 0.1 radian per second except in turns when sampling is near the turning loop cross-over frequency. It appears that sampling the turn and bank indicator is explained by the "needle-ball-and-air-speed" training rationale. It was more important to pilots who flew the standard panel in 1949 and was not as important to the pilots who flew the experimental panel in 1951, except in turns. The turn and bank indicator sampling might be modelled by fixation frequency equal to one-half the lateral-directional loop frequency bandwidth. One must then conclude in the case of the approach, Fig. 4 and 7, that the sampling rate of the turn indicator is actually much less than even half the loop cross-over frequency, simply because the indicator information is unimportant in controlling the landing. Appendix A shows that yaw damping is essential in the approach flight condition, but that the turn and bank indicator sampling rate is far too low to provide the bandwidth required. Therefore the pilot may employ vestibular sensing of lateral acceleration and yaw rate instead.

We next consider why certain of the instruments have significantly different fixation frequencies, depending on the flight maneuvers.

B. Fixation Frequency-Maneuver Relationship

There is a distinct influence of the maneuver on fixation frequencies for four flight instruments: airspeed, altitude, vertical speed, and turn and bank. Maneuver also has a pronounced influence on the fixation frequency associated with the engine group.

Consider first the airspeed indicator. In both Fig. 3B and 6B, that is, with both standard and experimental instrument arrangements, the fixation frequency for the airspeed indicator increases in the order of the following maneuvers: level turns, climbing and descending turns, and straight climb and descent. The additional fixations in these cases may be explained by the fact that the pilot knows that these maneuvers will disturb his air speed. Another explanation might be associated with increasing mental stress. Since the sampling rate, at most, triples the straight and level value, the addition of one or more signal paths of higher order than compensatory in the pilot's topological model might explain the observation. It is also interesting to find the highest airspeed fixation frequency near 2.5 radians per second, the same norm exhibited for the gyro horizon and directional gyro, which are normally important instruments.

Consider next the altimeter in climbing and descending turns, straight climbs and descents, the low approach (Fig. 3, 4, 6 and 7.) The fixation frequency for the altimeter decreases markedly with climbing and descending maneuvers. The compensatory altitude control loop is here open. It has probably been replaced by a compensatory vertical speed control loop. Possibly the instructions for the maneuvers were given in terms of airspeed and vertical speed rather than change in altitude. It may also be that the changes in altitude during the climbs and descents were small, and therefore not of paramount concern. Certainly the reduction of altimeter fixation frequency during the instrument low approach is expected because the pressure altimeter is not important as a flight control error sensor. Its function is performed by the glideslope displacement needle (cross-pointer) in the instrument low approach. However, in Fig. 8, wherein we plot data from an RAF Adcock Standard Beam Approach in which letdown is by pressure altimetry from outer to inner marker beacon, the altimeter fixation frequency is nearly three times the characteristic loop frequency bandwidth. We may expect similar attention to altimetry when dealing with the absolute altimeter in future studies.

Fixation frequency for the vertical speed indicator increases with maneuvers in the same order as did the airspeed fixation frequency increase

(Fig. 3B and 6B). Thus one may conclude that the pilot's compensatory vertical speed and airspeed loops are closed to perform the maneuvers again with extra sampling for higher order concern. The maximum vertical speed fixation frequency in Fig. 6B is 2.8 radians per second. In the case of the instrument low approach (Fig. 4 and 7), fixation frequency of the vertical speed indicator drops to a low value near the loop frequency bandwidth, probably because that instrument is not important to the approach control problem with a radio glideslope reference. In contrast, the RAF Standard Beam Approach data in Fig. 8 show the mean fixation frequency on vertical speed to be twice the characteristic frequency bandwidth. This instrument evidently played a compensatory role as explained by the RAF letdown procedure in Ref. 54, viz., "...the pilot passes the Outer Marker at 1,000 feet and then descends to 150 feet at 600 feet per minute. This height is maintained until the Inner Marker is heard, by which time the runway should be visible..."

Turning maneuvers increase the fixation frequency on the turn and bank indicator. (Figure 3A and 6A.) Climbing turn mean fixation frequency with the standard panel in 1949 is more than double that with the experimental panel in 1951. Since the pilots in 1949 were probably originally trained in the needle-ball-and-air-speed school of instrument flight, this result is reasonable. Level turn mean fixation frequency, however, is insignificantly higher with the standard panel than with the experimental pane. Both exhibit a maximum fixation frequency of about 0.8 radian per second, about 0.8 times the heading loop frequency bandwidth.

Finally, the fixation frequency for the engine group increases with turning, climbing and descending maneuvers, as we found in the case of airspeed and vertical speed. Here the pilot knows he must disturb the engines in order to perform the maneuvers. Therefore he samples more frequently to look for the expected increase in threshold exceedences. The increase in engine group fixation frequency is much greater with the standard Air Force panel in Fig. 3 than with the new experimental panel in Fig. 6. This is difficult to explain because the engine group was identical in both arrangements, as Fig. 1 shows.

C. Fixation Frequency-Instrument Arrangement Relationship

One of the most significant results found by Milton and his associates Ref. 36, 37 is the effect of instrument arrangement on fixation frequency. The most startling example is the cross-pointer indicator, which may be compared in Fig. 3 and 6. In all routine instrument flight maneuvers the cross-pointer indicator presented no signal. In Fig. 3, with the standard Air Force panel, the pilots made no fixations on the cross-pointer indicator, probably not only because it displayed no information but also because it was located at the extreme left edge of the panel. (Fig. 1S.) However, in Fig. 6, with the new experimental panel, the pilots fixed on the cross-pointer indicator at about the same rate as on the engine group, even though the cross-pointer had no signal on it! Evidently this was because the cross-pointer was located in the center of the instrument panel, immediately to the left of the gyro horizon. (Fig. 1X.)

We have already mentioned another example of the influence of instrument arrangement on the fixations of the vertical speed indicator in the experimental panel, Fig. 1X. Vertical speed is sampled at almost the frequency for the gyro horizon and directional gyro, probably only because the vertical speed indicator is located nearly between the other two.

One would hope that the subjects were exposed to sufficient pre-record training with the new instrument arrangement before the one-minute samples of data for publication were taken. There is no assurance of this in the statement of procedure. Hence, there may still be some non-stationary effects of learning or transfer of training in the data with the new experimental panel.

Since it is unlikely that one would locate an instrument which is most often dormant in the center of the instrument panel, the results of these experiments serve as a caution that the arrangement chosen may well influence the fixation frequencies which might have led to the choice of arrangement in the first place, if the arrangement contradicts the following hypotheses:

- (1) locate centrally those instruments having highest probability of fixation (Appendix B)
- (2) locate peripherally adjacent those instruments having highest link values (Appendix B) with central instrument(s)
- (3) locate peripherally remote those instruments having lowest probability of fixation and/or lowest link values.

D. Fixation Frequency-Instrument Co-relationship

There is informational redundancy and correlation among the instruments in an aircraft because of the intrinsic dynamic coupling among the several degrees of freedom. Pilots have learned this from their training. Now if the dynamic characteristics were all the pilot abstracted from the instrumentation, we might expect that he would sample each member of a redundant pair, or correlated pair, less often when both are present, compared with the situation where only one was present. However this does not seem to be entirely the way the pilot uses his instrumentation. In the first place he does not always have identical information on the correlated instruments. Therefore he learns to cross-check between members of a pair of similar or correlated instruments. Since cross-checking between members of a pair will usually be done on consecutive fixes, the cross-checking may tend to increase the apparent fixation frequency on both members of the pair. Finally, the pilot is often interested in the scale or quantitative value of excursions on each member of a pair of instruments which may be correlated dynamically. Thus he will certainly not decrease fixation frequency on either one when both are present, as compared with the case if only one were present. This reasoning may explain why most of the fixation frequencies examined in the Fig. 2, 3, 5 and 6 are well above the minimum values predicted by sampling- and reconstruction theory with and without first derivative sampling.

The problem of instrument correlation was investigated by Senders in Ref. 44. Although Senders had a rather coarse threshold exceedence criterion, he found that correlation did not significantly increase or decrease fixation frequency between the pair of correlated instruments relative to fixation frequencies on the same instruments with uncorrelated signals.

E. Summary and Conclusions for Fixation Frequency

- (1) The simple theory that fixation frequency should be slightly more than twice the bandwidth of the information does not hold water.
- (2) The pilot generally fixes on a given instrument much more frequently than is required by the bandwidth of the signal. A fixation frequency three to four times the bandwidth of the signal appears in the case of the principal flight instruments.

- (3) In particular maneuvers he will fix even more frequently on instruments displaying signals required by instructions to be nulled, and will fix less frequently on instruments displaying inessential information. He will also fix more frequently on instruments whose readings he expects to be disturbed. A vigilant sampling frequency between 2.5 and 3 radians per second appears for the C-45 data, independent of the instrument.
- (4) The partial redundancy of information is not often used to decrease the fixation frequency on a particular instrument.
- (5) There is probably an immense transfer of training effect from earlier displays and/or doctrines.
- (6) Instruments with inessential or no information may be fixated if they are centrally located near or between instruments which require attention.

F. Fixation (dwell) Time Relationships

Four sources of flight data on fixation time exist. Winblade's, Ref. 53 results with the X-15 have already been reported in Ref. 2 on p. 22. Winblade found dwell times in the range 0.5 to 0.6 second, for four instruments in the X-15.

A second source is the work of McGehee Ref. 17, in a Howard NH-1 airplane, in 1944, with Navy pilots. Figure 9 shows McGehee's results for each instrument. McGehee's sample runs were 4 minutes long. The proportion of each run given to a particular maneuver was not identified. Instead McGehee averaged all times for the entire sequence of maneuvers. This tends to reduce the variation among the means when compared with the last source, Fitts's data on dwell time. The small variation in dwell time with flight experience from McGehee's data does not appear to be significant. The dwell times found for the four most important instruments by McGehee are in exactly the same range found by Winblade. The concentration on the turn and bank and clock in McGehee's data reflects the importance of timed turns in the instrument flight practices in 1944.

A third source is the work of Watts and Wiltshire, Ref. 54, in an Avro 652A "Anson" Mk1 with one pilot and Royal Air Force Standard instrument panel. Figure 10 shows Watts' results for each instrument from a rather small sample,

compared with other sources. Five Adcock Standard Beam Approaches of approximately one minute time duration each were made on IFR. Data was recorded between outer and inner marker beacons. The extreme individual means for each instrument are shown with respect to the grand mean for 5 approaches. The grand averages tend to be slightly greater than found by McGehee. The unique importance of airspeed and vertical speed in this type of letdown without a true glideslope path reference is apparent from their long mean dwell times.

Finally, we turn again to Fitts' routine IFR data which has been plotted in Fig. 11 for the standard U. S. Air Force panel, and Milton's work in Fig. 12, with the experimental panel. The dwell times have been recorded by flight maneuver because Fitts experimented very carefully so as to keep the data for each maneuver separate. Instrument low approach dwell times are presented for both panel arrangements in Fig. 13. There is a significant dependency on instrument type (i.e., flight or engine) because the engine array was treated as a group. Within the flight instrument classification there is a secondary dependency on importance. Attitude, heading and airspeed form a "primary" group whose mean dwell time is in the range of 0.56 to 0.63 second, depending on the maneuver. Altitude, vertical speed and turn and bank form a "secondary" group whose mean dwell time is in the range 0.4 to 0.45 second, depending on the maneuver. These observations are labelled as finely quantized mean levels of dwell time in Fig. 11 and 12. With few exceptions the lower values of dwell time in each group are associated with the fact that the instrument did not have to be read in detail during the maneuver or was at a compensatory null value during that maneuver. The higher values of dwell time in each instrument group appear in maneuvers where a reading or reconstruction may have been necessary or where that instrument deviated from its null value.

One exception to the above statement is the directional gyro in straight and level flight. One would expect the dwell time to be about the same as that for other types of straight flight, but it is considerably higher. The increase may be attributable to the time spent reading the numerals on the instrument and interpolating for the purposes of navigation. A similar

exception for the engine group in straight and level flight may be associated with fuel management. We suggest that pilots are accustomed to do navigation and fuel management and have the time for it in straight and level flight and that force of habit is apparent in the results of the short-time experiments.

In the case of Fig. 11 another comment concerning straight and level flight is worthwhile. The grand average of all fixation times is much higher in straight and level flight than in the other maneuvers. It appears that the pilot has so much time available that he fixes somewhat longer on each instrument. When the mean dwell time for each instrument was revised downward in proportion to the ratio of grand mean values, the mean for each flight instrument exhibited a consistent pattern.

Some other discrepancies appear in Fig. 12. Vertical speed exhibits an unexplainable high and low dwell time in climbing and diving maneuvers, respectively, whereas it had a consistent value in both climbs and descents with the standard panel. The turn and bank indicator also exhibits a high dwell time and a low dwell time during turns, whereas it had a consistent dwell time during turns with the standard panel.

When one considers that the instrument panel must be designed for all classes of maneuvers, the dwell time of half a second is probably a suitable conclusion for all instruments in the flight group. A dwell time of one second appears reasonable for the engine group, since the pilot probably looks at paired instruments on each fixation in the case of a twin-engine aircraft, such as the C-45.

The cross-pointer dwell time is significant. In the instrument low approach in Fig. 13, a dwell time of about 0.8 second is probably required to smooth the localizer and glideslope noise appearing on the instrument. However in Fig. 12, where the cross-pointer was located centrally, yet inoperative, a minimum value of dwell time, quite consistent with a psychological refractory phase of voluntary ocular response, was observed at about 0.25 second. This may be the irrevocable fixation time after recognition or recall that this instrument was inoperative.

We have identified four finely quantized mean levels of dwell time in Fig. 12, the instrument low approach. That for the cross-pointer at 0.8 second we have already mentioned. Coincidentally, the engine group monitor dwell time is also about 0.8 second. This is about twice the 0.4-second dwell time required for monitoring the "secondary" group of flight instruments, viz., altitude, vertical speed and turn and bank. The directional gyro (moving scale), from which course was reconstructed, received a dwell interval of 0.55 second, its mean value in all cases. Finally, the mean duration of all other (miscellaneous) fixations was measured at 0.19 second, slightly lower than the mean threshold for the inoperative cross-pointer.

There may be another manifestation of the "needle-ball-and-airspeed" training rationale in the dwell time data for the gyro horizon, airspeed and turn and bank indicator in Fig. 13. On the standard panel in 1949, the airspeed sampling technique was one of more frequent shorter fixations compared with the technique on the new experimental panel in 1951 of fewer longer fixations. On the standard panel in 1949, the gyro horizon sampling technique was one of longer fixations compared with the technique of the experimental panel in 1951 of shorter fixations at nearly the same frequency. Fitts and Milton show in Ref. 16 and 37 that, although the combined fraction of time spent on airspeed and horizon was higher on the standard panel in 1949 than on the experimental panel in 1951, the relative proportion of attention between airspeed and horizon remained exactly the same in both arrangements with very different sampling techniques! Since we have some evidence* that more frequent shorter fixations are associated with lead compensation and longer fixations with smoothing, the shift in emphasis from airspeed IFR training to gyro horizon training during the 1941-1945 war may explain the observations.

Although the turn and bank indicator received a dwell time of about 0.35 second on the standard panel in 1949 during the low approach, the pilots in

*Clement, W. F., Cardinal Data Reconstruction Theory: A Method for Estimating the Effect of Fixation Dwell Time on Pilot Sampling Delay, Systems Technology, Inc. Working Paper, to be published and Appendix A of the present paper.

1951 with the new experimental panel did not even fixate on the turn and bank indicator located directly below the gyro horizon as shown in Fig. 1X. However, some pilots may have perceived it peripherally while apparently fixating on the gyro horizon.

Senders' (Ref. 44) minimum dwell time is approximately the same as that found by Fitts and Milton: 0.4 second. Again there is no need to hypothesize Senders' information theory formula to explain dwell time among Fitts', McGehee's or Senders' experimental results. This confirms the conclusion reached in Ref. 2, on p. 22, after a review of Winblade's X-15 data on dwell time.

Mackworth, Kaplan and Metlay in Ref. 32 also report eye fixation dwell times for their laboratory experiments in signal detection vigilance. Cumulative frequency distributions of eye dwell time intervals were obtained during 3.5 minutes of viewing time. The two subjects with lowest signal detection rates (less than 40%) sampled less frequently with most dwell intervals between 0.5 and 4 seconds. The two subjects with highest detection rates (about 60%) sampled more frequently with most dwell intervals between 0.25 and 1.5 seconds.

Sheridan (Ref. 49) reports measurements of operator tracking preview time interval by J. G. Kriefeldt and M. H. Merel in several forced-pace tracking experiments in the laboratory. Minimum smoothed tracking error was obtained for preview time intervals between 0.25 second and 0.5 second with 0.5 second preferred. Preview times up to 1 second produced little improvement over 0.5 second. The agreement between Sheridan's results and the flight test results appears more significant than coincidental.

G. Summary and Conclusions for Dwell Time

- (1) The more coarsely quantized mean levels of dwell time shown in Fig. 11 and 12 appear to be a sufficient summary of Fitts' and Milton's findings. The mean value of 0.5 second is termed a "reconstruction" dwell time, since it represents an average for all flight instruments. It is also supported by the average of all of McGehee's measurements in Fig. 9.

- (2) The mean value of 1 second is termed a "group-monitor" dwell time, since it represents an average for the engine group. If we hypothesize paired engine instrument sampling for the twin-engine C-45 on each group fixation, we may venture the same value of 0.5 second for dwell time on each member of the pair. However, Fitts and Milton supplied no data to support this paired-sampling hypothesis.
- (3) The approach data in Fig. 11 suggest revision of the "monitor" dwell time downward to 0.4 second, if attention to the instruments is not required for flight control.
- (4) A threshold or refractory interval for dwell time appears to be in the range 0.2 to 0.25 second. There may be at least four reasons for increasing dwell time above the threshold: (1) extrapolation and prediction for lead compensation; (2) interpolation and extrapolation for reproduction; (3) interpolation and smoothing for filtering or lag compensation; and (4) threshold exceedence monitoring. There is evidence that the more finely quantized mean levels of dwell time in Fig. 11, 12 and 13 are nearly integral multiples of the threshold or refractory period. An accompanying work* presents an analysis of a truncated cardinal reconstruction filter acting on the output of a random impulse sampler. The results show that dwell time and first derivative recognition do indeed influence the character of the filter in a rational way. Further investigation and experiment is required to determine whether a correlation exists between the pilot lead or lag compensation, introduced in the loop closures, and the dwell time observed in various flight conditions.
- (5) The results from four sources spanning 20 years of flight history in three distinctly different types of aircraft suggest that average dwell time on the class of instruments studies may be a physiological property of the pilot population — even including the 15 Naval Aviation cadets examined by McGehee.

*Clement, W. F., Cardinal Data Reconstruction Theory: A Method for Estimating the Effect of Fixation Dwell Time on Pilot Sampling Delay, Systems Technology, Inc. Working Paper, to be published.

H. Display Fixation Link Values

We have continued estimation of display fixation link values by Senders' approximate method in Ref. 46 and 47, Appendix 5, using only fixation frequencies and fixation times. Figure 14 presents a comparison of calculated link values with observed link values, for Fitts' instrument low approach in the C-45 with standard Air Force instrument panel. The agreement between the approximate calculation and the observation is quite acceptable in the range above a link value of 0.1. A by-product of this calculation is an estimator of the probability of fixation on each instrument. The calculations for this instrument low approach example are given in Appendix B to this working paper.

We conclude that this approximate method of calculating link values is quite satisfactory. We shall now apply this method in a weak test of our preliminary pilot scanning model hypotheses.

We have derived in subsection E (above) some conclusions for a pilots' eye fixation frequency model based on flight tests in a C-45 with two instrument arrangements in daytime under IFR. We have purposely avoided examining flight test data with the new experimental instrument arrangement in nighttime under IFR (Ref. 16, 37) because we want to test hypotheses against observations which did not contribute to the hypotheses. This test is, of necessity, weak because the aircraft approach flight condition and display-control loop bandwidth frequencies remain the same as for the conditions of derivation.

The mean fixation frequency hypotheses and mean dwell time hypotheses are listed by instrument in Table I for the instrument low approach (ILA). Two hypotheses are used for AS and DG. Although the values in parentheses match daytime observations somewhat better, the order of results is predicted acceptably by the other simpler hypotheses. Calculations are presented in Appendices C and D to this working paper. Calculated probabilities of eye fixation are compared with observed (Ref. 16, 20 and 37) proportions of time spent on each aircraft instrument in Fig. 15 and 16. The observations which led to the preliminary hypotheses are shown in Fig. 15 and 16, as well as the nighttime data. The GH night fixation frequency is not predicted as well as others.

TABLE I

HYPOTHESES FOR PILOTS' EYE FIXATION FREQUENCIES
AND DWELL TIMES FOR C-45 INSTRUMENT LOW APPROACH

FLIGHT INSTRUMENT	MEAN FIXATION FREQUENCY HYPOTHESIS*	MEAN DWELL TIME HYPOTHESIS (SECONDS)	ORDER OF CONTROL LOOP TOPOLOGY
XPT	$3\omega_b$	0.8	Major
AS	$3\omega_b$ ($2.4\omega_b$)	.5	Major (and Minor)
DG	$4\omega_b$ ($5 \omega_b$)	.5	Minor
GH	$4\omega_b$.5	Minor
ALT	ω_b	.4	Monitor
TF	0	.4	Monitor
VS	ω_b	.4	Monitor
ENG	0.1 RAD/SEC	.8	Monitor
MISC	0.1 RAD/SEC	.2	—

*Expressed in terms of low-pass display-control loop characteristic frequency bandwidth, ω_b , except for Eng and Misc groups. Improved modified hypotheses for AS and DG appear in parentheses.

Refer to Appendices C and D for calculations.

Calculated eye movement link values between aircraft instruments are compared with observed (Ref. 16, 20 and 37) link values in Fig. 17 and 18. The symmetric scatter in nighttime observations is not significantly altered by the modified AS and DG hypotheses (Fig. 16). The arrows on observed link values of 0.02 signify that the observation was recorded as "less than 0.02."

We now conclude that the preliminary pilot display-scanning hypotheses are ready for more critical test in application to a different aircraft. We suggest that the next application be the Boeing 707, since we find evidence in Ref. 30, p. 3, that flight test observations of fixation frequency and dwell time may exist for the 707 in Australia.

I. Display Arrangement

We are searching for a theory which will culminate in prediction and validation of the "best" instrument arrangement(s) for an assigned set of mission-vehicle-crew requirements. We have here suggested hypotheses which relate average ocular fixation frequencies on separate flight instruments to the compensatory topology of a low approach. This is but one of many branches in the structure of a theory. We now add one more branch to illustrate the application of hypotheses for arrangement based on the calculated probabilities of fixation in Fig. 15 or 16 and the calculated paired-instrument link values in Appendix C or D. A quantitative definition of a sense in which the resulting arrangement is "best" remains as a subject for continuing research.

We conclude in Table II with three instrument arrangement hypotheses paraphrased after McGehee and Fitts (Ref. 17, 20).

TABLE II
HYPOTHESES FOR DISPLAY ARRANGEMENT

- (1) Locate centrally those instruments having highest probability of fixation (McGehee suggested upper center for the single most important instrument.)
- (2) Locate peripherally adjacent those instruments having highest link values with central instrument(s). (McGehee suggested lower center for the next most important instrument.)
- (3) Locate peripherally remote those instruments having lowest probability of fixation and/or lowest link values.

An arrangement based solely on the calculated values for the instrument low approach is presented in Fig. 19. Since we would not locate the cross-pointer centrally in any other flight condition, the result of Fig. 19 logically suggests an integration of cross-pointer and gyro horizon or directional gyro. Indeed several examples of such combinations have been proposed, patented and developed. Reference 66 presents a recent example of a "bull's-eye" adaptation of the cross-pointer in combination with an attitude indicator for the C-5A heavy logistics transport.

SECTION III

EXPERIMENTS PROPOSED TO RESOLVE QUESTIONS, VALIDATE MODELS OR FILL VOIDS IN EXISTING RESULTS

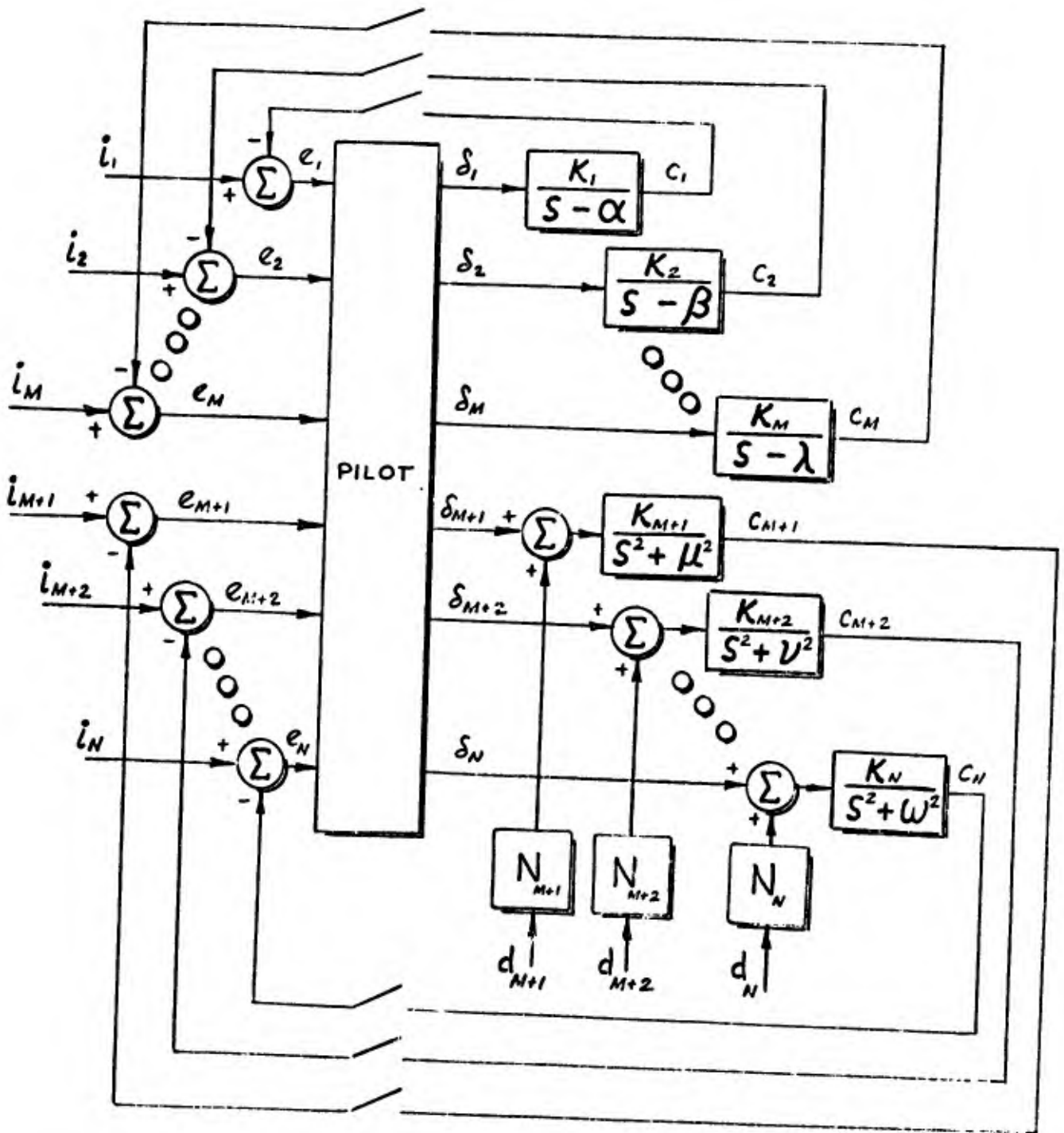
The following proposals for experiments have been motivated by the re-examination and analyses reported in this paper.

1. Frequency distribution measurements of ocular sampling interval and dwell time interval on separate instruments in a multiloop control situation

Although apparently a repetition of the same experiments conducted by those whose works have just been re-examined here, there are several controversial, weak or missing cornerstones in a theory of display for separate instruments which require exploration and erection:

- a. Observed frequency distribution of ocular sampling interval to classify probability distributions of sampling interval for signal reconstruction and monitoring tasks.
- b. Correlations among effective pilot sampling delay, reconstruction compensation and parametric statistics for ocular sampling interval and dwell time.
- c. A valid theory for determinism or randomness in policies for sampling from a multiplicity of displays.
- d. A valid theory for the role of peripheral sampling.

A sequence of experiments is required with ascending multiplicity of tasks to measure changes in effective pilot delay, compensation, and remnant among several tasks competing for attention. One possible topology for a multiplicity of compensatory tasks would build a hierarchy of uncorrelated "critical" tasks as in the sketch following.



Instrument references
 $i_1 \dots i_N$
 (include one aural
 channel such as
 Adcock tone generator)

Disable switches
 (to force dead
 instrument sampling
 and to build hierarchy
 of tasks)

Disturbances
 $d_{M+1} \dots d_N$

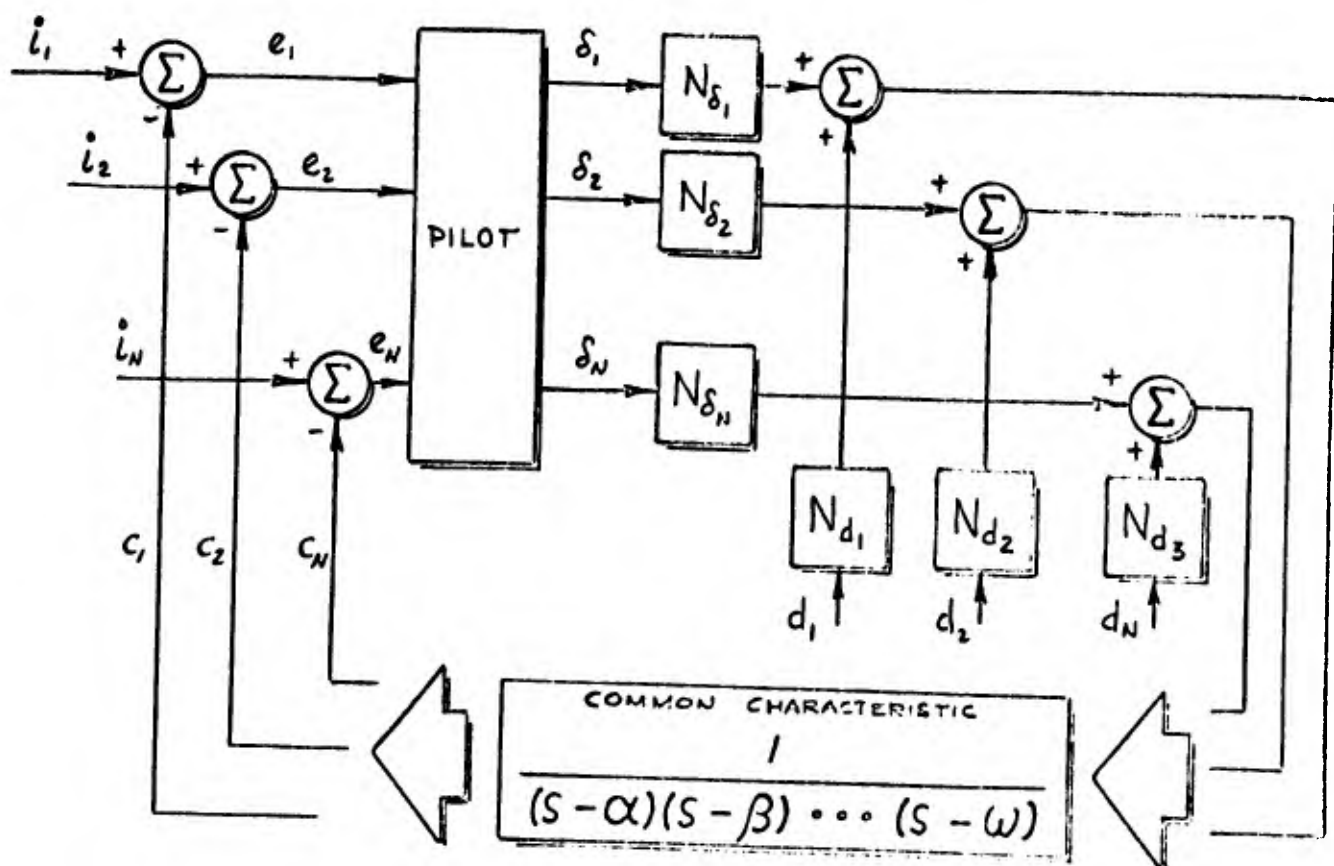
Controlled variables
 $C_1 \dots C_N$

Uncorrelated Multiple-Task Topology

A case with two uncorrelated tasks of matched priority having controlled elements with neutrally-stable first order poles has been studied (Ref. 61), and a case with two uncorrelated tasks of unequal priority having controlled elements with (unequal) unstable first order poles has been studied (Ref. 62). Results in both cases are inconclusive on the question of a relationship between effective pilot delay and ocular fixation statistics.

If each control point be uniquely associated with each unstable element, we should be able to use data already accumulated for a single task as representative of the continuous no-sampling case. Since $\alpha \neq \beta \neq \gamma \neq \dots \neq \omega$, one can give to the "pilot" different numbers and combinations of uncorrelated controlled elements, measure effective pilot delay, and find a sequence of uncorrelated "critical" and subcritical multi-display tasks.

Since instruments are in fact correlated in varying degrees in an actual airplane, a correlated loop structure as in the sketch below may be preferable for a different set of experiments. Attitude, velocity and position



control of a V/STOL approach would provide a multiplicity of partially correlated "critical" tasks.

In either case of task topology it will be preferable to include monitoring tasks as well as control tasks. The V/STOL approach example will provide inherent monitoring tasks.

Some of the present doubt regarding determinism or randomness in multi-display sampling policies may be removed by recording conditional instrument fixation link values as well as observed proportions of time spent on each instrument. Except for Ref. 54, which studied only one pilot subject in five instrument approaches, prior experimenters have not published conditional instrument fixation link values. There is clear evidence of some determinism in the sampling policies of the single subject in Ref. 54 among primary flight control instruments. There is, of course, an implied recognition of determinism in all of the work re-examined herein by the discrimination between instruments which are "monitored" and instruments from which signals are "reconstructed." More detailed subordinate classification of reconstruction sampling policies is desirable.

2. Reconstruction Theory and Dwell Time Measurements

We have alluded to this issue above. The purpose of this set of experiments would be to test at least three distinct reasons for increasing ocular fixation dwell time above a threshold or refractory period:

- (1) extrapolation (prediction or lead)
- (2) smoothing (filtering or lag)
- (3) monitoring for exceedence detection

Frequency distribution measurements of dwell time are desirable to confirm probability distribution(s) for dwell time in each task classification above in frequency domain, reason (1) should reduce phase lag of open loop; (2) should increase phase lag of open loop. Both involve reconstruction, but for different reasons. We should also try to confirm or reject multiple ocular refractory period hypothesis for dwell time.

The uncorrelated multi-task topology of the first sketch above seems preferable. Some ($-\infty < \omega < 0$) stable controlled elements might induce smoothing in the presence of external disturbance(s) and noisy reference inputs for tasks having equality of priority with "critical" tasks. Stable, neutral or unstable elements might also induce secondary exceedence detection tasks.

Dwell time measurements are needed on the same signal for the same task presented on

- (a) moving pointer instrument, circular or linear
- (b) moving scale instrument, circular or linear and
- (c) either integrated with a different signal.

Heading, airspeed and pressure altitude are familiar candidates for this. In (c) the different signal might be lateral deviation, Mach number, and absolute altitude or instantaneous vertical speed, respectively.

An alternative candidate sequence of instruments is provided by the remote attitude director indicator. An inside-to-outside view of roll attitude is always provided by a rotating horizon line. However, pitch attitude is alternatively provided by

- (a) moving pointer
- (b) moving horizon background

and director commands, speed error or vertical deviation error provide different integrated signals (c).

3. Ocular Sampling Interval-Dwell Time - Field of View Interactions for Integrated Displays

This experiment would be addressed to measure fixation field of view as a function of display boundaries in multiple tasks requiring

- (1) signal assimilation and reconstruction for control
- (2) monitoring for exceedence detection
- (3) reading alpha-numerics.

We need to establish bounds and guidelines in organizing a theory for interactions among fixation frequency, fixation dwell time, and fixation

field of view within which peripheral as well as foveal assimilation of signals can occur.

Contiguous multiple-bargraph displays would be candidates for (1) and (2). Contiguous multiple-"silver dollar" trend instruments would be candidates for (2). Integrated Attitude Director Indicator (ADI) and Horizontal Situation Indicator (HSI) or Pictorial Deviation Indicator (PDI) are candidates for (1) and (3).

A display line-synthesizer or raster-synthesizer will offer candidates for (1) within a wide field of view.

Alpha-numeric caution lights are candidates for (3). Since eye camera or electro-oculargraph (EOG) will record only center of fixation, it may be necessary to use higher frame rates than 8/sec or finer EOG potential quantization and to supply critical signal and failure detection tasks in order to obtain field of view boundaries.

BIBLIOGRAPHY

1. Anon., Application Study of a Theory for Manual Control Displays, Systems Technology, Inc., Tech. Proposal 105A, 25 October 1965.
2. Anon., Application of Analytical Techniques to Display Design and Evaluation, Systems Technology, Inc., Tech. Proposal 117, 7 December 1965.
3. Anon., Experiments for a Theory of Manual Control Displays, Systems Technology, Inc., Tech. Proposal 118, 28 January 1966.
4. Adams, J. J., and H. P. Bergeron, "Measured Variations in the Transfer Function of a Human Pilot," NASA Langley, Presented at the AIAA-ASD Vehicle Design and Propulsion Meeting, Dayton, Ohio, November 4-6, 1963.
5. Wezel, F., "Untersuchungen Uber die Willkurbewegung der Menschlichen Hand Mit Getastet Dargebotenen Reizmustern," Thesis, J. W. Goethe Univ., Frankfurt am Main, 1962; Systems Technology, Inc. Tech. Translation No. 3, July 1965.
6. Vossius, G., "Die Vorhersageeigenschaften des Systems der Willkurbewegung," Nenre Ergebnisse der Kybernetik, R. Oldenbourg, Munich, 1964; Systems Technology, Inc., Tech. Translation No. 2, The Prediction Capabilities of the System of Haphazard Motion, July 1965.
7. Bekey, G. A., A Survey of Techniques for the Analysis of Sampled-Data Systems with a Variable Sampling Rate, ASD-TDR-62-35, May 1962.
8. Bekey, G. A., An Investigation of Sampled Data Models of the Human Operator in a Control System, ASD-TDR-62-36, May 1962.
9. Bergen, A. R., The Synthesis of Optimum Random Sampling Systems, TR T-T/133, Electronic Research Labs., Columbia University, 1957.
10. Bergen, A. R., "On the Statistical Design of Linear Random Sampling Schemes," Proc. IFAC, Vol. 1, Moscow, June 1960, pp. 430-436.
11. Bergen, A. R., "Random Linear Systems: A Special Case," AIEE Trans. Part II, Applications and Industry, No. 55, July 1961, pp. 142-145.
12. Bond, C. R., Procedures for Determining Human Operator Information Requirements, GR-1462, Lear Siegler, Inc., July 1964.
13. Carbonell, J. R., "A Queueing Model of Many-Instrument Visual Sampling," Presented at the 7th IEEE Symposium on Human Factors in Electronics, May 5-6, 1966.
14. Chang, S. S. L., "Information Flow Criteria for Feedback Control Systems," Proc. IFAC, Vol. 2, Moscow, 1960, pp. 712-716; Butterworth, 1961.
15. Coffey, T. C., and I. J. Williams, Stability Analysis of Multiloop Multirate Sampled Systems, TDR-669(6540)-3, Aerospace Corporation, 15 October 1965.

16. Cole, E. L., J. L. Milton, and B. B. McIntosh, Routine Maneuvers under Day and Night Conditions, Using an Experimental Panel Arrangement, WADC-TR-53-220, March 1954.
17. Fitts, P. M., R. E. Jones, and J. L. Milton, Eye Fixations of Aircraft Pilots, I. A Review of Prior Eye-Movements Studies and a Description of a Technique for Recording the Frequency, Duration, and Sequences of Eye Fixations during Instrument Flight, AF TR-5837, September 1949.
18. Fitts, P. M., R. E. Jones, and J. L. Milton, Eye Fixations of Aircraft Pilots, III. Frequency, Duration, and Sequence Fixations when Flying Air Force Ground Controlled Approach System (GCA), AMC Technical Report No. 5967, February 1950.
19. Fitts, P. M., R. E. Jones, and J. L. Milton, Eye Fixations of Aircraft Pilots, VI. Frequency, Duration, and Sequence of Fixations during Routine Instrument Flight, AF TR-5975, December 1949.
20. Fitts, P. M., R. E. Jones, and J. L. Milton, "Eye Movements of Aircraft Pilots during Instrument-Landing Approaches," Aeronautical Engineering Review, Vol. 9, No. 2, February 1950, pp. 24-29.
21. Hsieh, H. C., "On the Optimum Synthesis of Random Sampling Multiple Filters with Stationary Inputs," AIEE Trans., Part II, Applications and Industry, November 1961, pp. 239-247.
22. Jex, H. R., and V. J. Kovacevich, Apollo Attitude Control using Pilot-Vehicle System Analysis, Systems Technology, Inc., Tech. Report 236-1, 15 September 1962.
23. Jury, E. I., Sampled-Data Control Systems, John Wiley and Sons, New York, 1958.
24. Jury, E. I., and F. J. Mullin, "The Analysis of Sampled-Data Control Systems with a Periodically Varying Sampling Rate," IRE Trans. on Auto Control, Vol. AC-4, May 1959, pp. 15-20.
25. Jury, E. I., and T. Nishimura, "Analysis of Finite Pulse Systems with a Periodically Varying Sampling Rate and Pulse Width," AIEE Conference Paper 60-866, June 1960.
26. Jury, E. I., "Sampling Schemes in Sampled-Data Control Systems," IRE Trans. on Automatic Control, Vol. AC-6, February 1961.
27. Jury, E. I., Theory and Application of Z-transform Method, John Wiley and Sons, New York, 1964.
28. Kalman, R. E., and J. E. Bertram, "A Unified Approach to the Theory of Sampling Systems," J. Franklin Institute, Vol. 267, May 1959, pp. 405-436.

29. Kalman, R. E., "Control of Randomly-Varying Linear Dynamical Systems," American Mathematical Society Conference on Hydrodynamic Instability, Providence, R. I., 1962, pp. 287-298.
30. Lennox, D., Airline Pilots' Eye Movements during Take-Off and Landing in Visual Meteorological Conditions, Note ARL-HE 15, Australian Defence Scientific Service, August 1963.
31. Leondes, C. T., Modern Control System Theory, McGraw-Hill, New York, 1965.
32. Mackworth, N. H., I. T. Kaplan, and W. Metlay, "Eye Movements during Vigilance," Perceptual and Motor Skills, 1964, 18, pp. 397-402.
33. Magdaleno, R., Sampling Behavior for the Human Operator, Systems Technology, Inc., Tech. Memorandum 115-4, 27 July 1962.
34. Magdaleno, R., Human Operator Average Performance in Single-Loop Tasks, Systems Technology, Inc., Working Paper 134-3, January 1964.
35. Magdaleno, R., and D. T. McRuer, Implications of Remnant Data for Human Operator Models, Systems Technology, Inc., Working Paper 154-2 25 May 1966.
36. Milton, J. L., R. E. Jones, and P. M. Fitts, Eye Fixations of Aircraft Pilots, II. Frequency, Duration, and Sequence of Fixations when Flying the USAF Instrument Low Approach System (ILAS), AF TR-5839, October 1949.
37. Milton, J. L., B. B. McIntosh, E. L. Cole, Eye Fixations of Aircraft Pilots, IV. Fixations during Day and Night ILAS Approaches using an Experimental Instrument Panel Arrangement, AF TR-6570, October 1951.
38. Milton, J. L., and F. J. Wolfe, Fixations during Zero-Reader Approaches in a Jet Aircraft, WADC-TR-52-17, February 1952.
39. Mullin, F. J., and E. I. Jury, "A Note on the Operational Solution of Linear Difference Equations," J. Franklin Institute, Vol. 266, September 1958, pp. 189-205.
40. Murphy, G. J., "On the Exact Analysis of Sampled-Data Feedback Systems with Appreciable Pulse Width," National Electronics Conference, Vol. 17, Chicago, October 1961, pp. 214-221.
41. Nishimura, T., "Operational Analysis of Finite-Pulsed Sampled-Data Systems," IRE Trans. on Automatic Control, Vol. AC-6, No. 3, September 1961, pp. 344-346. Also Electronics Research Laboratory, University of California, Berkeley, Series No. 60, Issue No. 279.

42. Phatak, A. V., and R. E. Magdaleno, The Status of Sampled Data Models as Human Operator Data Descriptors, Systems Technology, Inc., Working Paper 134-4, 5 February 1964.
43. Senders, J. W., 'The Human Operator as a Monitor and Controller of Multi-Degree of Freedom Systems,' Presented at the 4th National Symposium on Human Factors in Electronics, Men, Machines and Systems, Washington, D. C., May 2-3, 1963.
44. Senders, J. W., J. I. Elkind, M. C. Grignetti, and R. Smallwood, An Investigation of the Visual Sampling Behaviour of Human Observers, Report No. 1246, Job No. 11154, Bolt Beranek and Newman, Inc., 10 May 1965.
45. Senders, J. W., and J. L. Ward, "Multiple Criteria for Assessing Tracking Performance," Presented at the 7th IEEE Symposium on Human Factors in Electronics, Washington, D. C., May 5-6, 1966
46. Senders, J. W., "A Re-Analysis of the Pilot Eye-Movement Data," IEEE Trans. on Human Factors in Electronics, Vol. HFE-7, No. 2, June 1966, pp. 103-106.
47. Senders, J. W., "The Estimation of Pilot Workload," AGARD Ad Hoc Panel on Guidance and Control Symposium on "The Human Operator and Aircraft and Missile Control", Paris, September 5-6, 1966.
48. Sheridan, T. B., "Experimental Analysis of Time-Variation of the Human Operator's Transfer Function," Proc. of IFAC, Vol. 2, Moscow, June 1960, pp. 629-635.
49. Sheridan, T. B., "On Precognition and Planning Ahead in Manual Control," Presented at the IEEE 4th National Symposium on Human Factors in Electronics, Washington, D. C., May 2-3, 1963.
50. Stapleford, R. L., Case I - Data Notebook: Jet Transport Landing, Systems Technology, Inc., Working Paper No. 163-1, 15 October 1966.
51. Thomas, E. L., "The Eye Movements of a Pilot during Aircraft Landing," Aerospace Medicine, May 1963, pp. 424-426.
52. Weir, D. H., Compilation and Analysis of Flight Control System Command Inputs, AFFDL-TR-65-119, January 1966.
53. Winblade, R. L., Current Research on Advanced Cockpit Display Systems, AGARD Report No. 491, October 1964.
54. Watts, A. F. A., D.C.Ae., and H. C. Wiltshire, M.Sc., Investigation of Eye Movements of an Aircraft Pilot under Blind Approach Conditions, Note No. 26, The College of Aeronautics, Cranfield, England, May 1955.

55. McRuer, D. T., D. Graham, E. Krendel, and W. Reisener, Human Pilot Dynamics in Compensatory Systems, AFFDL-TR-65-15, July 1965.
56. McRuer, D. T., and D. Graham, Pilot-Vehicle Control System Analysis, Progress in Aeronautics and Astronautics, Vol. 13, Guidance and Control-II, Academic Press, New York, 1964, pp. 603-621.
57. Senders, J. W., "Man's Capacity to Use Information from Complex Display," in Information Theory in Psychology, H. Quastler (ed.), The Free Press, Glencoe, Illinois, 1955.
58. Senders, J. W., Tracking with Intermittently Illuminated Displays, WADC-TR-55-197 (AD 80941), Wright Air Development Center, Ohio, 1955.
59. Senders, J. W., Tracking with Intermittent Stimuli (Forced Sampling), ARDC-TR-56-8; Vol. 51, Air Research and Development Command, Washington, D. C., June 1956.
60. Senders, J. W., "Information Input Rates to Human Users: Recent Research Results," WADC Symposium on Air Force Flight Instrumentation Program, Wright Air Development Center, Ohio, 1958.
61. Elkind, J. F., and W. H. Levison, Results from Studies of Two-Variable Manual Control Systems, Presented at AGARD Symposium on "The Human Operator and Aircraft and Missile Control," Paris, France, 5-6 September 1966.
62. Jex, H. R., Two Applications of the Critical Instability Task to Secondary Work Load Research, Systems Technology, Inc., Tech. Report 155-1, 21 February 1967.
63. Nyquist, H., "Certain Topics in Telegraph Transmission Theory," Trans. of the AIEE, Vol. 47, April 1928, p. 617.
64. Shannon, C. E., "Communication in the Presence of Noise," Proc. of the IFE, Vol. 37:1, January 1949, pp. 10-21.
65. White, W. J., The Effect of Dial Diameter on Ocular Movements, Speed and Accuracy of Check Reading Groups of Simulated Engine Instruments, USAF Technical Report No. 5726, Air Materiel Command, Dayton, Ohio, 1949.
66. Stein, K. J., "Bendix Offers Dual-Model Flight Director — System gives bull's-eye presentation of IIA Approach Gate or conventional flight director display," Aviation Week, 13 March 1967, pp. 81, 82, 84.

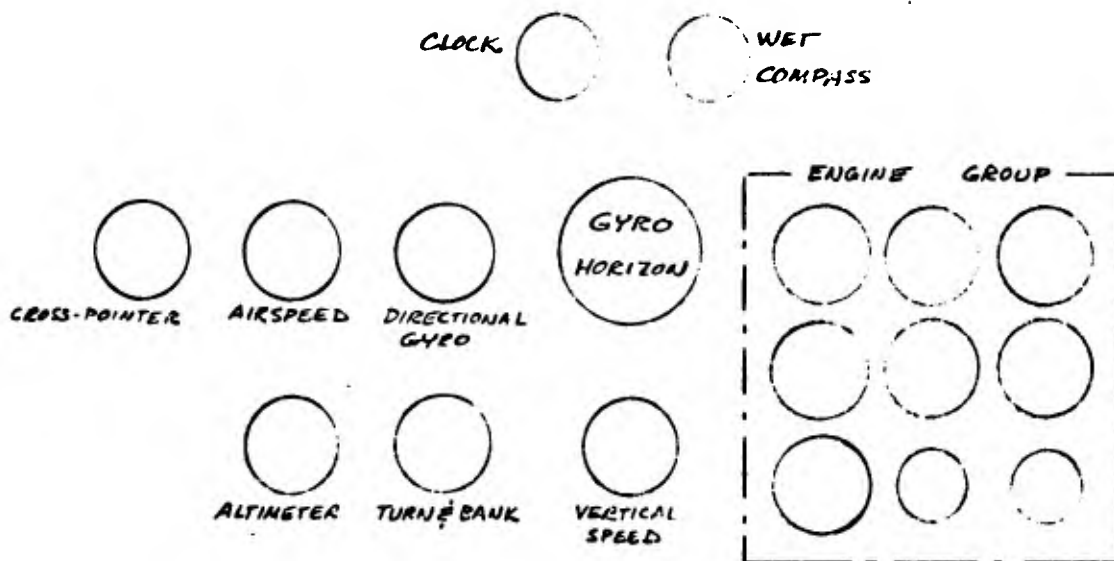


FIGURE 1S STANDARD AIR FORCE INSTRUMENT
ARRANGEMENT USED IN BEECH C-45
BY FITTS, JONES AND MILTON (1949-1950)

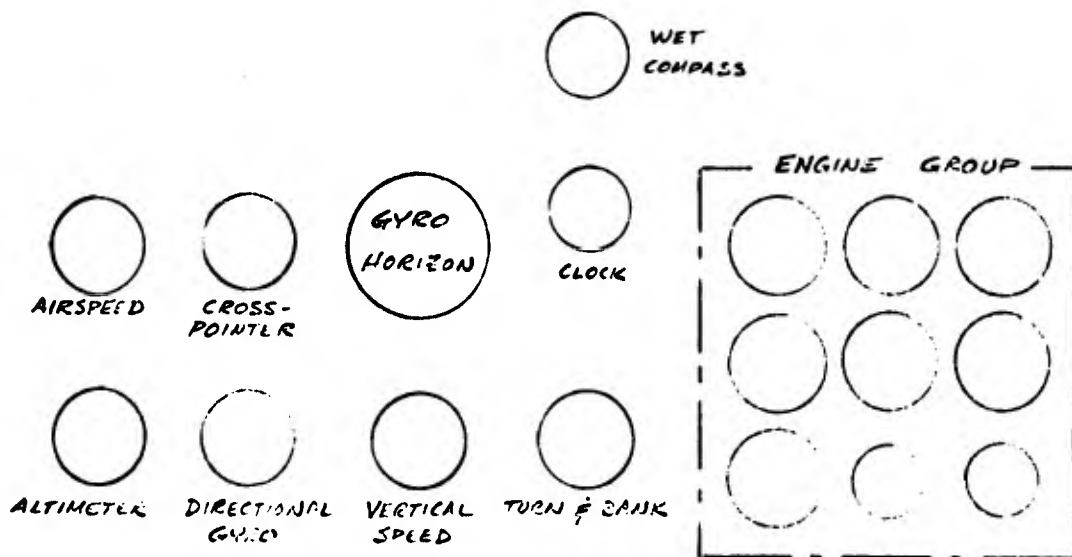


FIGURE 1X EXPERIMENTAL INSTRUMENT ARRANGEMENT
USED IN BEECH C-45 BY MILTON, MCINTOSH
AND COLE (1951-1954)

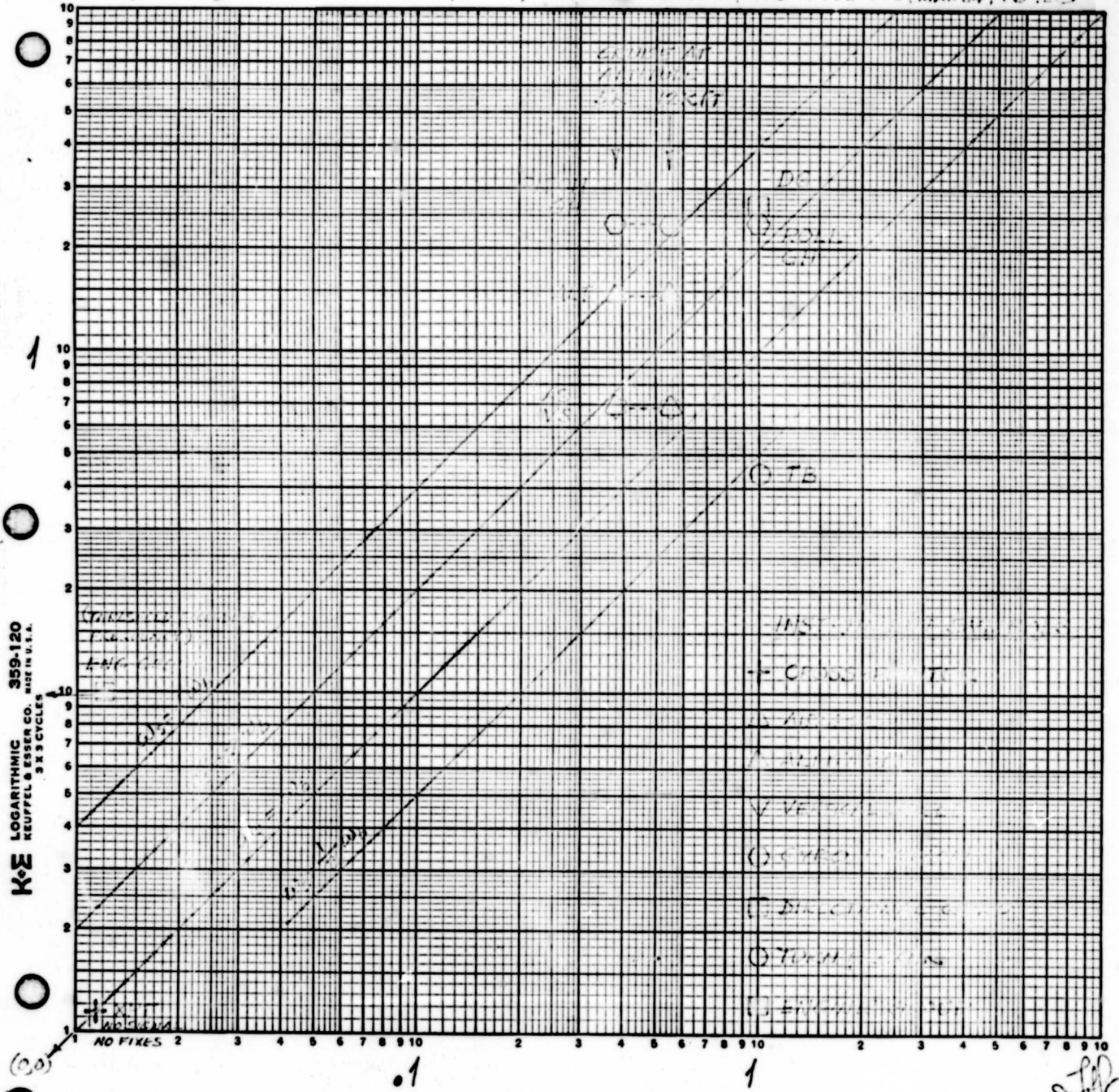
EYE FIXATION FREQUENCY AS A FUNCTION OF DISPLAY-CONTROL LOOP FREQUENCY BANDWIDTH

FIG 2

STRAIGHT & LEVEL IFR C-45 STD AF PANEL

FIXATION
FREQUENCY, ω_s
(RAD/SEC)

REF: MILTON, ET AL., ROUTINE MANEUVERS, WADC TR 55-220, MAR 54, PG 25



K&E LOGARITHMIC KEUFFEL & ESSER CO. MADE IN U.S.A. 359-120 3.5 CYCLES

DISPLAY-CONTROL LOOP CHARACTERISTIC FREQUENCY BANDWIDTH, ω_b , (RAD/SEC)

JPC
22 NOV 66
REV 20 FEB 67

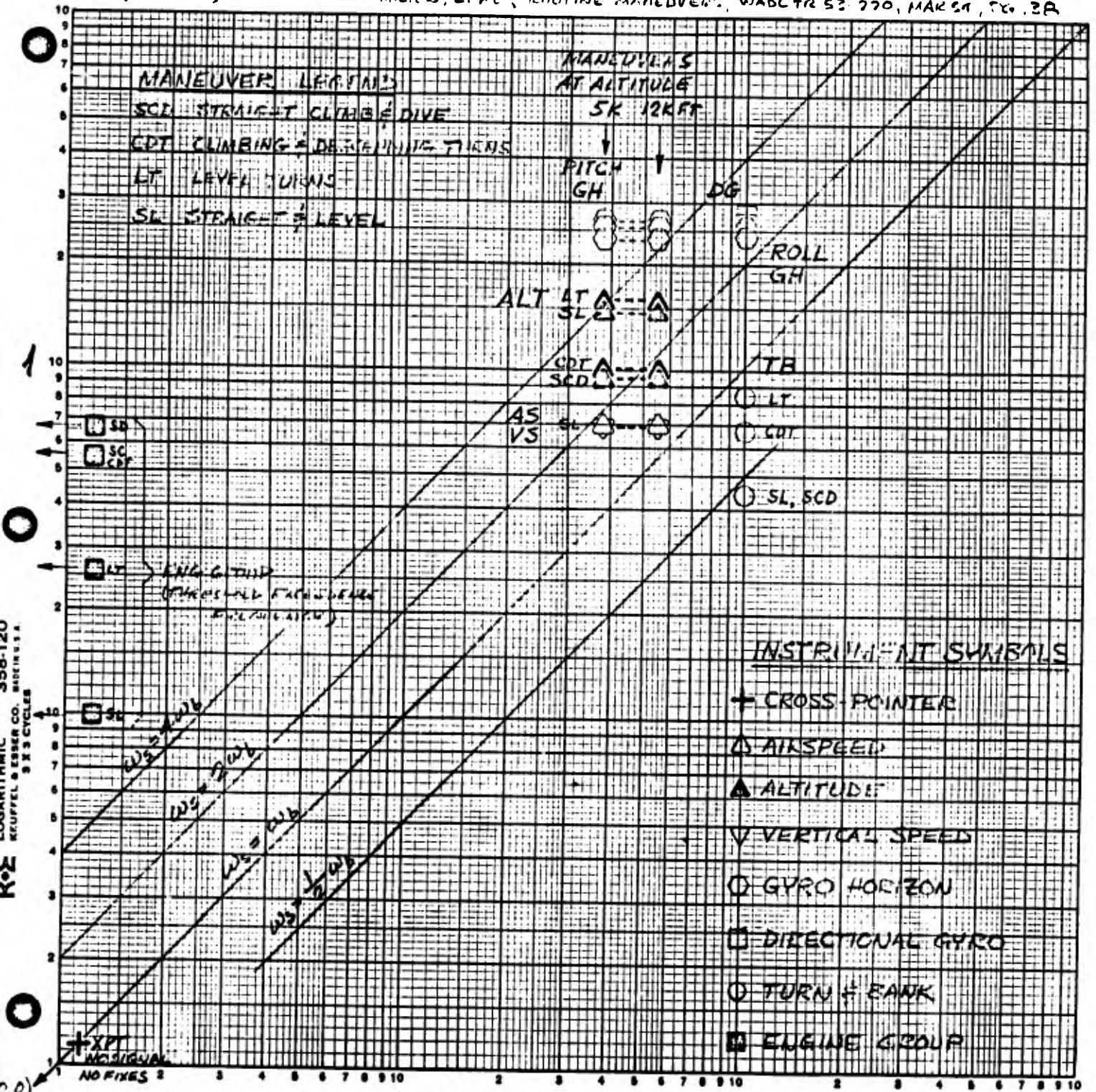
EYE FIXATION FREQUENCY AS A FUNCTION OF DISPLAY-CONTROL LOOP FREQUENCY BANDWIDTH

FIG 3A

ROUTINE IFR C-45 STD AF PANEL

FIXATION FREQUENCY, ω_s (RAD/SEC)

REF: FITTS, ET AL, EYE FIXATIONS..., AF TR 5975, DEC 49, PG 6.
MILTON, ET AL, ROUTINE MANEUVERS, WADC TR 52-770, MAR 51, PG 2A



DISPLAY-CONTROL LOOP CHARACTERISTIC FREQUENCY BANDWIDTH, ω_b (RAD/SEC)

ω_b (RAD/SEC)

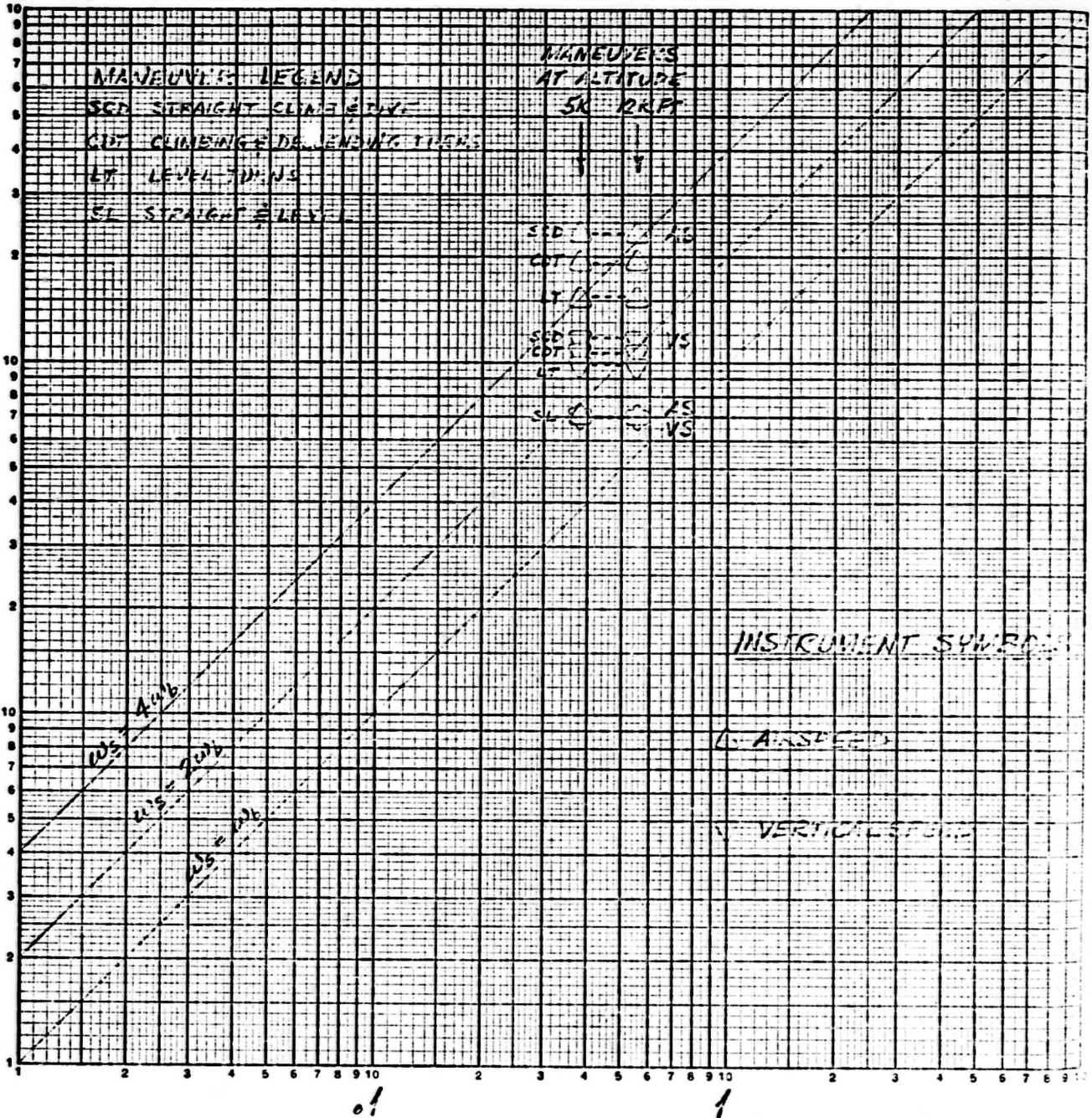
J.C.
2217066
REV 20 FEB 64

EYE FIXATION FREQUENCY AS A FUNCTION OF DISPLAY-CONTROL LOOP FREQUENCY BANDWIDTH

FIG 3B

FIXATION FREQUENCY, ω_s (RAD/SEC) ROUTINE IFR C-45 STD AF PANEL

REF: FITTS, ET AL., EYE FIXATIONS..., AF TR 5975, DEC 49, PG 6.
MILTON, ET AL., ROUTINE MANEUVERS, WADC TR 53-220, MAR 54, PG 23



KE LOGARITHMIC 46 7402
 MADE IN U.S.A.
 KEUFFEL & ESSER CO.

DISPLAY-CONTROL LOOP CHARACTERISTIC FREQUENCY BANDWIDTH,
 ω_b (RADIAN/SECOND)

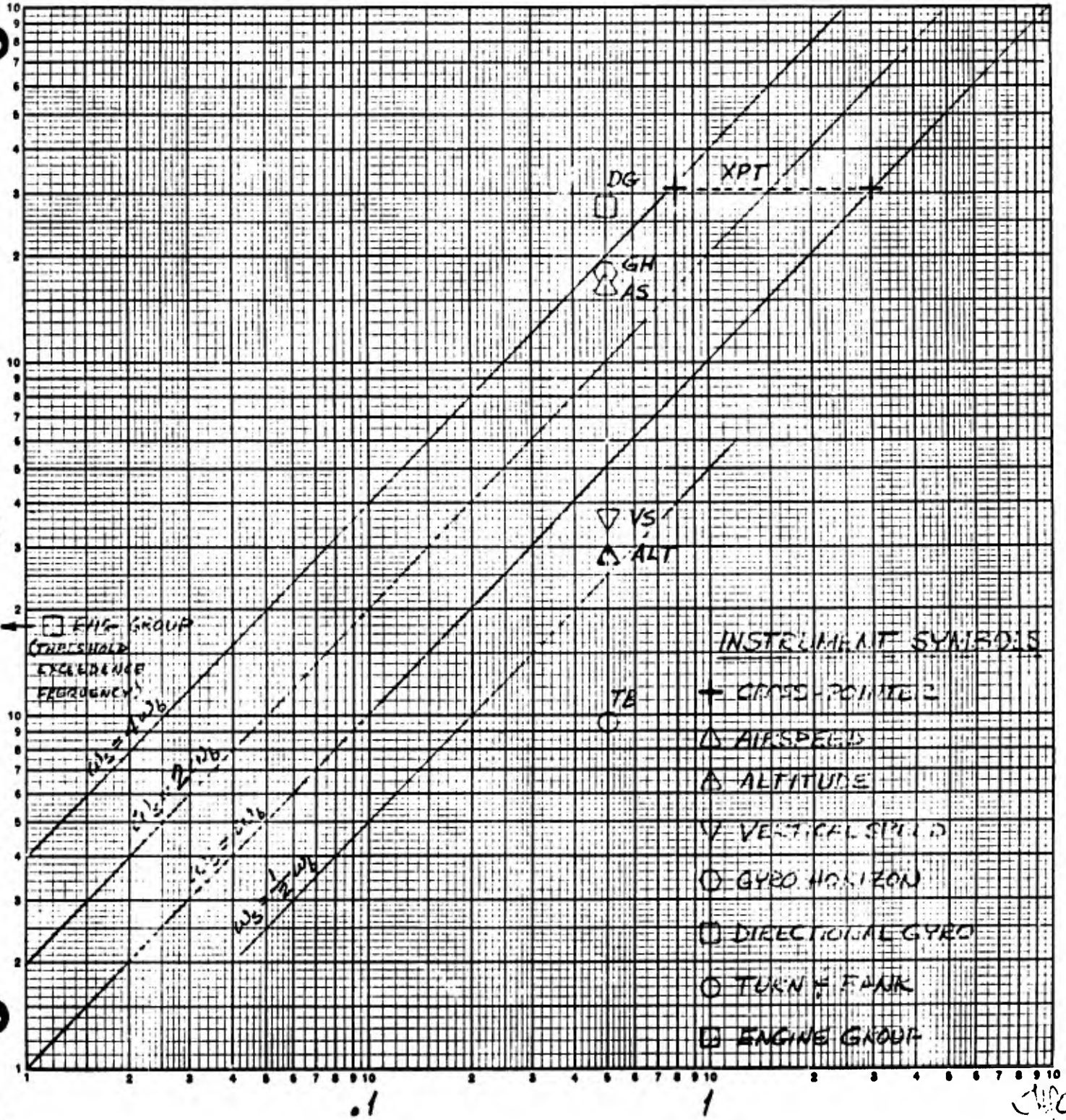
REV 50

EYE FIXATION FREQUENCY AS A FUNCTION OF
DISPLAY-CONTROL LOOP FREQUENCY BANDWIDTH

ILAS C-45 STD AF PANEL

FIXATION
FREQUENCY, ω_s
(RAD/SEC)

REF: FITTS, ET AL, EYE MOVEMENTS..., AEC 9:2, 1949, PG. 27



DISPLAY-CONTROL LOOP CHARACTERISTIC FREQUENCY BANDWIDTH, REV 20 FEB 67

ω_b (RAD/SEC)

JWC
14 OCT 66

KEUFFEL & ESSER CO. MADE IN U.S.A. 3 X 3 CYCLE

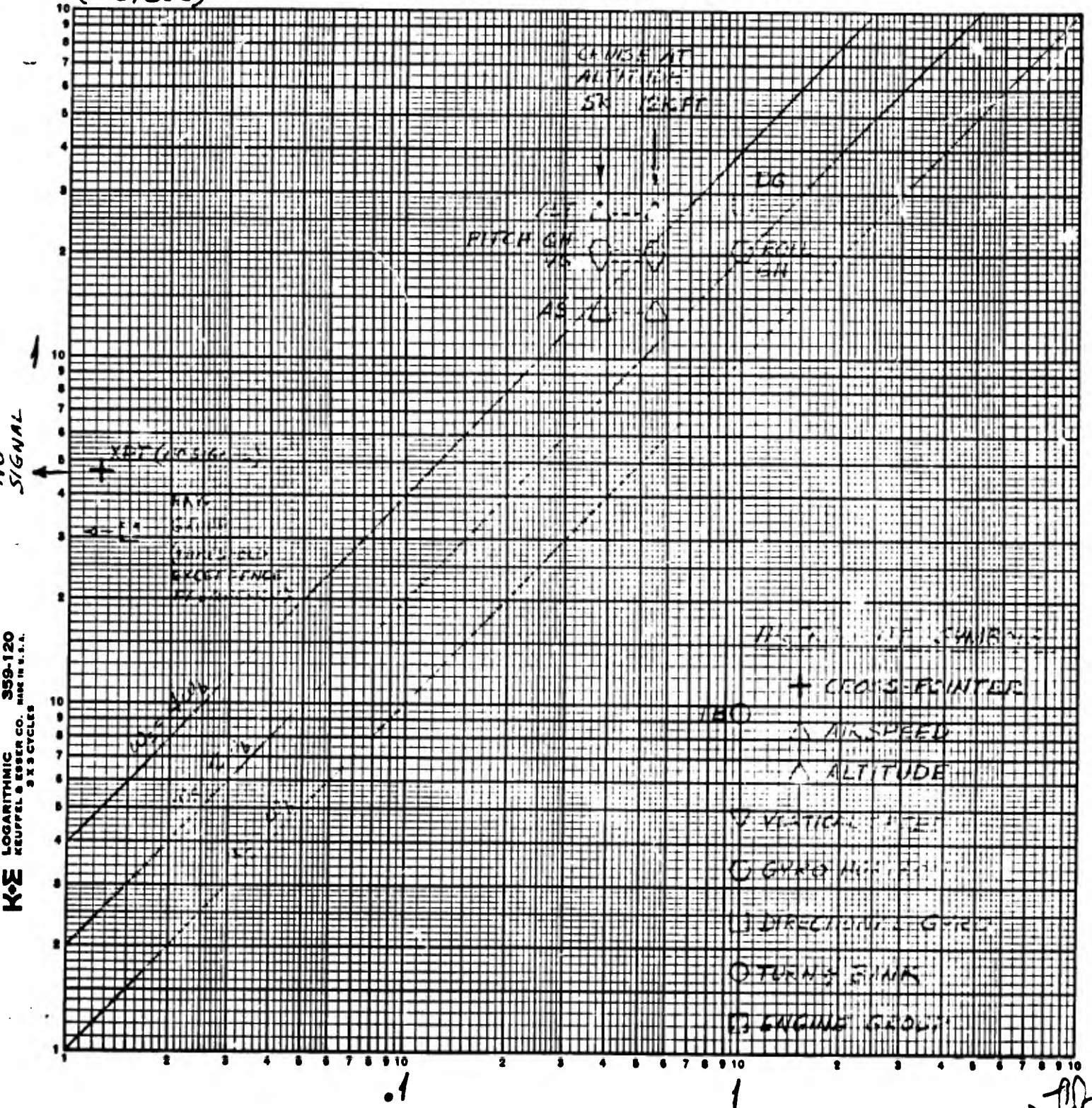
EYE FIXATION FREQUENCY AS A FUNCTION OF DISPLAY-CONTROL LOOP BANDWIDTH FREQUENCY

FIG 5

STRAIGHT & LEVEL IFR C-45 NEW EXPERIMENTAL PANEL

FIXATION FREQUENCY, ω_s (RAD/SEC)

REF: MILTON, ET AL, ROUTINE MANUEVERS...; WADCTR 53-22G, MAR 54, PPS, 22



K&E LOGARITHMIC KEUPEL & ESSER CO. MADE IN U.S.A. 3 1/2 CYCLES

DISPLAY-CONTROL LOOP CHARACTERISTIC FREQUENCY BANDWIDTH, ω_b (RAD/SECOND)

JAC
23 NOV 66
REV 20 FEB 67

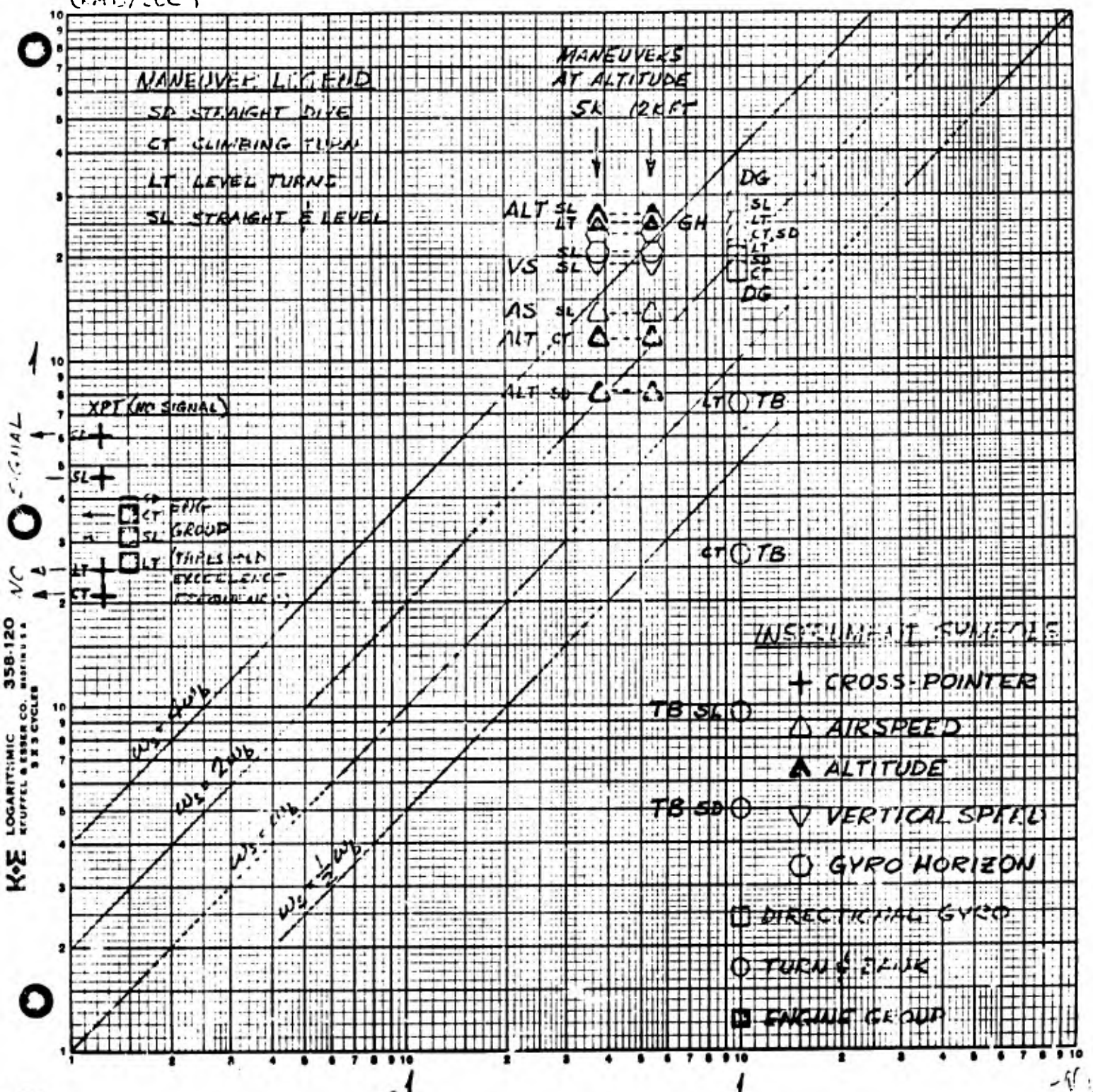
EYE FIXATION FREQUENCY AS A FUNCTION OF DISPLAY-CONTROL LOOP BANDWIDTH FREQUENCY

FIG 6A

ROUTINE IFR C-45 NEW EXPERIMENTAL PANEL

FIXATION FREQUENCY, ω_s (RAD/SEC)

REF: MILTON, ET AL, CONTROL MANEUVERS, WADCTR 53-270, MAR 54, PPS, 22



DISPLAY-CONTROL LOOP CHARACTERISTIC FREQUENCY BANDWIDTH, ω_b (RADIAN/SECOND)

22/10/67
REV 20 FEB 67

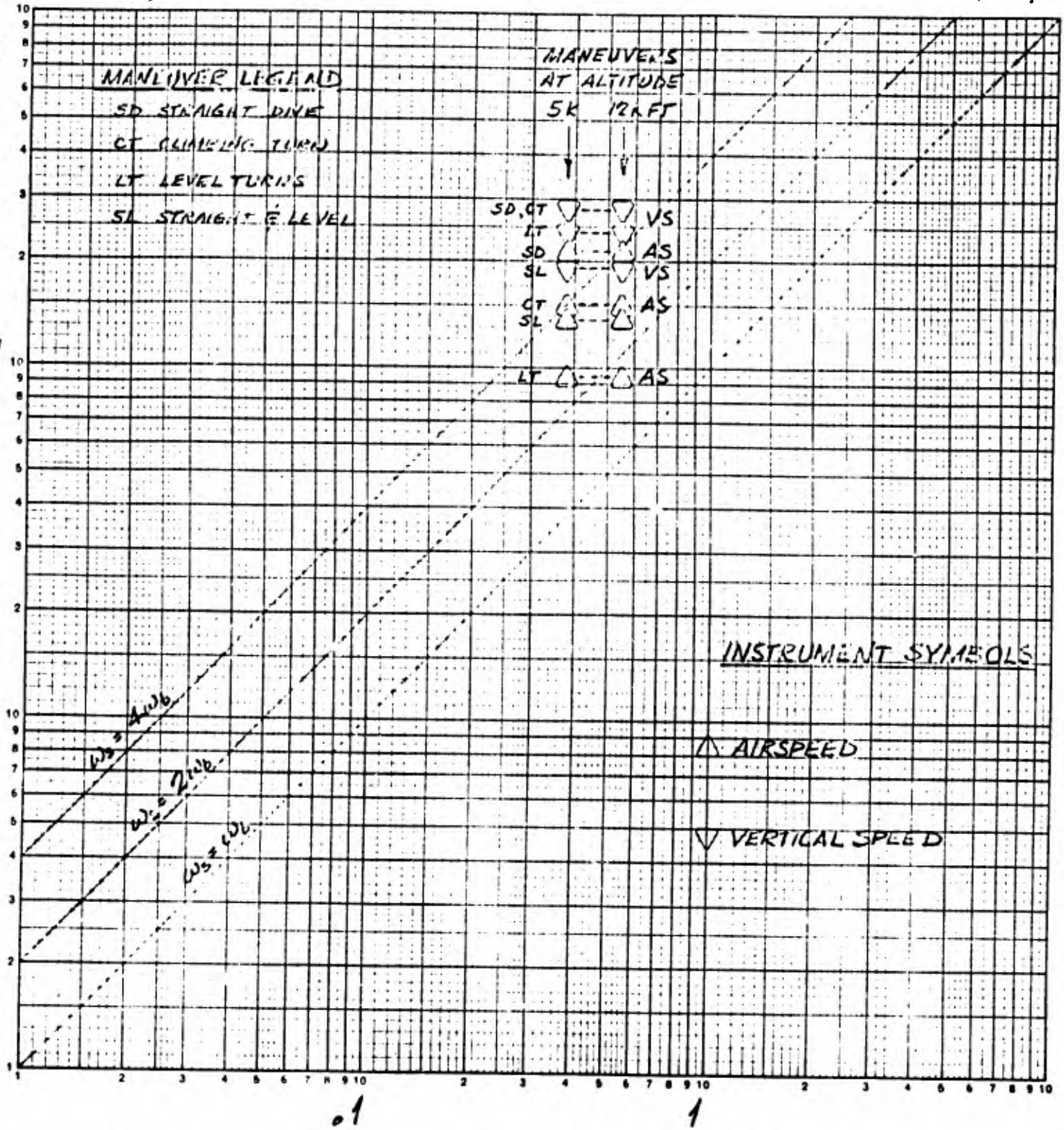
EYE FIXATION FREQUENCY AS A FUNCTION OF DISPLAY-CONTROL LOOP FREQUENCY BANDWIDTH

FIG 6B

FIXATION
FREQUENCY, ω_s
(RAD/SEC)

ROUTINE IFR C-45 NEW EXPERIMENTAL PANEL

REF: MILTON, ET AL, ROUTINE MANEUVERS..., WADCTIC 53-220, MAR '61, PP 5, 22.



DISPLAY-CONTROL LOOP CHARACTERISTIC FREQUENCY BANDWIDTH ω_b ,
 ω_b (RADIANS/SECOND)

REV 20 FEB 67

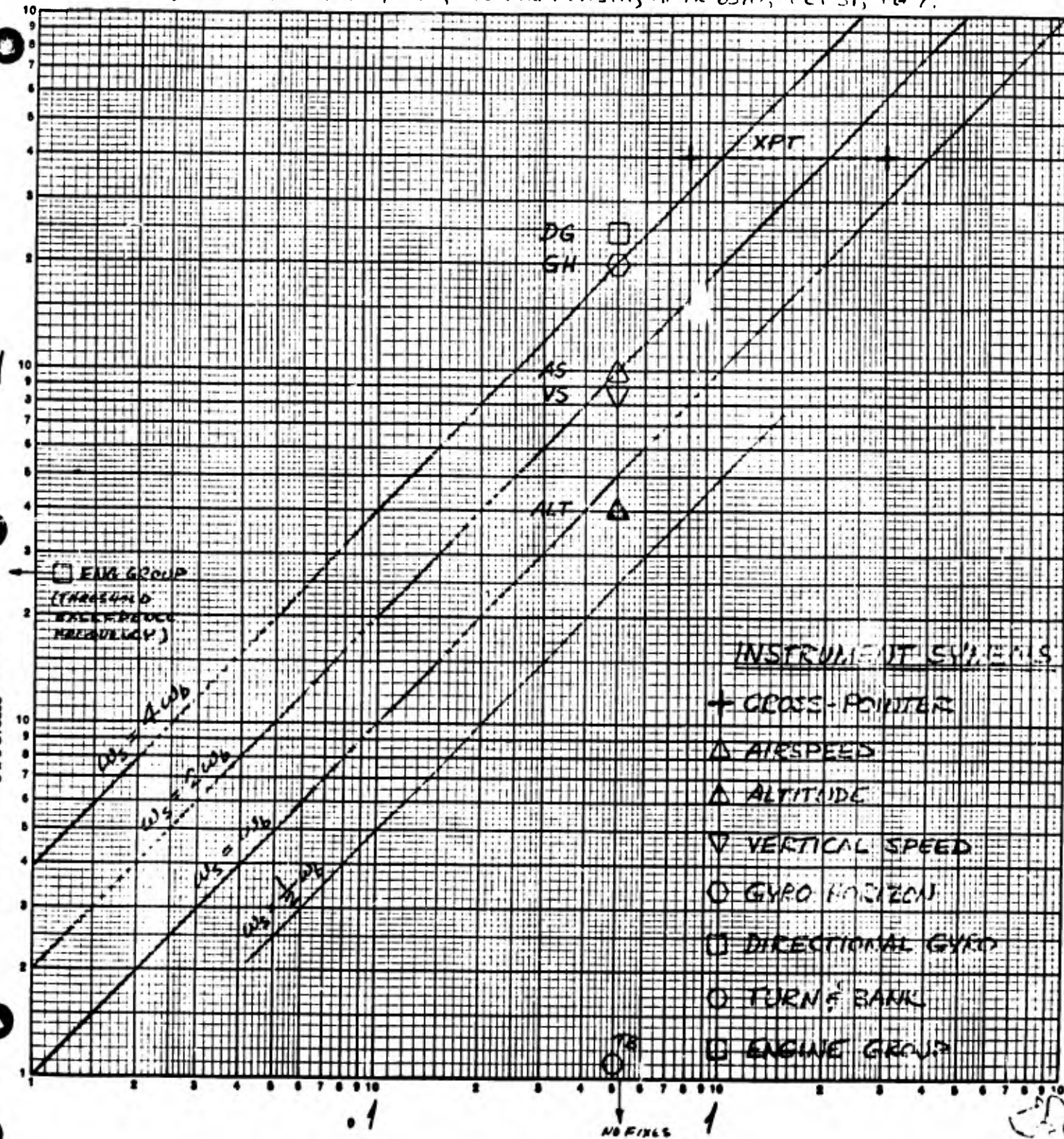
KEUFFEL & ESSER CO.
 46 7402
 LOGARITHMIC
 3 X 3 CYCLES
 MADE IN U.S.A.

EYE FIXATION FREQUENCY AS A FUNCTION OF DISPLAY-CONTROL LOOP BANDWIDTH FREQUENCY

ILAS C-45 NEW EXPERIMENTAL PANEL

FIXATION FREQUENCY, ω_s (RAD/SEC)

REF: MILTON, ET AL, EYE FIXATIONS..., AFTR 6570, OCT 51, PG 7.



K&E LOGARITHMIC 358-120 KEUFFEL & ESSER CO. MADE IN U.S.A. 2 X 3 CYCLES

INSTRUMENT SYSTEMS

- + CROSS-POINTER
- △ AIRSPEED
- ▲ ALTITUDE
- ∇ VERTICAL SPEED
- GYRO HORIZON
- ◻ DIRECTIONAL GYRO
- TURN & BANK
- ◻ ENGINE GROUP

DISPLAY-CONTROL LOOP CHARACTERISTIC FREQUENCY BANDWIDTH, ω_b (RAD/SECOND)

ω_b (RAD/SECOND)

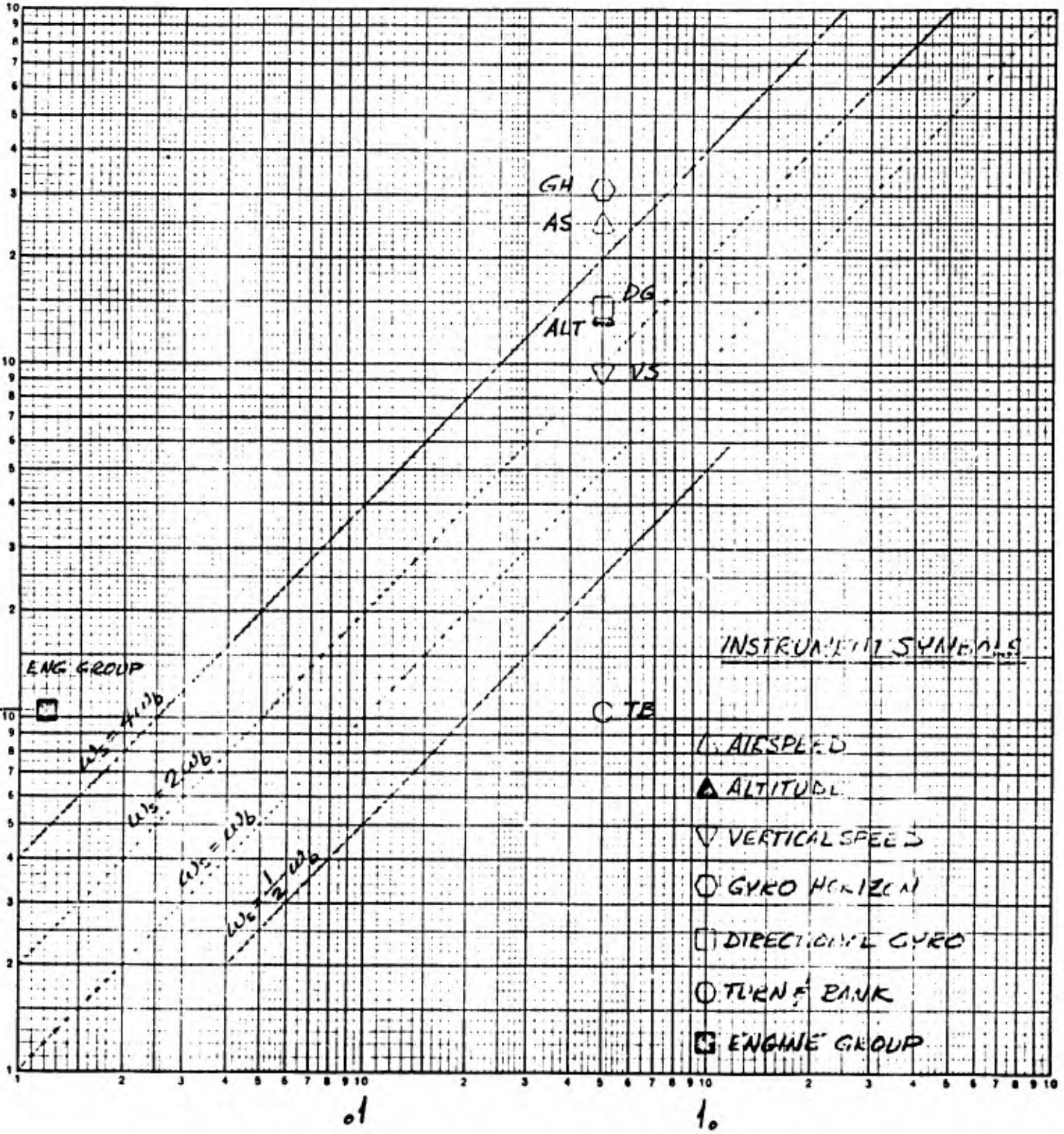
35A0006G REV 20 FEB 67

EYE FIXATION FREQUENCY AS A FUNCTION OF
DISPLAY-CONTROL LOOP FREQUENCY BANDWIDTH

ADCOCK 5RA AVRO 652A "ANSON" MK1 STD RAF PANEL

FIXATION
FREQUENCY, ω_s
(RAD/SEC)

REF: WATTS, ET AL., INVESTIGATION OF EYE MOVEMENTS..., CRAFIELD COA NOTE 26, MAY 55, P. 15.



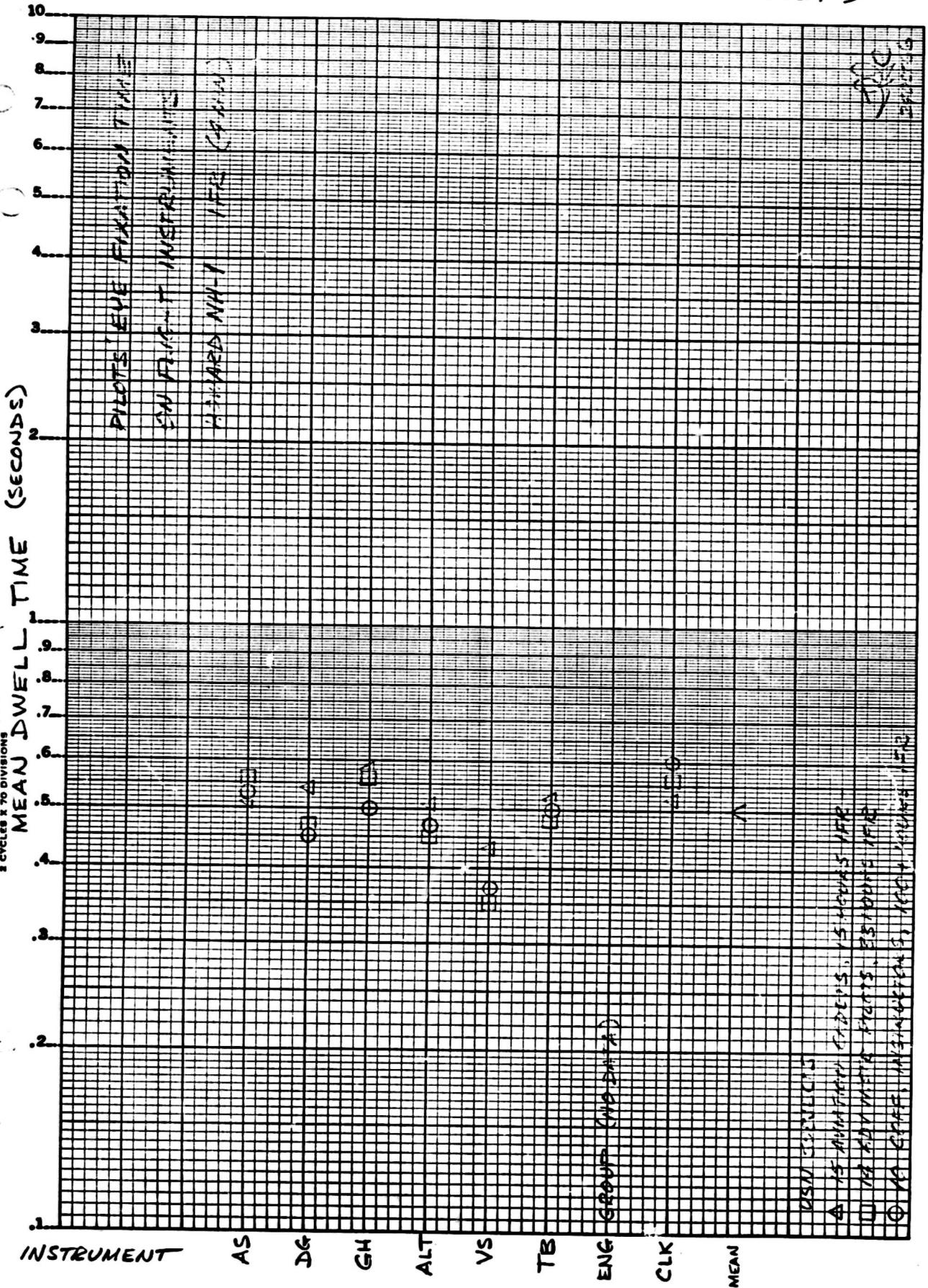
DISPLAY-CONTROL LOOP CHARACTERISTIC FREQUENCY BANDWIDTH,
 ω_b (RAD/SEC)

WTC
20 FEB 67

40 7402
QUARTERMASTER
MADE IN U.S.A.
KEUFFEL & ESSER CO.

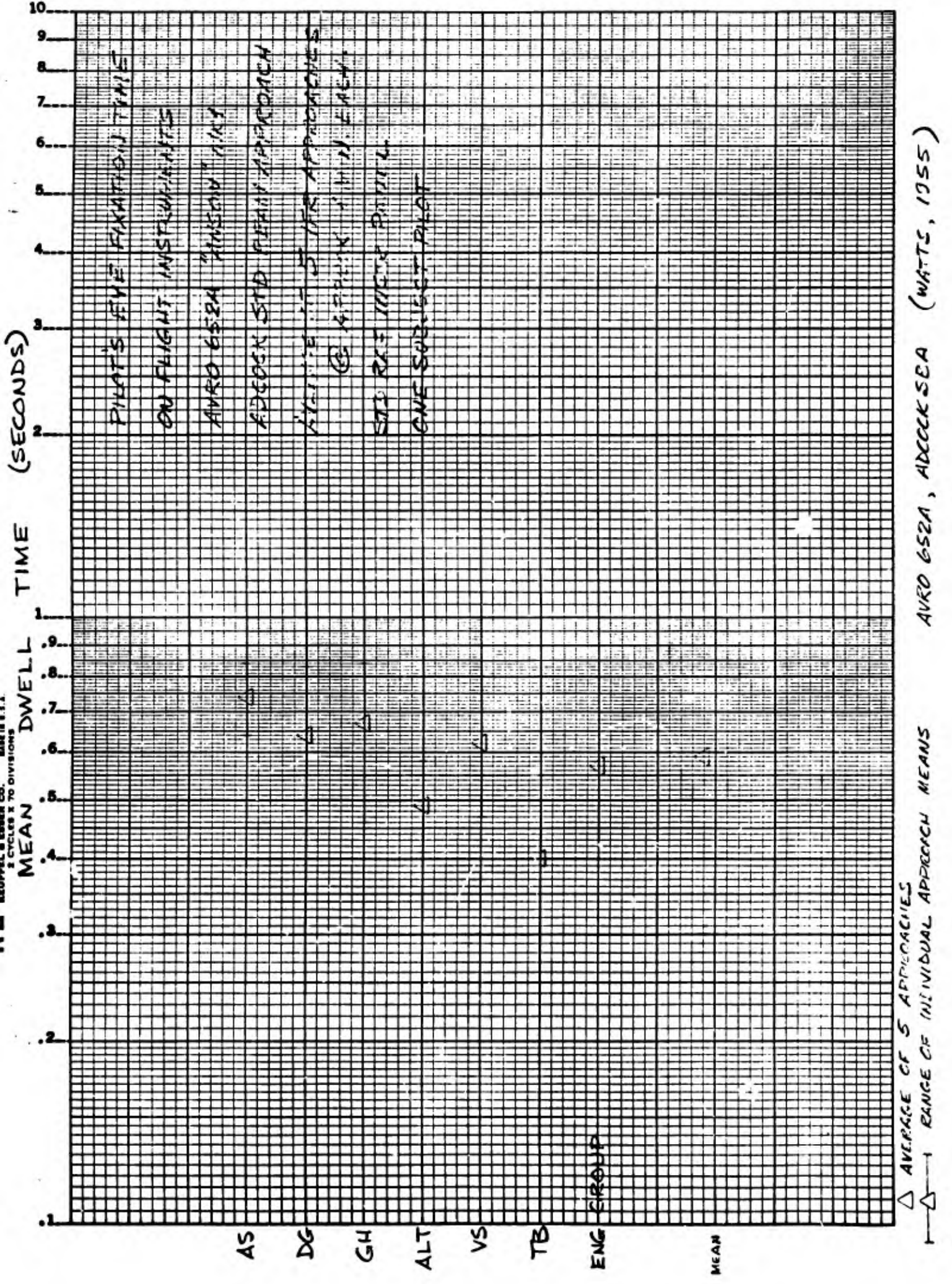
FIG. 9

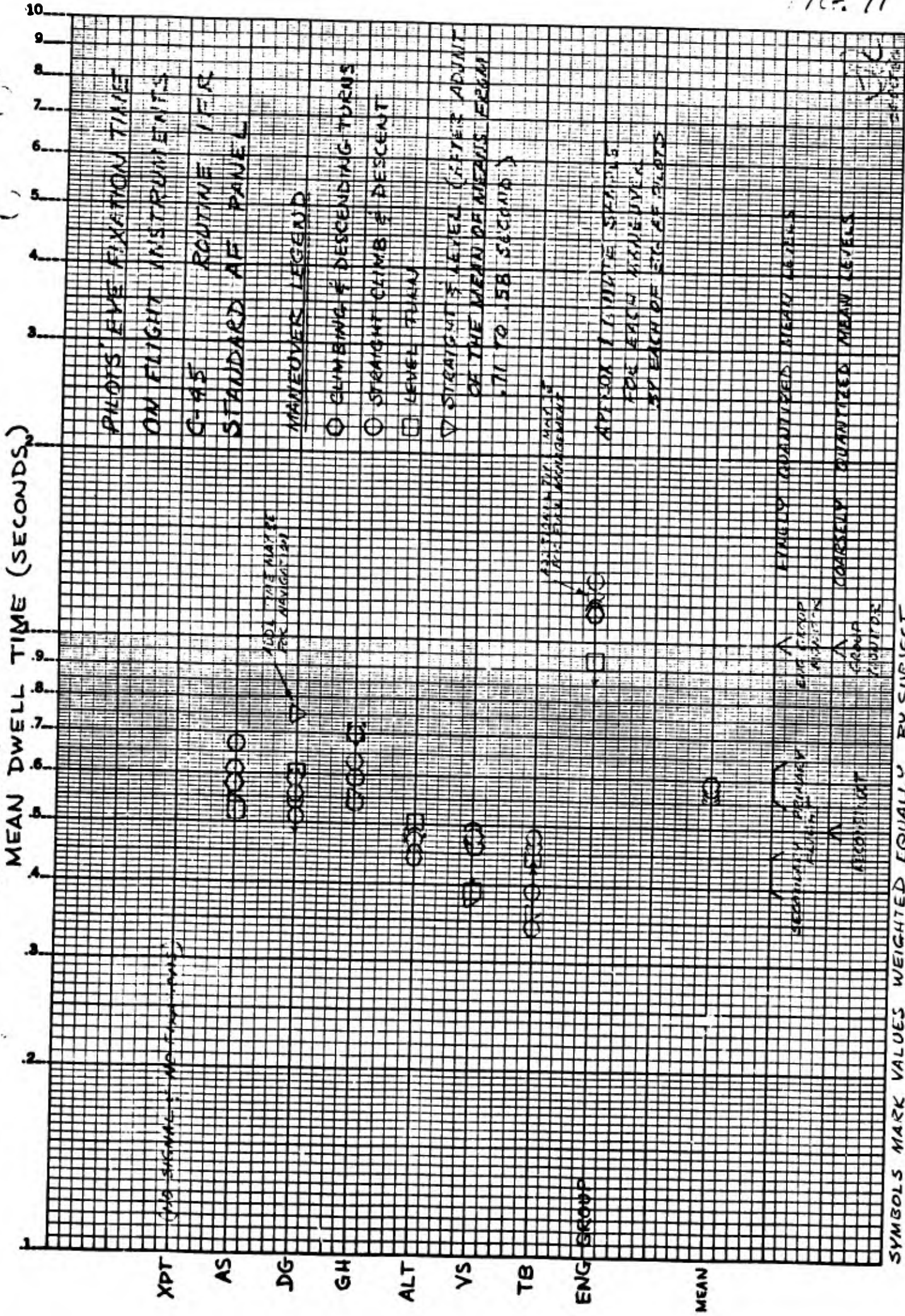
KOE SEMI-LOGARITHMIC 359-61
 KEUFFEL & ESSER CO. MADE IN U.S.A.
 5 CYCLES X 70 DIVISIONS



HOWARD NH-1, IFR (McGEE, 1944)

FIG. 10



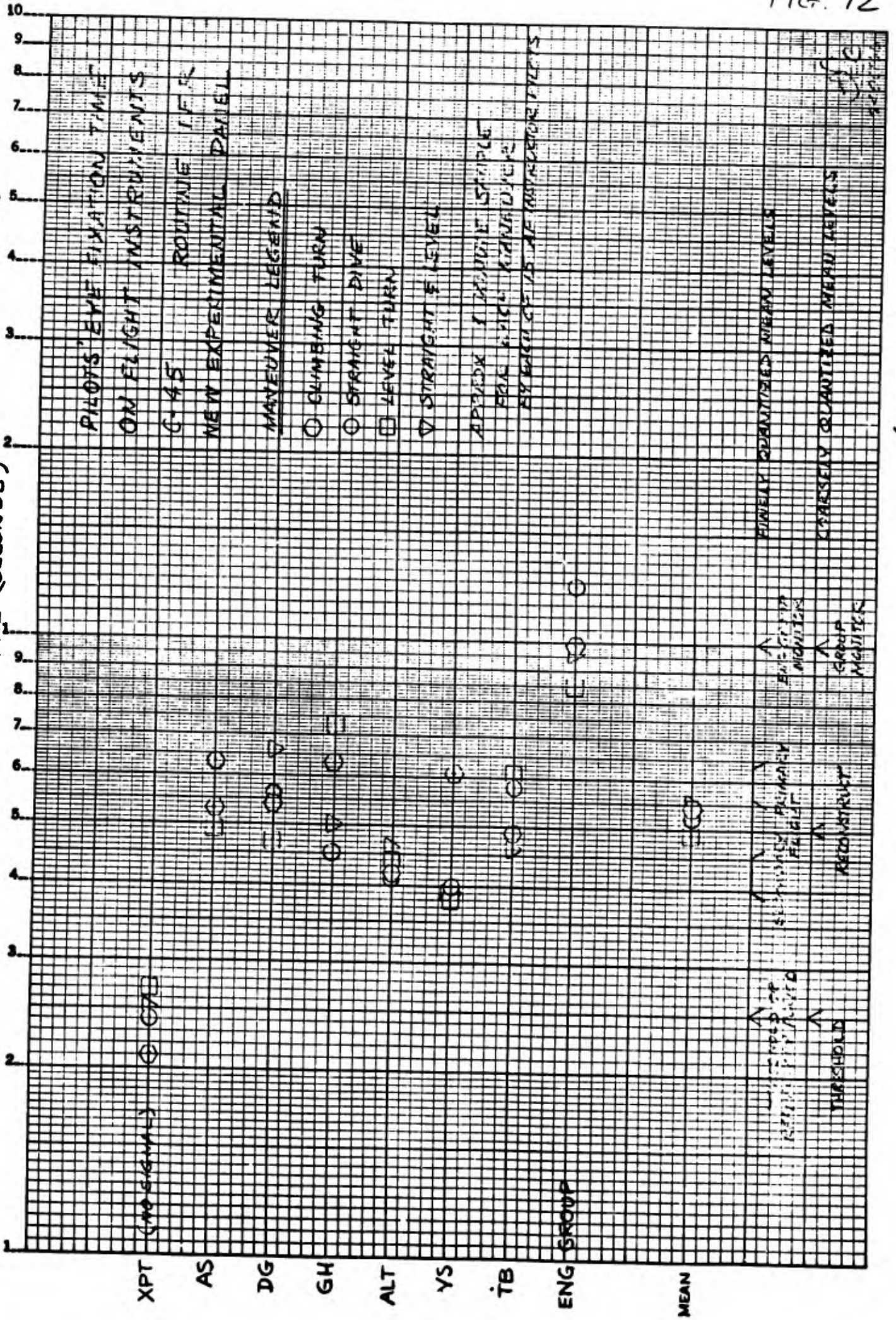


(FITTS, 1949 & MILTON, 1954)

FIG. 12

300-01
 KRUPP & ESSER CO.
 MADE IN U.S.A.
 2 CYCLES X 70 DIVISIONS

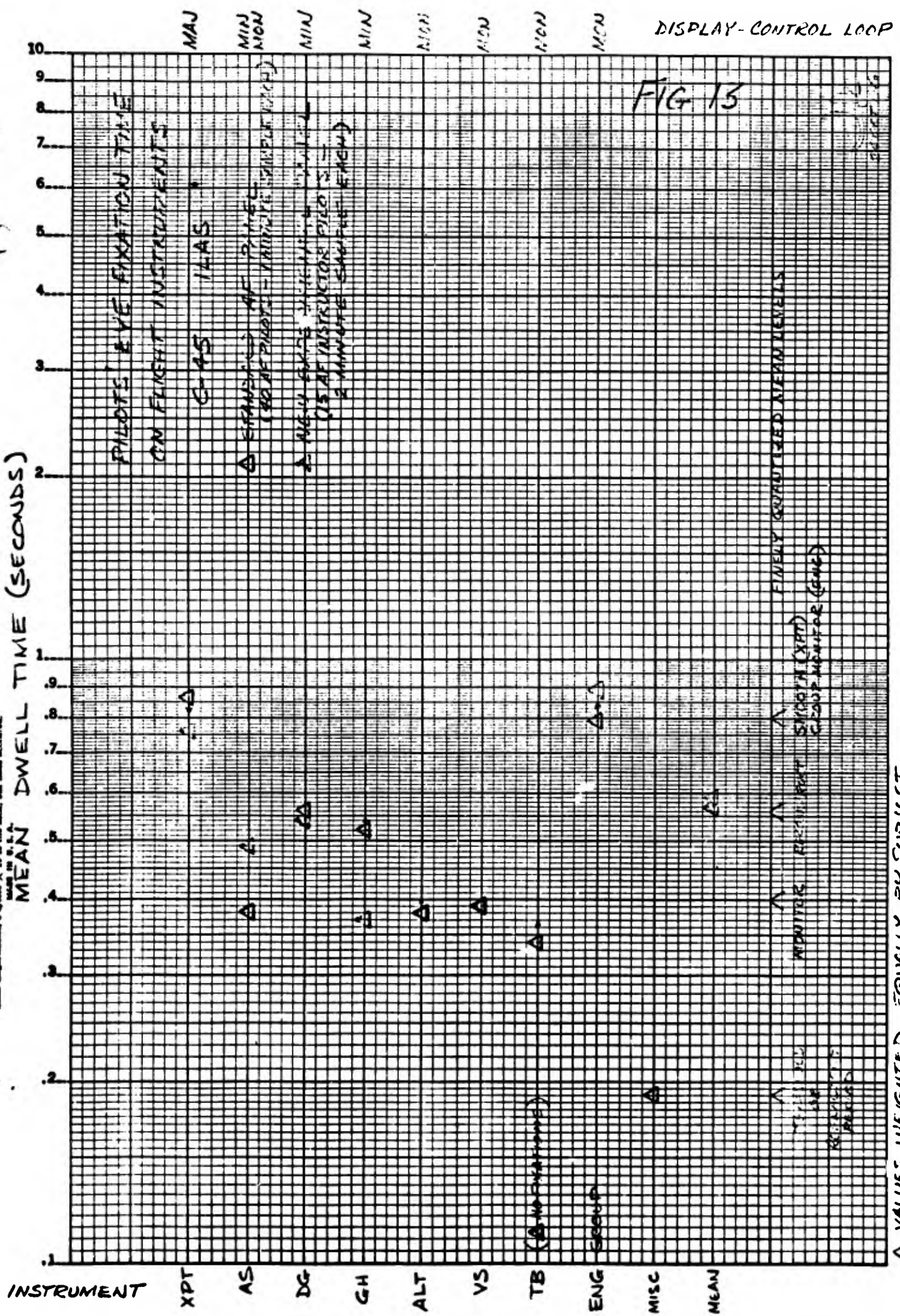
MEAN DWELL TIME (SECONDS)



(MILTON, 1954)

Standard Error of Mean (SEM) = 0.15
 Mean = 1.5
 Standard Deviation (SD) = 0.3

MEAN DWELL TIME (SECONDS)



DISPLAY-CONTROL LOOP

FIG 13

▲ VALUES WEIGHTED EQUALLY BY SUBJECT
 ▲• VALUES WEIGHTED EQUALLY BY FIXATION
 C-45, ILAS (FITZ, 1940 & MILTON, 1951)

EYE MOVEMENT LINK VALUES BETWEEN AIRCRAFT INSTRUMENTS

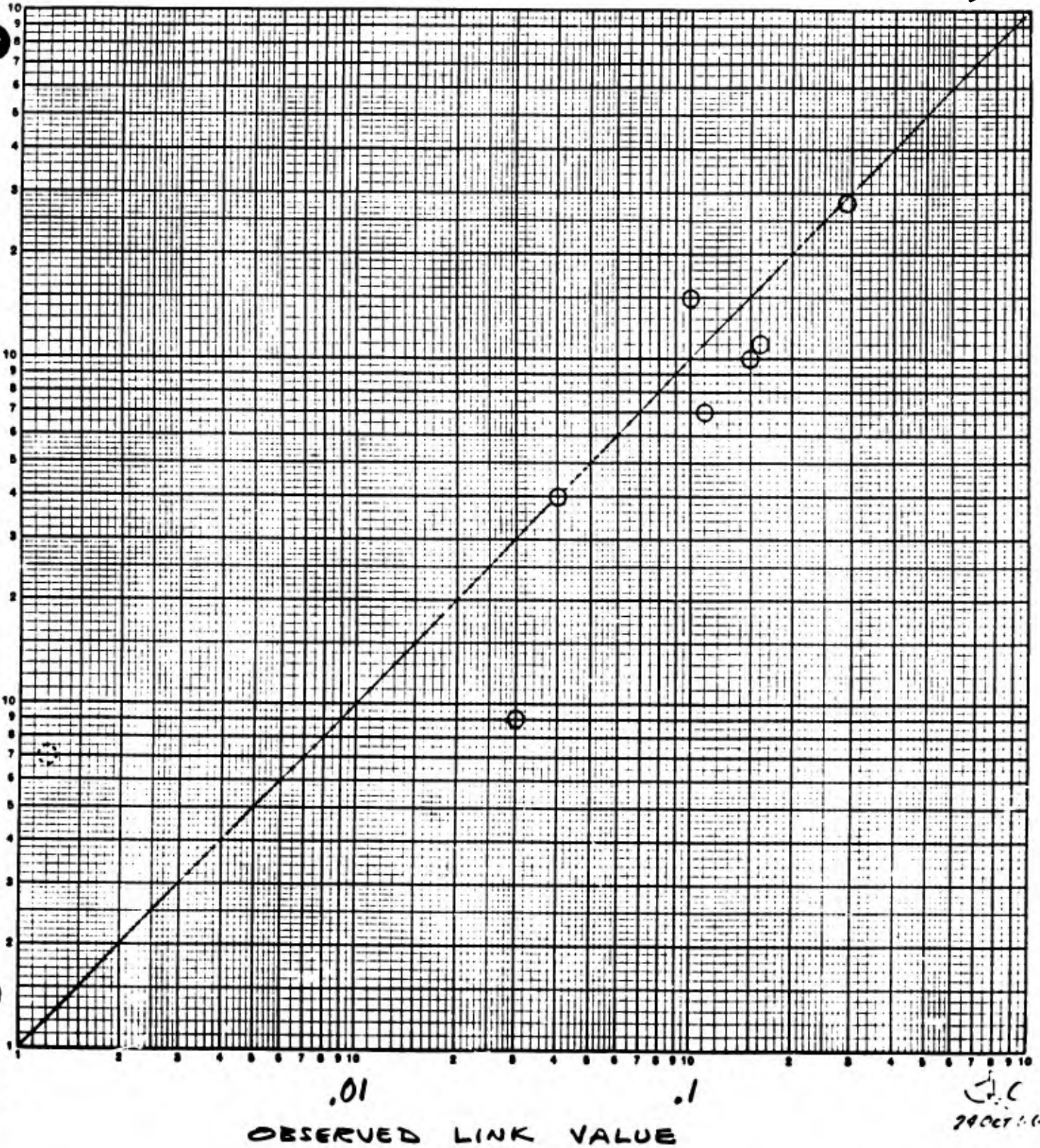
FIG 14

ILAS G-45 STD AF PANEL

CALCULATED

LINK
VALUE

(BY THE METHOD OF SENDERS, A RE-ANALYSIS OF THE PILOT
EYE-MOVEMENT DATA, IEEE TRANS ON HFE, HFE-7:2, JUN 66)



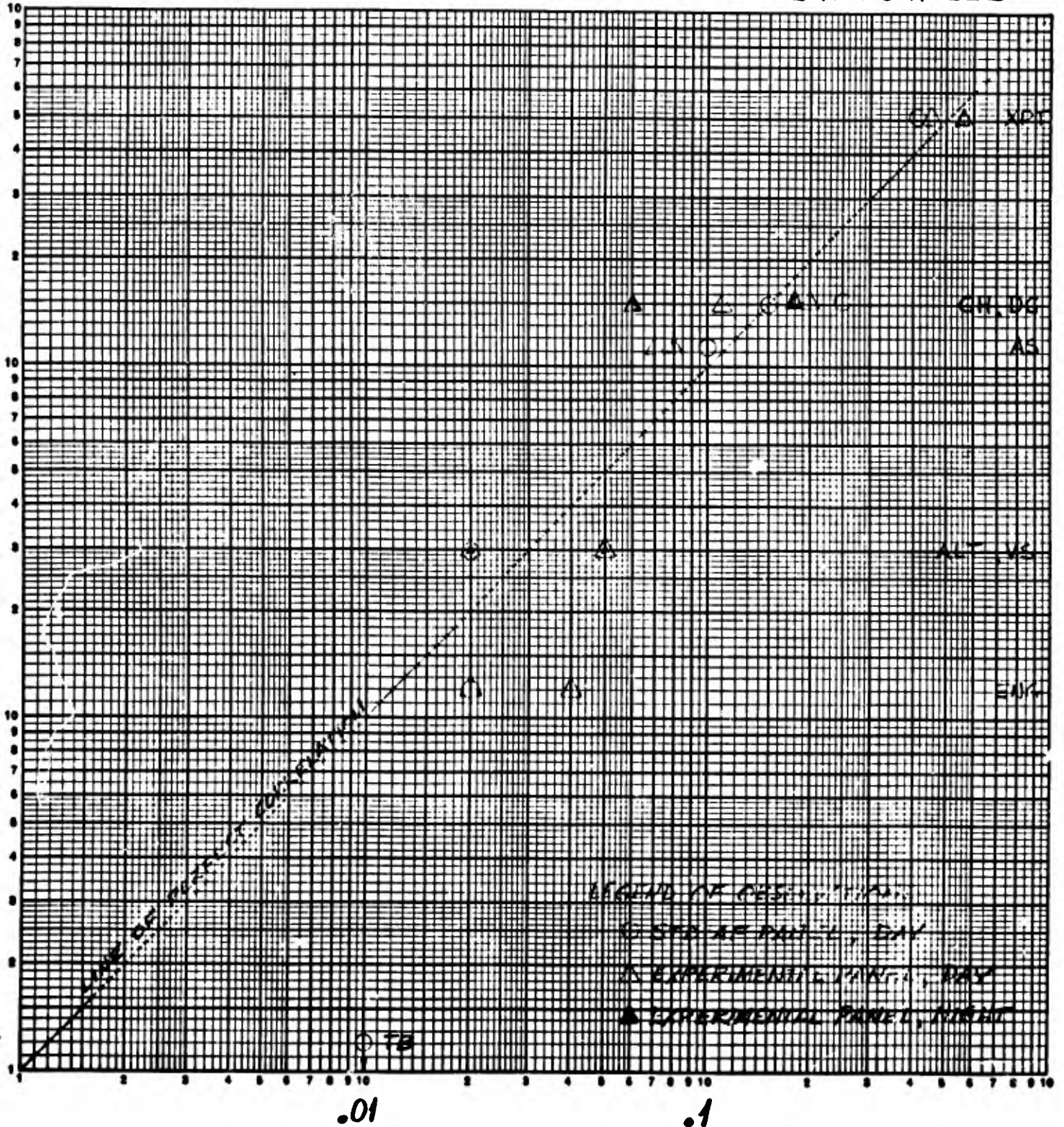
REF: FITTS, JONES & MILTON, EYEMOVEMENTS..., AER 9:2, 1949, PG. 27

CALCULATED PROBABILITIES OF EYE FIXATION
ON EACH AIRCRAFT INSTRUMENT
FOR C-45 INSTRUMENT LOW APPROACH

FIG 15

CALCULATED
PROBABILITY
OF FIXATION

BASED ON PRELIMINARY SCANNING MODEL HYPOTHESES



OBSERVED PROPORTION OF TIME SPENT ON EACH INSTRUMENT

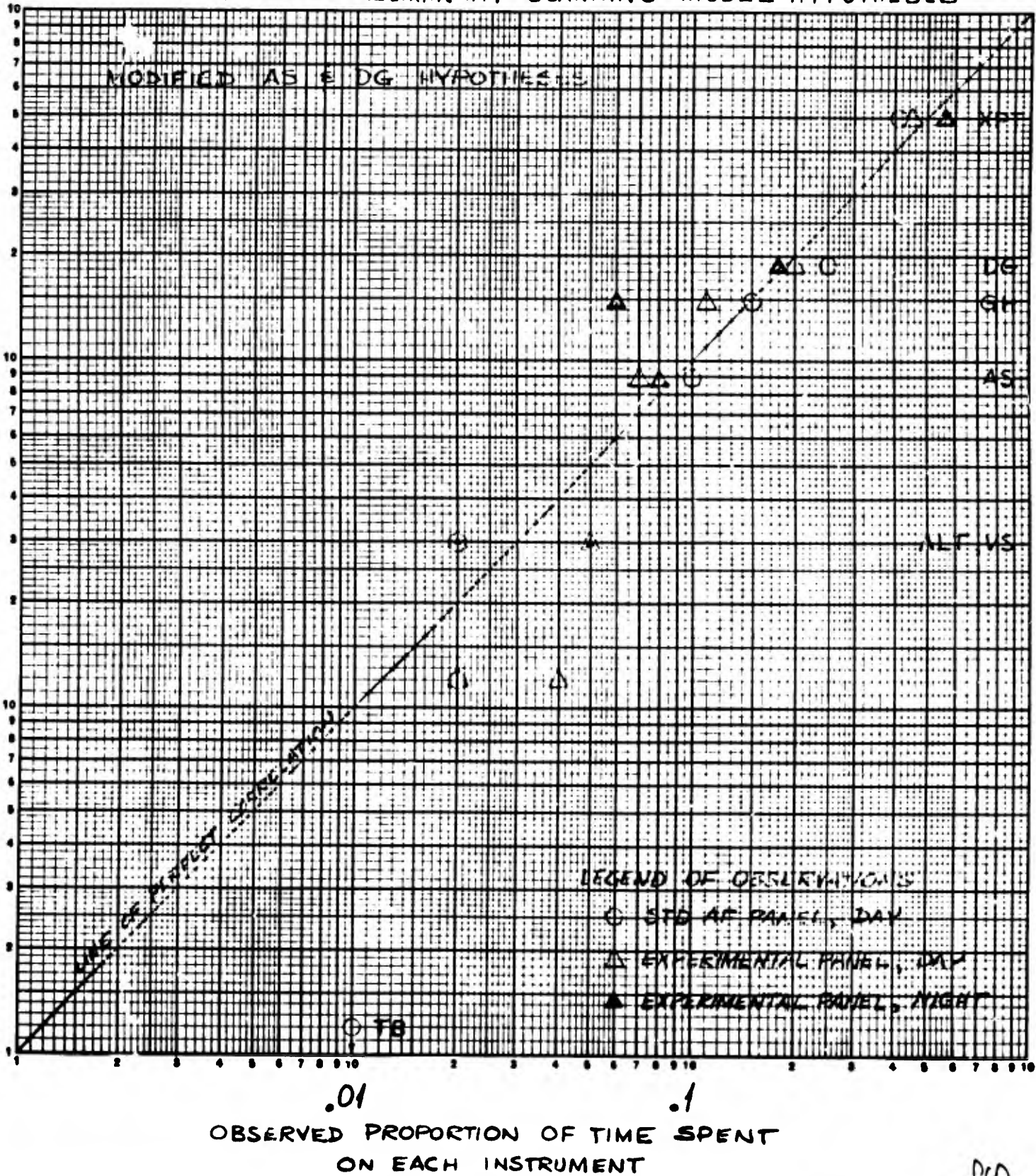
REF.: FITTS, JONES & MILTON, EYE MOVEMENTS..., AER 9:2, 1949, PG. 27
MILTON, JONES & FITTS, EYE FIXATIONS..., II, AFTR 5839, 1949, PG. 9
MILTON, MCINTOSH & COLE, EYE FIXATIONS..., VI, AFTR 6570, 1951, PP. 8, 9

JJC
5 DEC 66
REV 21 FEB 67

CALCULATED PROBABILITIES OF EYE FIXATION
ON EACH AIRCRAFT INSTRUMENT
FOR C-45 INSTRUMENT LOW APPROACH

FIG 16

CALCULATED PROBABILITY OF FIXATION BASED ON PRELIMINARY SCANNING MODEL HYPOTHESES



K&E LOGARITHMIC 46 7403 MADE IN U.S.A. BRUNNEN & EBER CO.

REF.: FITTS, JONES & MILTON, EYE MOVEMENTS..., AER 9:2, 1949, PG.27
MILTON, JONES & FITTS, EYE FIXATIONS..., II, AFTR 5839, 1949, PG.9
MILTON, MCINTOSH & COLE, EYE FIXATIONS..., VI AFTR 6570, 1951, PP. 8,9

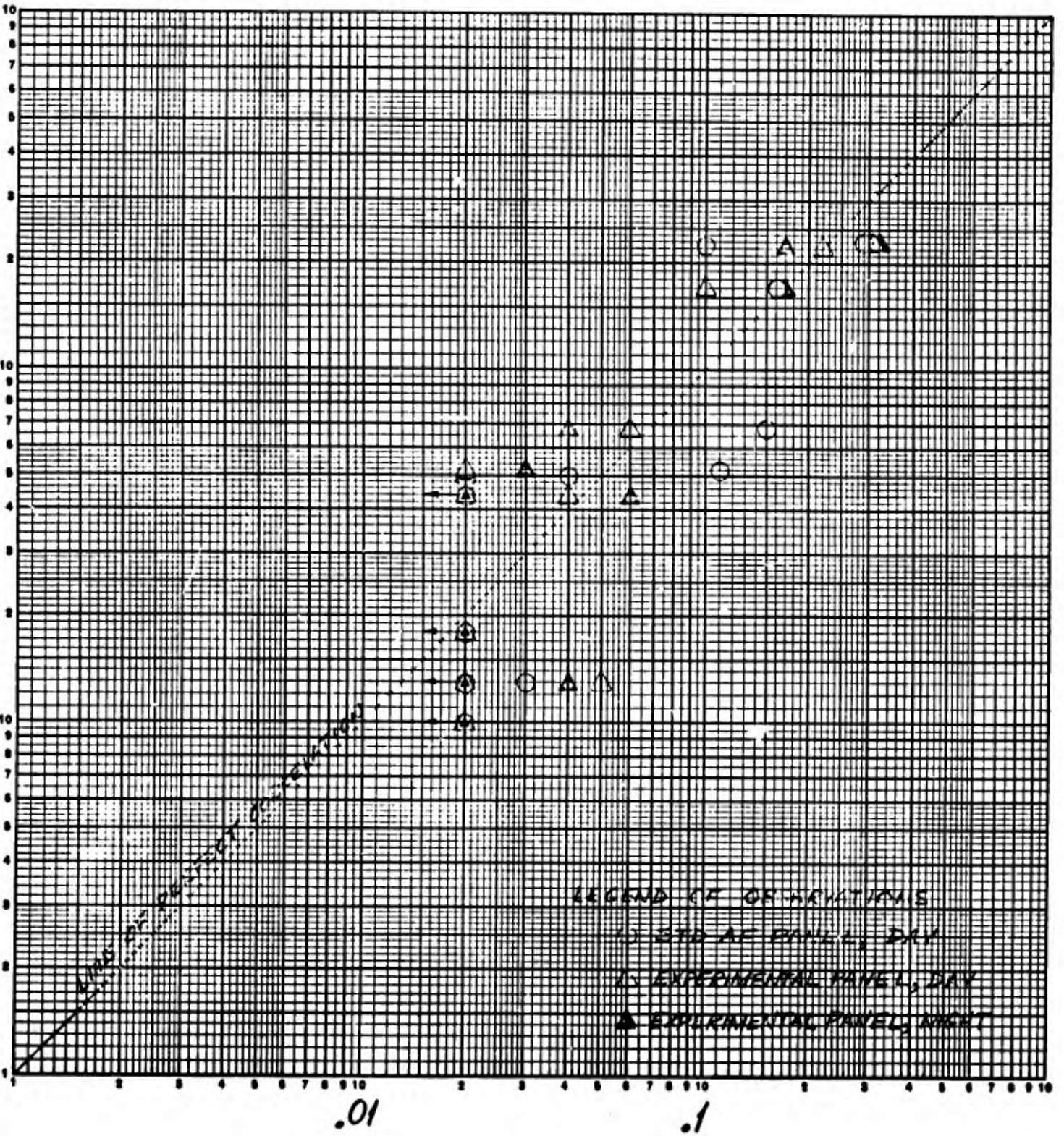
JHC
5 DEC 66
REV 21 FEB 67

FIG 17

CALCULATED EYE MOVEMENT LINK VALUES
BETWEEN AIRCRAFT INSTRUMENTS
FOR C-45 INSTRUMENT LOW APPROACH

CALCULATED LINK VALUE BASED ON PRELIMINARY SCANNING MODEL HYPOTHESES

K&E LOGARITHMIC 359-120
Kruppel & Esser Co. Made in U.S.A.
3 X 3 Cycles



LEGEND OF OBSERVATIONS
 ○ STD. AC PANEL, DAY
 △ EXPERIMENTAL PANEL, DAY
 ▲ EXPERIMENTAL PANEL, NIGHT

OBSERVED LINK VALUE

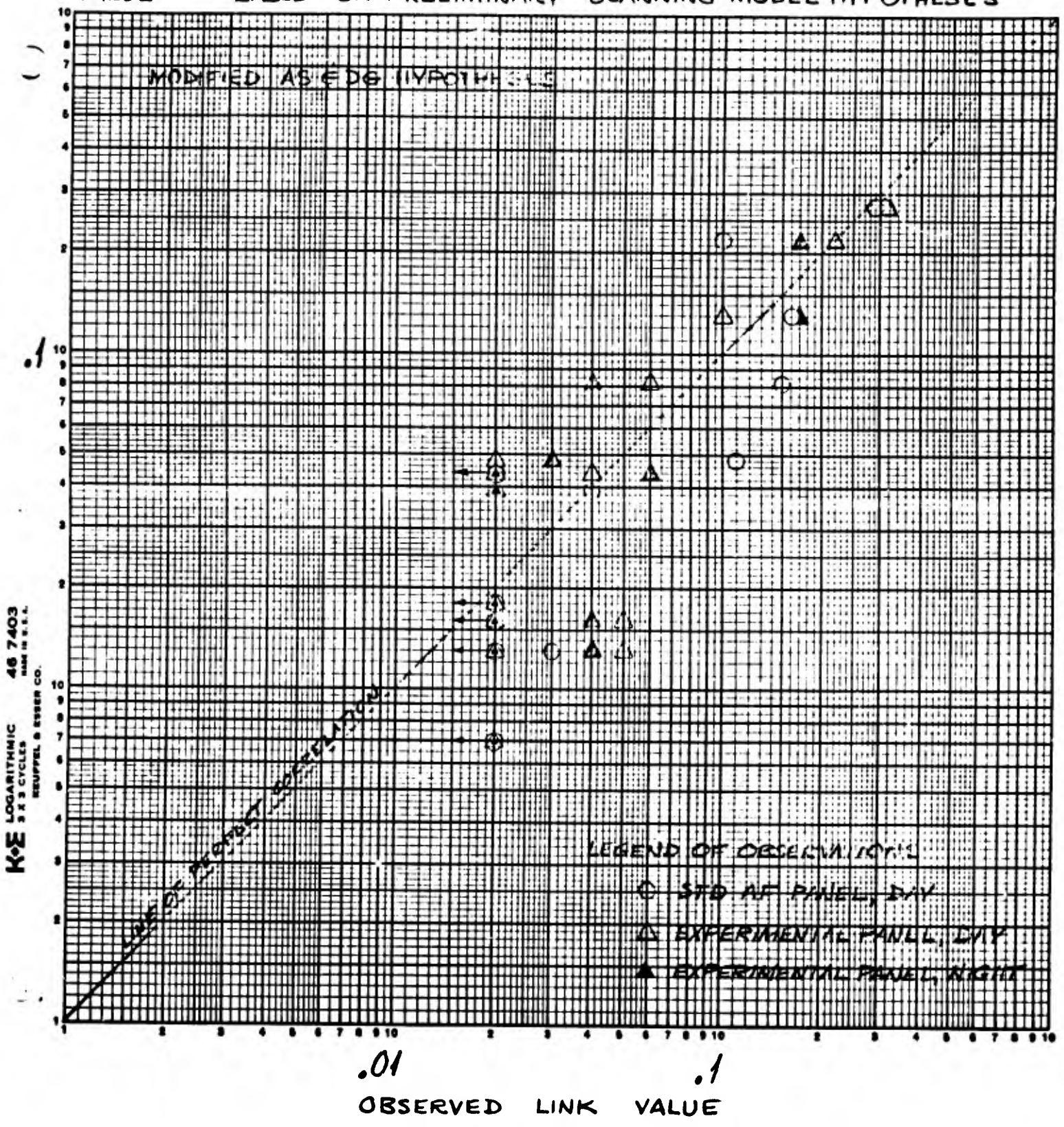
REF.: FITTS, JONES & MILTON, EYE MOVEMENTS..., AER 9:2, 1949, PG. 27
 MILTON, JONES & FITTS, EYE FIXATIONS..., II, AFTR 5839, 1949, PG. 16
 MILTON, MCINTOSH & COLE, EYE FIXATIONS..., VI, AFTR 6570, 1951, PP. 18, 19

JJC
 5 DEC 66
 REV 21 FEB 67

CALCULATED EYE MOVEMENT LINK VALUES
 BETWEEN AIRCRAFT INSTRUMENTS
 FOR C-45 INSTRUMENT LOW APPROACH

FIG 18

() CALCULATED LINK VALUE BASED ON PRELIMINARY SCANNING MODEL HYPOTHESES
 () MODIFIED AS EDG HYPOTHESES



K&E LOGARITHMIC 46 7403 MADE IN U.S.A. REUPPEL & ESSER CO.

REF.: FITTS, JONES & MILTON, EYE MOVEMENTS..., AER 9:2, 1949, PG. 27
 MILTON, JONES & FITTS, EYE FIXATIONS..., II, AF TR 5839, 1949, PG. 16
 MILTON, McINTOSH & COLE, EYE FIXATIONS..., VI, AFTR 6570, 1951, PP. 18, 19

JDC
 5 DEC 66
 REV 21 FEB 67

The arrangement in this figure remains identical to the experimental rearrangement in Fig. 1X employed by Milton, et al., in the second sequence of C-45 pilot eye fixation measurements, 1951-54.

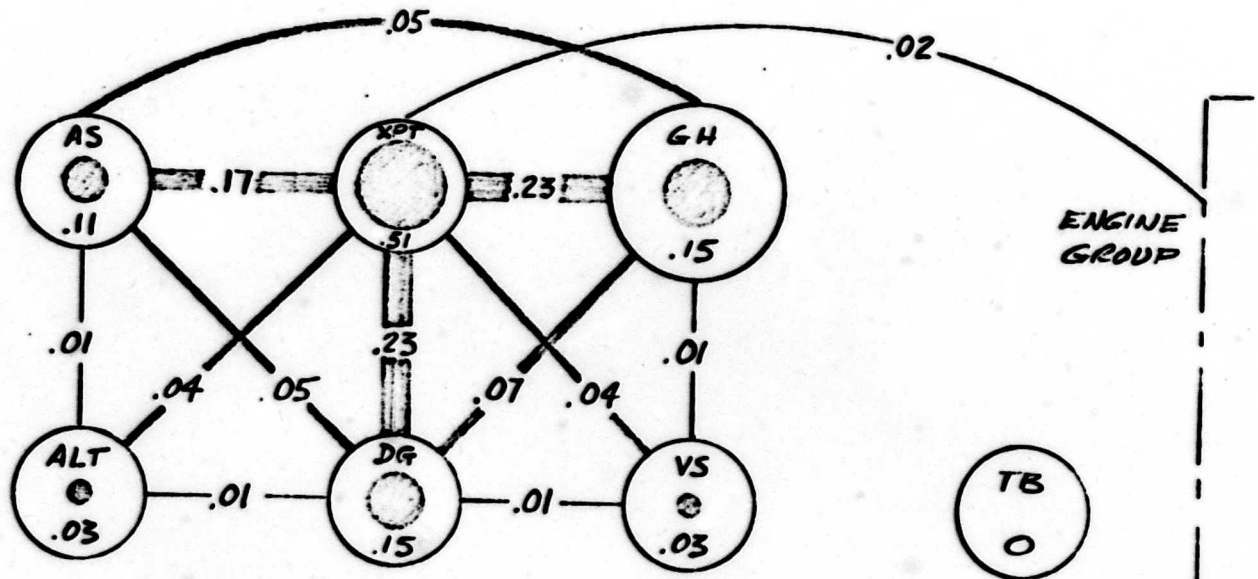


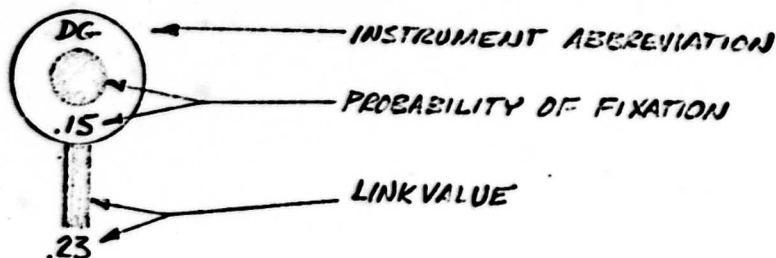
FIGURE 19

C-45 DISPLAY ARRANGEMENT

BASED ON CALCULATED PROBABILITIES OF FIXATION
AND LINK VALUES IN APPENDIX C

FOR INSTRUMENT LOW APPROACH

LEGEND:



APPENDIX A

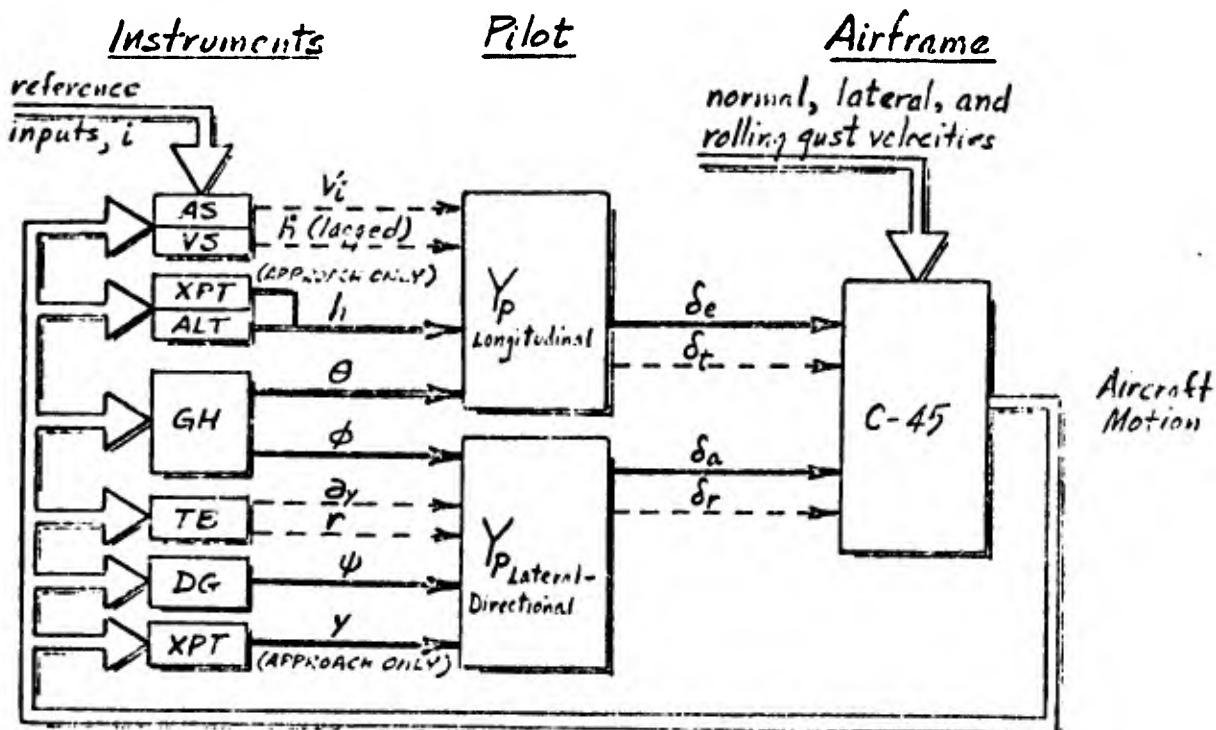
ANALYSIS OF DISPLAY-CONTROL LOOP DYNAMICS FOR THE C-45

This Appendix presents an analysis of manual control of the C-45 under IFR conditions. The results were used in Section II to correlate the sampling behavior of the pilot with closed-loop control characteristics. Specifically, the pilot's observed instrument sampling rate (fixation frequency) was compared with the dominant frequency of the displayed signal (under closed loop conditions) calculated in this Appendix.

In this examination of display-control loop dynamics only the most important aspects of the system for instrument flight are considered. Control feel, control surface actuator dynamics and instrument dynamics are neglected. In the longitudinal case throttle or blade pitch inputs are not considered, although in the landing approach condition they might play a role since the aircraft is operating near speed for minimum required power. In the lateral case rudder inputs are of secondary importance in cruise, but essential in approach. The analysis shows that a very lightly damped Dutch roll mode exists at both cruise and approach conditions. Dutch roll damping is only slightly increased by the aileron closures in cruise. The pilot very likely does use the rudder to add Dutch roll damping. Since the Dutch roll lies outside the closed loop system bandwidth in cruise, and since the selection of loop gain is not determined by the Dutch roll resonant peak in this case, the determination of the precise damping ratio of this mode is unimportant here. In approach, however, the Dutch roll is lower in frequency and even more poorly damped to the extent that satisfactory aileron closures are impossible without a modicum of yaw damping through the rudder.

A compensatory system topology for this display-control situation is shown in the sketch. Those features unimportant to the determination of closed loop characteristics are shown with dashed lines. Two conventional linear, uncoupled sets of three rigid-body aircraft perturbation equations of motion are used. The dimensional stability derivatives are given in Table A-I. Two flight conditions are examined: straight and level flight at 5,000 feet altitude (referred to as "Cruise" in this Section) and low-level

instrument flight (referred to as "ILA," instrument low approach, in this Section). The data for Cruise were taken from Ref. A-1.¹ The data for ILA were extrapolated from the Cruise data by accounting for the airspeed and altitude difference between the flight conditions with the help of Ref. A-7 through A-10.



Compensatory System Topology for C-45 Analysis

Rolling and yawing moments of inertia were not given in Ref. 1. Therefore values of rolling and yawing radii of gyration were scaled from values for the B-25 and C-47 based on span-wise similarity. An average of the scaled radii of gyration was employed to compute each moment of inertia for the C-45.

Reference A-7 was used to estimate parasite drag coefficient as 0.02 and Oswald's drag efficiency factor as 0.8 for a parabolic drag function. The computed lift coefficient for ILA was then used to estimate total drag coefficient and nondimensional partial derivative $C_{D_{C_L}}$.

¹See end of Appendix A for References indicated A-

Constant throttle and propeller blade pitch settings were assumed to maintain approximately constant thrust horsepower in approach, from which the airscrew contribution to X_u was estimated directly by partial differentiation. Compressibility effects and trimmed aerodynamic pitching moment were assumed zero.

Static margin and nondimensional partial derivatives $C_{L\alpha}$, $C_{m\delta_e}$, $C_{m\dot{\alpha}}$ and $C_{m\dot{q}}$ were assumed invariant between cruise and approach. Lateral-directional nondimensional cross-coupled partial derivatives $C_{n\dot{p}}$ and $C_{l\dot{r}}$ were assumed directly proportional to lift coefficient between cruise and approach. This is equivalent to neglecting the tail contribution with respect to the dominant wing contribution. (Ref. A-8, A-9, A-10.) All other significant lateral-directional nondimensional partial derivatives were assumed invariant between cruise and approach.

Results of closures for the Cruise flight conditions have also been applied to climbing, diving and turning flight conditions in Section II. Justification for this may be found in the one-minute time duration of instrument maneuvers performed with the performance-limited C-45. We assume path angle and bank angle departures from straight and level flight were small. Reference A-11 shows that even large steady path and bank angles have a relatively small effect on the perturbation dynamics of the airframe estimated for straight and level flight.

Table A-II gives approximate transfer function characteristics for all pertinent input-output quantities. These were derived from the data in Table I, using the information provided by Ref. A-2. The aircraft dynamics correspond with what one might expect of the C-45 except perhaps for the near-zero $1/T_{h1}$ in the ILA condition. This corresponds to operation near the minimum power required as a function of speed.

TABLE A-I
DIMENSIONAL STABILITY DERIVATIVES FOR C-45

	<u>CRUISE</u>	<u>APPROACH</u>
U ₀ (fps)	220	≅ 140
Pressure Altitude (ft.)	5,000	≅ 500
X _u	- .0341	(- .0408**) - .063
Z _u	- .294	- .494
M _u	0	0
X _w	+ .0329	+ .106
Z _w	- 1.44	- 1.08
M _w	- .0677	- .0462
Z _{ẇ}	0	0
M _{ẇ}	- .00472	- .0053
Z _q	0	0
M _q	- 2.29	- 1.67
Z _{δ_e}	0	0
M _{δ_e}	+ 15.0*	+ 6.97*

*Note sign inversion with respect to NACA convention for aft control.

**This value neglects the airscrew contribution which is probably present in the value for cruise. The airscrew contribution in ILA will increase X_u (in a negative sense) about 50 percent to - .063.

TABLE A-I (Concluded)

	<u>CRUISE</u>	<u>APPROACH</u>
Y_v	- .199	- .145
L_β	- 9.35	- 4.33
N_β	+ 6.68	+ 3.10
L_p	- 4.58	- 3.24
N_p	- .0314	- .0493
L_r	+ .336	+ .527
N_r	- .425	- .31
L_{δ_α}	+ 7.50*	+ 3.47*
N_{δ_α}	0	0
Y_{δ_r}	0	0
L_{δ_r}	0	0
N_{δ_r}	- .380	- .176
I_{yz}	$\dot{=} 0$	$\dot{=} 0$

*Note sign inversion with respect to NACA convention.

TABLE A-II

C-45 LONGITUDINAL CHARACTERISTICS

		<u>CRUISE</u>	<u>APPROACH</u>
Δ	ζ_p	.09	.07
	ω_p	.19 rad/sec	.29 rad/sec
	ζ_{sp}	.56	.6
	ω_{sp}	4.27 rad/sec	2.9 rad/sec
$N_{\delta_e}^{\theta}$	A_{θ}	15.1/sec ²	7.1/sec ²
	$1/T_{\theta_1}$.041 rad/sec	.089 rad/sec
	$1/T_{\theta_2}$	1.47 rad/sec	1.12 rad/sec
$sN_{\delta_e}^h$	A_h	4750. ft/sec ⁴	1057. ft/sec ⁴
	$1/T_{h_1}$.011 rad/sec	$\doteq 0$
$N_{\delta_e}^u$	A_u	- 373. ft/sec ⁴	- 121. ft/sec ⁴
	$1/T_{u_1}$	1.86 rad/sec	2. rad/sec
Integral Scale of Isotropic Turbulence, L		1000 ft	500 ft
Normal Gust Bandwidth		.38 rad/sec	.5 rad/sec
$\omega_{wg} = \frac{\sqrt{3} U_0}{L}$			
Forcing Function Decrement in Effective Pilot Delay		.03 sec	.04 sec
$\Delta\tau_e(\omega_{wg})$			
(from Fig. 75, Ref. A-4)			

TABLE A-II (Continued)

$$N_{wg}^{\theta} = \frac{M_q}{U_0} s \left[s^2 - \left(X_u + Z_w + \frac{U_0 M_w}{M_q} \right) s + X_u Z_w - X_w Z_u + \frac{U_0 M_w}{M_q} X_u \right]$$

if $M_u = 0$, $|M_w| \ll |M_q|$

	<u>CRUISE</u>		<u>APPROACH</u>
$\frac{M_q}{U_0} s$	- .0104s	$\frac{M_q}{U_0} s$	- .0119s
	(s + .0322)		(s + .045)
	(s - 5.06)		(s - 2.78)

$$sN_{wg}^h = Z_w \left\{ s^3 - \left[2M_q + \left(X_u - \frac{X_w Z_u}{Z_w} \right) \right] s^2 + \left[2M_q \left(X_u - \frac{X_w Z_u}{Z_w} \right) + \frac{g M_q Z_u}{U_0 Z_w} \right] s - \frac{g Z_u M_w}{Z_w} \right\}$$

if $M_u = 0$, $|M_w| \ll |M_q|$

	<u>CRUISE</u>		<u>APPROACH</u>
Z_w	- 1.44	Z_w	- 1.08
ζ_h	≈ 0	ζ_h	≈ 0
ω_h	.345 rad/sec	ω_h	.442 rad/sec
	(s + 4.61)		(s + 3.45)

TABLE A-II (Continued)

		<u>CRUISE</u>	<u>APPROACH</u>
Δ	$1/T_S$	≈ 0	≈ 0
	$1/T_R$	4.80 rad/sec	3.63 rad/sec
	ζ_d	.075	.019
	ω_d	2.60 rad/sec	1.76 rad/sec
N_{ϕ}^{ϕ}	A_{ϕ}	+ 7.50 1/sec ²	+ 3.47 1/sec ²
	ζ_{ϕ}	.12	.129
	ω_{ϕ}	2.60 rad/sec	1.76 rad/sec ²
sN_{ϕ}^{ψ}	A_{ψ}	- .235 1/sec ³	- .171 1/sec ³
	$1/T_{\psi_1}$	+ 5.7 rad/sec	+ 3.88 rad/sec
	$1/T_{\psi_2}$	- 5.5 rad/sec	- 3.73 rad/sec
$s^2N_{\phi}^y$	A_y		112 ft/sec ⁴
	ζ_y		.08
	ω_y		1.76 rad/sec
N_{ϕ}^r	A_r		- .176
	$1/T_{r1}$		3.24 rad/sec
	ζ_r		.045
	ω_r		.555 rad/sec
	Gust Bandwidth		
	Rolling (ω_{pg})	1.6 rad/sec	1.7 rad/sec
	estimated from Fig. 7, Ref. A-3)		
	Lateral ($\omega_{vg} = \frac{\sqrt{3} U_0}{L}$)	.38 rad/sec	.5 rad/sec
	Forcing Function Decrement		
	in Effective Pilot Delay		
	$\Delta\tau_e (\omega_{pg})$.13 sec	.14 sec
	(from Fig. 75, Ref. A-4)		
	$\Delta\tau_e (\omega_{vg})$.03 sec	.04 sec

TABLE A-II (Concluded)

$$N_{\beta g}^{\phi} \doteq -Y_v \frac{L_{\beta}}{N_{\beta}} \left[s - \left(N_r - \frac{N_{\beta}}{L_{\beta}} L_r \right) \right] \quad \text{if } |\dot{\beta} - Y_v \beta| \ll \left| -\frac{g}{U_0} \phi + r \right|$$

	<u>CRUISE</u>	<u>APPROACH</u>
$-Y_v L_{\beta} / N_{\beta}$	- .278	- .202
	(s + .185)	(s - .066)

$$N_{\beta g}^{\psi} \doteq -Y_v \left[s - \left(L_p - \frac{L_{\beta}}{N_{\beta}} N_p \right) \right] \quad \text{if } |\dot{\beta} - Y_v \beta| \ll \left| -\frac{g}{U_0} \phi + r \right|$$

	<u>CRUISE</u>	<u>APPROACH</u>
- Yv	+ .199	+ .145
	(s + 4.6)	(s + 3.28)

$$sN_{\beta g}^Y \doteq U_0 \left[1 + Y_v \left(L_p - \frac{L_{\beta}}{N_{\beta}} N_p \right) \right] \quad \text{if } |\dot{\beta} - Y_v \beta| \ll \left| -\frac{g}{U_0} \phi + r \right|$$

	<u>CRUISE</u>	<u>APPROACH</u>
$sN_{\beta g}^Y = \frac{sN_{\beta g}^Y}{U_0}$	1.925	1.475

$$N_{p g}^{\phi} \doteq - \left(L_p - \frac{L_{\beta} N_p}{N_{\beta}} \right) \quad \text{4.6} \quad \text{3.28}$$

$$sN_{p g}^{\psi} \doteq \frac{g}{U_0} N_{p g}^{\phi} \quad \text{.674} \quad \text{.755}$$

$$s^2 N_{p g}^Y \doteq U_0 s N_{p g}^{\psi} \quad \text{148} \quad \text{106}$$

The Simple Pilot Model

It is not our present purpose to validate or even to announce a particular model of the pilot which accurately describes his sampling behavior. This is one objective of the entire program of which this work is only a part. However, it is necessary to account in some gross way for the pilot's sampling behavior in the present analysis. Otherwise the results and their application in Section II will not be realistic.

A model to account for the gross nature of sampling is developed in the following simple way. A pure delay due to sampling is postulated. It is associated with a given instrument and is a function of the mean sampling period, T_s and the mean dwell time, T_d

$$\Delta\tau_{(INST)}(T_s, T_d)$$

Consider first the limiting case when the dwell time is zero (negligible with respect to the sampling period). We assume that the pilot acts as a zero order hold which can be represented approximately by a pure delay of $T_s/2$ seconds.* Then,

$$\Delta\tau_{(INST)}(T_s, 0) = \frac{T_s}{2}$$

Consider next the limiting case when the dwell time is equal to the sampling period. This is the continuous attention case. In effect there is no "off time" and, of course, it is logical to set the sampling delay equal to zero.

*This assumption can be justified by the implied notion of data reconstruction from single impulsive samples. We assume the dwell time to be sufficiently short that no derivatives can be sampled. We also assume that the contribution of sample history is negligible (forgotten). The only unbiased intersample reconstruction filter is the zero-order hold whose transfer function is

$$G_h(s) = \frac{1 - e^{-T_s s}}{s} \approx \frac{1 - \frac{1 - sT_s/2}{1 + sT_s/2}}{s} \approx \frac{T_s}{\left(1 + \frac{sT_s}{2}\right)} \approx T_s e^{-\frac{T_s}{2} s}$$

$$\Delta\tau(\text{INST}) (T_s, T_d) = 0$$

It is now assumed that for dwell times intermediate between zero and the full sampling period the sampling delay decreases linearly with increasing dwell time

$$\frac{\partial}{\partial T_d} \Delta\tau(\text{INST}) = - \text{constant}$$

The function which has these characteristics is

$$\Delta\tau(\text{INST}) = \frac{T_s - T_d}{2} = \frac{T_s}{2} (1 - \eta)$$

$$\text{where } \eta = T_d/T_s.$$

Applying this formula, for instance, to the gyro horizon during straight and level flight, we find:

$$T_s = 2.6 \text{ seconds}$$

$$T_d = .55 \text{ seconds}$$

$$\Delta\tau(\text{GH}) = \frac{2.6 - .55}{2} = 1.03 \text{ seconds.}$$

In addition to this sampling delay a component is added to account for the basic pilot neuromuscular lag which obtains when he continuously monitors and controls a signal. The case of continuous compensatory control has been the subject of both analytical and experimental research for many years, and there are rules for selecting pilot characteristics, including his reaction time delay (Ref. A-4). The symbol $\tau(\omega_1, Y_c)$ is used to denote the basic pilot delay where ω_1 represents the input signal bandwidth and Y_c indicates the nature of the controlled element. For instance, a typical situation might be one in which $\tau(\omega_1, Y_c) = .20$ corresponding approximately to $\omega_1 = 2.0$ radians/second and $Y_c = 1/s$. In general ω_1 and Y_c must be estimated. They are taken here to be the isotropic gust disturbance input break

frequency and the approximate nature of the appropriate airframe transfer function near ω_1 . In the closure of the pitch angle-to-elevator loop in straight and level flight $\tau(\omega_1, Y_c)$ is estimated to be .33 seconds. For this closure the total pilot delay is

$$\tau_\theta = \tau(\omega_1, Y_c) + \Delta\tau_{GH} = .33 + 1.03 = 1.36 \text{ secs}$$

The increment in τ due to sampling is in all cases a large fraction of the total τ . Thus the τ 's are very much larger than those one is accustomed to finding in the case of continuous monitoring of an instrument.

Table A-III gives the sampling rates, dwell times and computed sampling delay times for five instruments. The airspeed indicator and the vertical speed indicator are included to show the larger sampling delay times associated with these instruments which are of secondary importance to control.

TABLE A-III PILOT SAMPLING BEHAVIOR

CRUISE	INSTRUMENTS				
Sampling Parameters	GH	AS	ALT	VS	DG
ω_B (rps)	2.4	0.7	1.5	0.7	2.8
T_B (sec)	2.6	9.0	4.2	9.0	2.25
T_d (sec)	.55	.54	.48	.38	.75
$\Delta\tau$ (INST)(sec)	<u>1.03</u>	4.23	<u>1.86</u>	4.31	<u>.75</u>

ILA	INSTRUMENTS				
Sampling Parameters	GH	AS	XPT	VS	DG
ω_B (rps)	1.8	1.6	3.1	.37	2.8
T_B (sec)	3.5	3.9	2.0	17.0	2.25
T_d (sec)	.55	.38	.86	.39	.55
$\Delta\tau$ (INST)(sec)	<u>1.47</u>	<u>1.76</u>	<u>.57</u>	8.3	<u>.85</u>

Dominant instruments are indicated by short sampling delays which have been underlined for emphasis.

Note that $\Delta\tau(\text{INST})$ as shown in Table A-III reaffirms the dominance of those instruments thought to be of primary importance in control. It is interesting to note that, in the ILA the airspeed indicator, AS, has a moderate sampling delay associated with it. This is not surprising in view of the fact that this aircraft, in the landing approach, is near the speed for minimum power required. A piloting technique known to be successful in this case, (See, e.g., Ref. A-5), is the closing of an airspeed-to-throttle loop. Although we are not sure that this compensatory loop was closed in flight tests, if it were it would explain the moderate fixation frequency associated with the airspeed indicator. There may also be another explanation for the attention given to airspeed in the ILA. An airspeed-to-elevator closure is an alternative method (to pitch attitude-to-elevator) for damping the phugoid, although extraordinarily low frequency pilot lead is required in the airspeed-to-elevator closure, because the fixation frequency is not sufficiently high as our subsequent analysis will show.

The effective pilot delays for the loop closures examined are summarized in Table A-IV.

TABLE A-IV
EFFECTIVE PILOT TIME DELAYS FOR C-45

CRUISE	INSTRUMENT \rightarrow CONTROL LOOP			
	$\theta \rightarrow \delta_e$	$h \rightarrow \delta_e$	$\phi \rightarrow \delta_a$	$\psi \rightarrow \delta_a$
Pilot Time Delay (sec)				
$\tau_0 (Y_c)$.36	.36	.36	.36
$-\Delta\tau_e (\omega_1)$	- .03	- .03	- .13	- .13
$+\Delta\tau(\text{INST})$	+ 1.03	+ 1.86	+ 1.03	+ .75
$\tau_e(\text{sec})$	1.36	2.19	1.26	0.98

TABLE A-IV (Concluded)

ILA	INSTRUMENT → CONTROL LOOP					
Pilot Time Delay (sec)	u → δ _e	θ → δ _e	h → δ _e	φ → δ _a	ψ → δ _a	y → δ _a
τ ₀ (Y _c)	.36	.36	.36	.36	.36	.36
- Δτ _e (ω ₁)	-.04	-.04	-.04	-.14	-.14	-.04
+ Δτ(INST)	+1.79	+1.47	+0.57	+1.47	+0.85	+0.57
τ _e (sec)	2.11	1.79	.89	1.69	1.07	.89

Longitudinal Control

Figure A-1 illustrates the simplified continuous equivalent topology and symbology used in parallel loop closures for elevator longitudinal control.

The u → δ_e closure is significant only in ILA. Figures A-2 and A-3 show the results. The appropriate pilot model for this closure requires low frequency phase lead:

$$Y_{p_u} = K_{p_u} \left(s + \frac{1}{T_{L_u}} \right) e^{-\tau_u s} ,$$

even when continuous attention is given to airspeed control, if the pilot is to increase phugoid damping ratio as well as bandwidth. (Cf. Ref. A-6.) Alternatively we may speak of the phase lead as acceleration-recognition above a frequency 1/T_{L_u}. Now in the sampled attention case which we treat, the average airspeed fixation frequency is sufficiently low that the phase lead is significantly compromised. Two lead break frequencies have been shown: 1/T_{L_u} = 0.1 and 0.29 rad/sec. Notice how low in frequency the phase lead (or acceleration-recognition) must occur even to increase phugoid damping and bandwidth slightly.

The exponential form itself is used for the large effective pilot reaction time delay, although a second order Padé approximant is acceptable for

the phugoid mode. Both closures are satisfied with 40 degrees phase margin by the same gain. The results demonstrate the importance of increasing fixation frequency to render the pilot lead effective. The delicate trade-off between fixation and acceleration-recognition frequencies appears consistent with the stress concentration of "needle-ball-and-airspeed" instrument technique prior to the universal acceptance of the gyro horizon, closures for which are studied next. Since the airspeed closures alter the phugoid so slightly, we shall proceed with pitch attitude closures from the characteristic modes of the open loop aircraft.

Figures A-4 and A-5 show the $\theta \rightarrow \delta_e$ closures for Cruise and ILA. The appropriate pilot model for this closure has the form

$$Y_{p\theta} = K_{p\theta} e^{-\tau\theta s}.$$

At both flight conditions the phugoid is well damped by the closure as shown by the root loci. The exponential form itself is used for the large effective pilot reaction time delay, because first and second order Pade approximations are inaccurate and introduce improper poles in the characteristic determinant of the attitude loop closures. The criteria upon which the loop gain is selected is a gain margin of 6db for the Cruise condition and a gain margin of 5 db for the ILA condition. Increasing X_u about fifty percent in the ILA to account for the airscrew contribution produces negligible effect on the chosen closed-loop poles. The effect of an increase in $1/T_{\theta_1}$ from 0.089 to 0.1 radian/second tends to counterbalance the effect of an increase in the phugoid damping ratio from 0.07 to 0.11. Since $|Z_w| \gg |X_u|$, $1/T_{\theta_2}$ is relatively unaltered by inclusion of the airscrew contribution to X_u .

Notice how much more effective is $\theta \rightarrow \delta_e$ in damping the phugoid and in increasing its bandwidth than was $u \rightarrow \delta_e$ with phase lead. There are two significant reasons:

- (1) the smaller aircraft numerator zero $1/T_{\theta_1}$ provides inherent phugoid phase lead and

- (2) the aircraft numerator zero $1/T_{\theta 2}$ (whose modulus is less than $|1/T_{u1}|$) provides inherent sampling phase lead. In fact, there is a remarkable correspondence between $|2/T_{\theta}|$ and $(1/T_{\theta 2})$ in both flight conditions. This suggests a simple rational hypothesis for making an initial estimate of pitch attitude fixation frequency, viz.:

$$\omega_s(\text{GH}) = \frac{2\pi}{T_s(\text{GH})} \doteq \frac{(1 - \eta) \pi}{\Delta\tau(\text{GH})} \quad \text{where } \eta = \frac{T_d}{T_s}$$

$$\text{but } \Delta\tau(\text{GH}) = \tau_{\theta} - \tau(\omega_1, Y_c) \doteq 2T_{\theta 2} - \tau(\omega_1, Y_c)$$

$$\text{therefore } \omega_s(\text{GH}) \doteq \frac{(1 - \eta) \pi}{2T'_{\theta 2} - \tau(\omega_1, Y_c)}$$

Figures A-6 and A-7 show the $h \rightarrow \delta_e$ closure. The airscrew contribution in X_u changes $1/T_{h1}$, from < 0 to > 0 . Therefore $1/T_{h1}$ has been chosen $\doteq 0$ in ILA. The pilot model chosen for this closure is

$$Y_{Ph} = K_{Ph} \left(s + \frac{1}{T_{Lh}} \right) e^{-\tau_h s}.$$

Again the exponential itself is used for the large different pilot reaction time delay, because it is more accurate and simpler than collecting a multitude of poles and zeros. The pilot phase lead is required to compensate for the phase lag contributed by the time delay in Cruise. In ILA the pilot phase lead break frequency has been doubled, because the large dwell time on the cross-pointer reduces the effective sampling delay in the altitude closure. The phugoid roots again become complex but their damping and natural frequency are both much higher than in the open loop aircraft. Primed notation is used to indicate closed loop values. The closure criterion is again the achievement of about 6 db of gain margin for both flight conditions. However, the gain margin has been left at about 10 db in ILA, because the short period damping ratio will be higher, the phugoid damping will be relatively insensitive to gain, and the phugoid frequency will be

more than twice the gust bandwidth anyway. The closed loop asymptotic characteristics given in Fig. A-6 and A-7 indicate that the system bandwidths exceed the vertical gust break frequency for both flight conditions. This marks each closed loop system as a relatively good one from the viewpoints of gust suppression and altitude-hold accuracy.

Lateral-Directional Control

The lateral-directional closures for Cruise are shown in Fig. A-8 through A-12. Figure A-8 defines the parallel loops. Figures A-9 and A-10 show the minor loop closure ($\phi \rightarrow \delta_a$). The pilot model chosen is

$$Y_{P\phi} = K_{P\phi} \left(s + \frac{1}{T_{L\phi}} \right) e^{-\tau_{\phi}s}$$

where $1/T_{L\phi} = 2.0 \text{ rad/sec}$

and $\tau_{\phi} = 1.17 \text{ sec}$

The reaction time delay is retained in exponential form to insure accuracy up to the rolling subsidence inverse time constant frequency, $1/T_R$.

The pilot phase lead is required to compensate for the phase lag contributed by the pilot's delay. A greater lead time constant than that actually used, $T_{L\phi} = .5 \text{ sec}$, depresses the roll-spiral bandwidth and results in a poor heading closure. The value selected is thought to be near the optimum. Notice that the pilot's delay causes the rolling subsidence mode to become a damped (and eventually unstable) oscillatory mode, denoted by $[\zeta'_R, \omega'_R]$.

Figures A-11 and A-12 show the heading closure $\psi \rightarrow \delta_a$ with the bank angle closure as an inner loop. Again pilot lead is required, but because of the Dutch roll resonant peak only a modest amount of lead is possible. The closed loop system bandwidth is on the order of 1 radian per second. Since the pilot can easily damp the Dutch roll with a rudder closure, the pilot lead time constant $T'_{L\psi}$ may be increased from .33 to .5 sec in these

circumstances. Then the closed-loop heading control bandwidth will be limited only by the roll attitude control bandwidth, which is somewhat low for rolling gust suppression.

The bandwidth of the rolling gust input to the aircraft at the Cruise condition is estimated to be 1.6 radians per second from Ref. A-3. Even if the pilot could devote full attention to lateral control it is doubtful that the resulting pilot-vehicle bandwidth could be extended to 2 radians per second. Certainly the pilot cannot devote full attention to lateral control when other flight tasks consume 60-70 percent of his time. Consequently the pilot regresses; that is, he reduces the system bandwidth and accepts larger errors. In return he can spend more time performing other flight tasks.

Since the transfer function from roll rate gusts to the heading angle response contains an integration, the DG displays only the average (or low frequency components) of the gust input. The gyro horizon displays the complete error spectrum. However the bandwidth for rolling gust inputs has been used to estimate pilot time delay regression for heading control in Table A-IV, because the pilot's vestibular awareness of rolling disturbances may reduce his delay in heading control far more than his awareness of yawing disturbances.

The lateral-directional closures for ILA are shown in Fig. A-13 through A-20. Figure A-13 defines the parallel loops which are closed through aileron control. This aileron loop topology requires yaw damping in the C-45 approach flight condition because of the low Dutch roll natural frequency (1.76 radians/second) and damping ratio (.019). Therefore the first loop closure (denoted by single prime, ') will be assumed without detailed analysis through rudder control to augment Dutch roll damping ratio such that $\zeta'_D \doteq \zeta_\phi$ by the pilot's low gain closure $a_y, r \rightarrow \delta_r$. (Cf. Ref. A-15) We shall assume vestibular sensing to insure shorter time delay than the very large needle and ball instrument sampling delay of 33.2 sec.* An

$$*T_s = 66.7 \text{ sec}; T_d = .34 \text{ sec.}$$

$$\Delta\tau_{(TB)} \doteq \frac{66.7 - .34}{2} \doteq 33.2 \text{ sec.}$$

approximate $r \rightarrow \delta_r$ closure locus is shown in Fig. A-14. The pilot model chosen is

$$Y_{Pr} = K_{Pr} e^{-\tau_r s}$$

where

$$\tau_r = .3 \text{ sec.}$$

The condition $\zeta'_D \doteq \zeta_\phi$ is easily satisfied at low gain without significant change in characteristic moduli.

Figures A-15 and A-16 show the roll attitude minor loop closure $\phi \rightarrow \delta_a$. The pilot model chosen is

$$Y_{p\phi} = K_{p\phi} \left(s + \frac{1}{T_{L\phi}} \right) e^{-\tau_\phi s}$$

where

$$1/T_{L\phi} = 1.5 \text{ rad/sec}$$

and

$$\tau_\phi = 1.69 \text{ sec}$$

The closure is an exact analogy of the Cruise closure at reduced bandwidth. The pilot phase lead time constant ($T_{L\phi} = .67 \text{ sec}$) has been chosen to compensate for the large reaction time delay and to give the best compromise between roll rate bandwidth and roll spiral bandwidth, both of which are low.

Figures A-17 and A-18 show the heading closure $\psi \rightarrow \delta_a$. A greater pilot lead time constant ($T_{L\psi} = .9 \text{ sec}$) can be used to maintain a semblance of roll rate and roll spiral bandwidth with $\tau_\psi = 1.07$ second preparatory to the lateral

displacement closure, because the Dutch roll is slightly better damped than in Cruise. However, the 6db gain margin is dominated by the low bandwidth roll rate and roll spiral modes anyway, so that the choice of pilot lead is forced. Notice that the roll rate bandwidth has regressed to about one-half the rolling gust bandwidth of 1.7 rad/sec.

Finally Fig. A-19 and A-20 show the $y \rightarrow \delta_a$ closure through the localizer deviation cross-pointer (XPT) instrument. The pilot model chosen is

$$Y_{Py} = K_{Py} e^{-\tau_y s}$$

where

$$\tau_y = .89 \text{ sec}$$

The closed loop system bandwidth is about 0.5 rad/sec, which matches the lateral isotropic turbulence bandwidth in the approach flight condition. This marks the lateral approach control as a good one from the standpoint of lateral gust suppression and center-line-hold accuracy, at the expense of some roll attitude disturbance. This is typical of manual approach control technique, since a very precise roll attitude loop is not required until immediately prior to touchdown when heading control is transferred to rudder.

Discussion

Table A-V presents a summary of the closed loop system characteristics. In the Cruise columns, the gust bandwidth is presented as a range of values. The lower value corresponds to that Cruise flight condition of 5K ft pressure altitude herein analyzed ($U_0 = 220 \text{ ft/sec}$). The higher value is that for Cruise at 12K ft pressure altitude ($U_0 = 320 \text{ ft/sec}$, according to Ref. A-14).

First, the following observations are made with respect to gust disturbance suppression. The longitudinal, lateral and directional loops provide good control. The system half-power bandwidth is about twice the normal

TABLE A-V

SUMMARY OF C-45 ALTITUDE, HEADING AND LATERAL DEVIATION CONTROL CHARACTERISTICS IN THE FREQUENCY DOMAIN. ALL FREQUENCIES ARE IN UNITS OF RAD/SEC

	LONGITUDINAL		LATERAL-DIRECTIONAL	
	CRUISE h → δe	ILA h → δe	CRUISE ψ → δa	ILA ψ → δa
Flight Condition				
Control Loop				
Gust Bandwidth, ω _g	(Normal) .38 to .55	.5	(Lateral) .38 to .55 (Rolling) 1.6 to 2.3	(Lateral) .5 (Rolling) 1.7
IIS Radio "Noise" Bandwidth, ω _n		(Est.) .5		1. to 1.4
System Low Pass Bandwidth, ω _b for reference input, 1	.8	(1.2)* 1.5	1.	.5
Gain Crossover, ω _c	.5	(1.2)* 1.5	.4	.3
Phase Crossover, ω _u (or ω _{pm} = 0)	1.	3.	1.	.55
IIS Error Passband Peak Amplitude Frequency, ω _{pIIS}		(.8)* 1.1		.8 to 1.
IIS Error Pass Bandwidth Δω _{pbIIS}		(3.)* 3.5		2.5 to 2.9
Instrument Sampling Frequency, (Standard Panel) ω _s	1.4	3.1	2.7	3.1
Ratios ω _s /ω _g	3.7 to 2.6	6.+	(Lateral) 7 to 5 (Rolling) 1.7 to 1.2	(Lateral) 6.+ (Rolling) 1.8
ω _s /ω _b	1.9	(2.6)* 2.1	2.7	6.+
ω _s /ω _{pIIS}		(3.9)* 2.8		3.9 to 3.1
ω _s /Δω _{pbIIS}		(1.)* .9		1.2 to 1.1

*Values in parentheses obtain with 10db gain margin, 600 phase margin and higher short period damping ratio.
Values in bold outline determine significant characteristic bandwidth frequency.

and lateral gust bandwidth except in lateral approach control where bandwidths are matched. In the lateral case the rolling gust bandwidth exceeds the system bandwidth. As was previously pointed out, this means that the gyro horizon displays large errors in the region between the system bandwidth and the rolling gust bandwidth, which the pilot is prepared to accept throughout Cruise and the approach until just prior to touchdown. Because of the integration which occurs in going from bank angle to heading angle, the directional gyro is not excited by the rolling gusts.

Second, instrument sampling rates are compared with loop closure characteristics. Two important loop closure parameters are the gain and phase crossover frequencies. For systems whose open loop transfer function has a crossover region approximated by

$$\frac{e^{-sT}}{s}$$

the phase crossover frequency is approximately equal to 2 times the gain crossover frequency when the stability criterion is either 45° of phase margin or 6db of gain margin. This fact appears in the data of Table A-V.

The instrument sampling frequencies vary from 1 to $2 \frac{1}{2}$ times the phase crossover frequencies and from 2 to 5 times the gain crossover frequencies. From a signal reconstruction point of view this result is encouraging because it is compatible with the Nyquist sampling theorem and its subsequent generalization (Ref. A-12).

Finally, instrument sampling frequencies are compared with the system bandwidth, ω_b for reference input i . For systems having a crossover region approximated by the function

$$\frac{e^{-Ts}}{s}$$

Figures A-21 and A-22 illustrate three cases of disturbance suppression for isotropic turbulence having bandwidth $\omega_g \equiv \omega_d$ viz.,

- (1) $\omega_b < \omega_d$, or insufficient suppression bandwidth;
- (2) $\omega_b = \omega_d$, or matched bandwidth;
- (3) $\omega_d < \omega_b$, or excessive suppression bandwidth approaching diminishing returns. Notice that the pilot can easily achieve cases (2) or (3) in Table A-V, since $\omega_g \leq \omega_b$ in all except rolling turbulence wherein we have case (1). Thus the displayed signal bandwidth will be dominated by the turbulence bandwidth for both attitude and position instruments in cruising flight.

Figure A-23 illustrates disturbance suppression bandwidth for ILS radio "noise-like" disturbances caused by irregularities in the radiation pattern. The irregularities enter the loop through the receiver at the error signal point and are distinguishable from the desired error signal only by their higher frequency content. Reference A-13 reveals average conventional localizer "noise" bandwidths, ω_n , in the range 1 to 2 radians/second, above lateral-directional path control system bandwidth in ILS. (Directional waveguide localizers with lower "noise" bandwidth did not exist in 1949.) Reference A-13 reveals nonstationarity in glideslope "noise," because continuous analyses were made from the outer marker to the transmitter and truncation errors were feared in analyses of shorter records. However, we have used an average waveguide localizer noise bandwidth of 0.5 rad/sec as an estimator of the glideslope noise bandwidth in Table A-V, since the UHF transmission band at about 330 mc/sec tends to improve directivity of the glideslope anyway.

The three cases of ILS radio disturbance suppression in Fig. A-23 for $\omega_n \equiv \omega_d$ are:

- (1) $\omega_b < \omega_d$, or underlapped suppression bandwidth;
- (2) $\omega_b = \omega_d$, or matched suppression bandwidth; and
- (3) $\omega_d < \omega_b$, or overlapped suppression bandwidth.

Evidently case (1) or (2) applies to the localizer in Table A-V, because the pilot learns to perform spectral filtering on his signal reconstruction from the error on the cross-pointer indicator. The net result in the loop may approach case (3), although the instrument error to be sampled by the pilot is from case (1) or (2). Evidently case (2) or (3) applies to the glideslope in Table A-V. Since the error is not a low pass but rather a

band pass function, the notion of error bandwidth for sampling and reconstruction depends on the center frequency and the amplitude-frequency gradients above and below the center frequency.

Estimates of the half-power glideslope and localizer error bandwidth are made in Fig. A-24. The glideslope "noise" amplitude-frequency gradient is unknown. We have assumed a first order gradient, which is typical of directional localizers in Ref. A-13. Since the closed loop error transfer function is not purely high pass but has a suppressed low pass characteristic, the resulting closed loop glideslope error exhibits a hybrid low pass-band pass property. The overlapped suppression bandwidth is such that the low pass character dominates. Thus we have approximated the half-power bandwidth as 3 radians/second, commensurate with the uncertainty in glideslope bandwidth.

The localizer closed loop error has a bandpass characteristic. The half-power bandwidth is estimated in Fig. A-24 as 2.9 radians/second centered on 1 radian/second. Results are summarized in Table A-V and several ratios of instrument sampling frequency to bandwidth frequency are computed.

The instrument sampling frequencies vary from more than 1 to over 3 times the disturbance error or system bandwidth, depending on which applies in each column of Table A-V in bold enclosure. Since the displayed signals form the basis for a signal reconstruction hypothesis of piloted control, the result remains compatible with the generalized Nyquist sampling theorem. We shall use the ratios ω_s/ω_g , ω_s/ω_b , ω_s/ω_p , and $\omega_s/\Delta\omega_{pb}$ in Section II of this working paper to establish correlative hypotheses for instrument sampling frequencies.

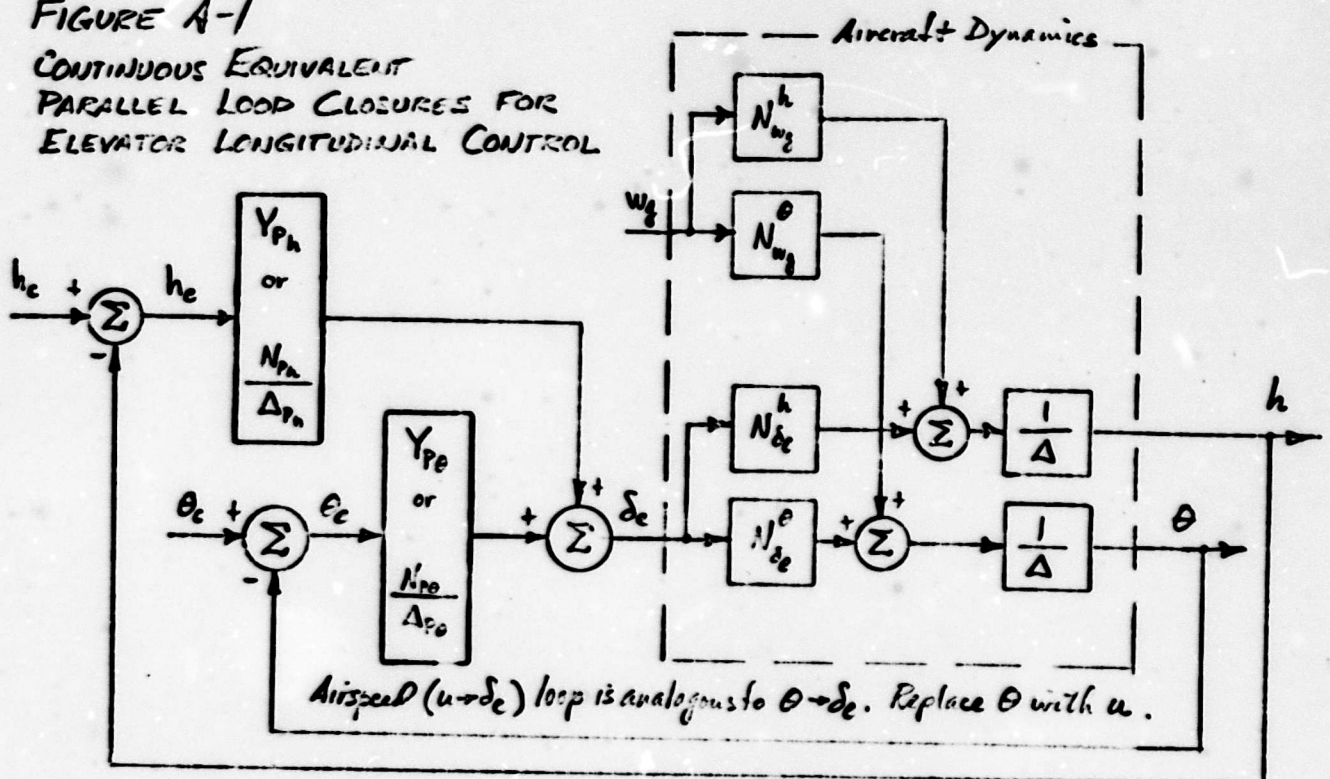
REFERENCES

- A-1. Kidd, E. A., Theoretical Investigation of Methods for Artificially Stabilizing the Modes of Motion of a C-45 Aircraft, Cornell Aeronautical Laboratory, Buffalo, New York, Report No. TB-754-F-1, October 1951.
- A-2. Ashkenas, I. L., and D. T. McRuer, Approximate Airframe Transfer Functions and Application to Single Sensor Control Systems, WADC-TR-58-82, June 1958.
- A-3. Eggleston, J. M., and F. W. Diederich, Theoretical Calculation of the Power Spectra of the Rolling and Yawing Moments on a Wing in Random Turbulence, NACA TN-3864, December 1956.
- A-4. McRuer, D. T., D. Graham, E. Krendel, and W. Reisinger, Human Pilot Dynamics in Compensatory Systems, AFFDL-TR-65-15, July 1965.
- A-5. Stapleford, R. L., Analysis of Several Handling Qualities Topics Pertinent to Advanced Manned Aircraft: Part V, Altitude Control During Approach and Other Topics, Systems Technology, Inc., Tech. Rept. 156, October 1966.
- A-6. McRuer, D. T., I. L. Ashkenas, and D. Graham, Vehicle Dynamics and Automatic Control, Systems Technology, Inc., Tech. Rept. 129-1, August 1966.
- A-7. Hoerner, S. F., Fluid-Dynamic Drag, Published by the author, Midland Park, New Jersey, 1958.
- A-8. Perkins, C. D., and R. E. Hage, Airplane Performance, Stability and Control, John Wiley and Sons, New York, 1949.
- A-9. Etkin, B., Dynamics of Flight, Stability and Control, John Wiley and Sons, New York, 1959.
- A-10. Seckel, E., Stability and Control of Airplanes and Helicopters, Academic Press, New York, 1964.
- A-11. Abzug, M. J., "Effects of Certain Steady Motions on Small-Disturbance Airplane Dynamics," Journal of the Aeronautical Sciences, 21:11 (November, 1954), pp. 749-752, and 762.
- A-12. Linden, D. A., and N. M. Abramson, "A Generalization of the Sampling Theorem," Information and Control, 3:1 (1960), pp. 26-31.
- A-13. Weir, D. H., Compilation and Analysis of Flight Control System Command Inputs, AFFDL-TR-65-119, January 1966.

- A-14. Bridgman, Leonard (ed.), Jane's All the World's Aircraft, 1942, Macmillan Company, New York, 1943.
- A-15. Graham, D., and J. J. Best, Analysis of Several Handling Quality Topics Pertinent to Advanced Manned Aircraft, Part II. Augmented Handling Qualities for Advanced Manned Aircraft, Systems Technology, Inc., Tech. Report 156, July 1966.

FIGURE A-1

CONTINUOUS EQUIVALENT
PARALLEL LOOP CLOSURES FOR
ELEVATOR LONGITUDINAL CONTROL



$$\left[\frac{e_c}{\theta_c} \right]' = \frac{\Delta_{Pe} \Delta}{\Delta_{Pe} \Delta + N_{Pe} N_{\delta_c}^\theta} = \frac{\Delta}{\Delta'}$$

$$\left[\frac{\theta}{e_c} \right]' = \frac{N_{Pe} N_{\delta_c}^\theta}{\Delta_{Pe} \Delta + N_{Pe} N_{\delta_c}^\theta} = \frac{Y_{Pe} N_{\delta_c}^\theta}{\Delta'}$$

$$\left[\frac{\theta}{w_2} \right]' = \frac{N_{w_2}^\theta \Delta_{Pe}}{\Delta_{Pe} \Delta + N_{Pe} N_{\delta_c}^\theta} = \frac{N_{w_2}^\theta}{\Delta'}$$

$$\left[\frac{h_c}{h_c} \right]'' = \frac{[\Delta_{Pe} \Delta + N_{Pe} N_{\delta_c}^\theta] \Delta_{Ph}}{\Delta_{Ph} \Delta_{Pe} \Delta + \Delta_{Ph} N_{Pe} N_{\delta_c}^\theta + \Delta_{Pe} N_{Ph} N_{\delta_c}^h} = \frac{\Delta_{Ph} \Delta'}{[\Delta_{Ph} \Delta' + N_{Ph} N_{\delta_c}^h]} = \frac{\Delta'}{\Delta''}$$

$$\left[\frac{h}{h_c} \right]'' = \frac{N_{Ph} N_{\delta_c}^h \Delta_{Pe}}{\Delta_{Ph} \Delta_{Pe} \Delta + \Delta_{Ph} N_{Pe} N_{\delta_c}^\theta + \Delta_{Pe} N_{Ph} N_{\delta_c}^h} = \frac{N_{Ph} N_{\delta_c}^h}{[\Delta_{Ph} \Delta' + N_{Ph} N_{\delta_c}^h]} = \frac{Y_{Ph} N_{\delta_c}^h}{\Delta''}$$

$$\left[\frac{h}{w_2} \right]'' = \frac{\Delta_{Ph} \Delta_{Pe} N_{w_2}^h + \frac{\Delta_{Pe} N_{Pe}}{\Delta} [N_{w_2}^h N_{\delta_c}^\theta - N_{\delta_c}^h N_{w_2}^\theta]}{\Delta_{Ph} \Delta_{Pe} \Delta + \Delta_{Ph} N_{Pe} N_{\delta_c}^\theta + \Delta_{Pe} N_{Ph} N_{\delta_c}^h} = \frac{N_{w_2}^h + \frac{Y_{Pe}}{\Delta} [N_{w_2}^h N_{\delta_c}^\theta - N_{\delta_c}^h N_{w_2}^\theta]}{\Delta''}$$

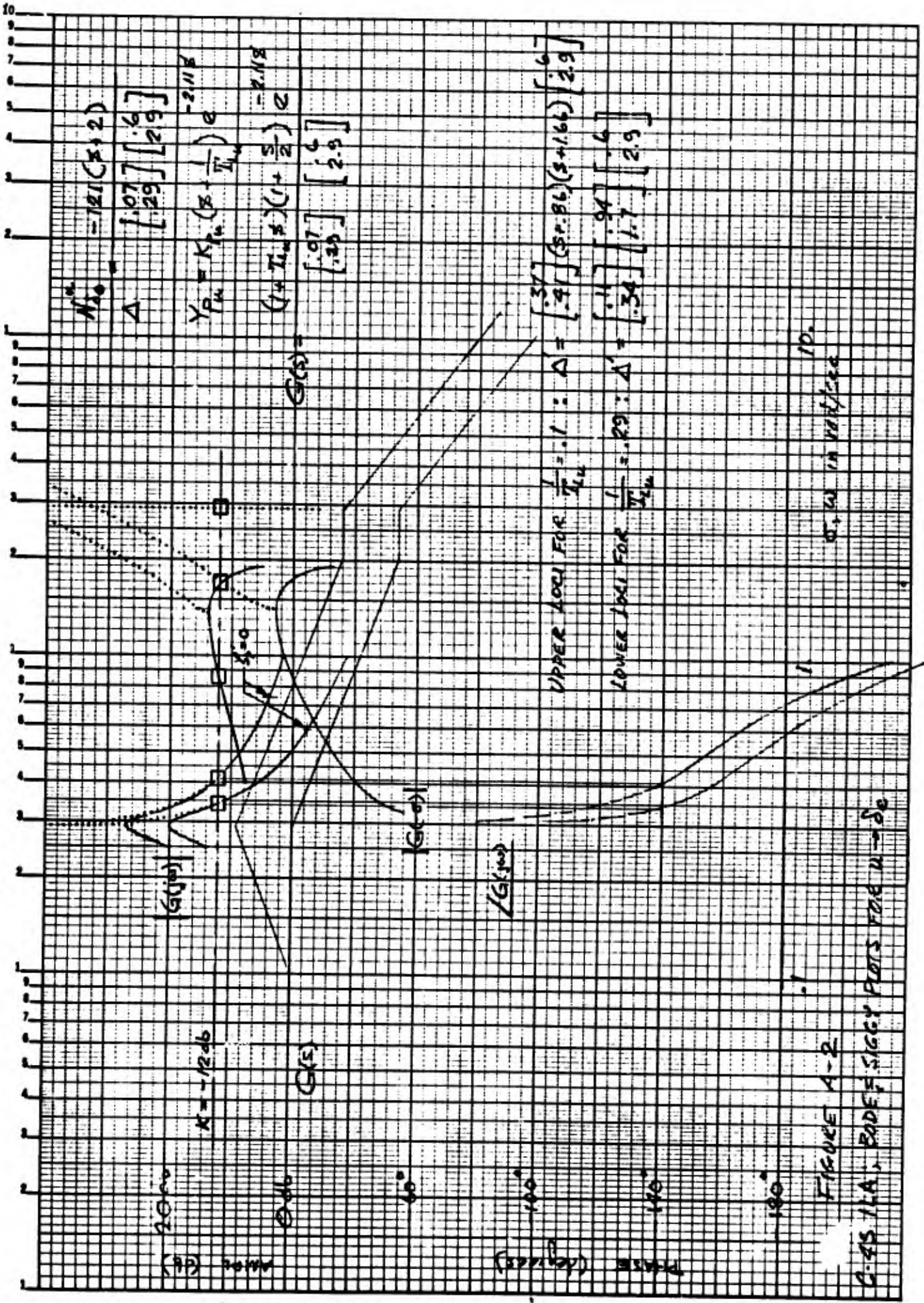


FIGURE A-2

C-45 1/A, BODE F-SIGGY PLOTS FOR N=50

sigma_c, w in rad/sec

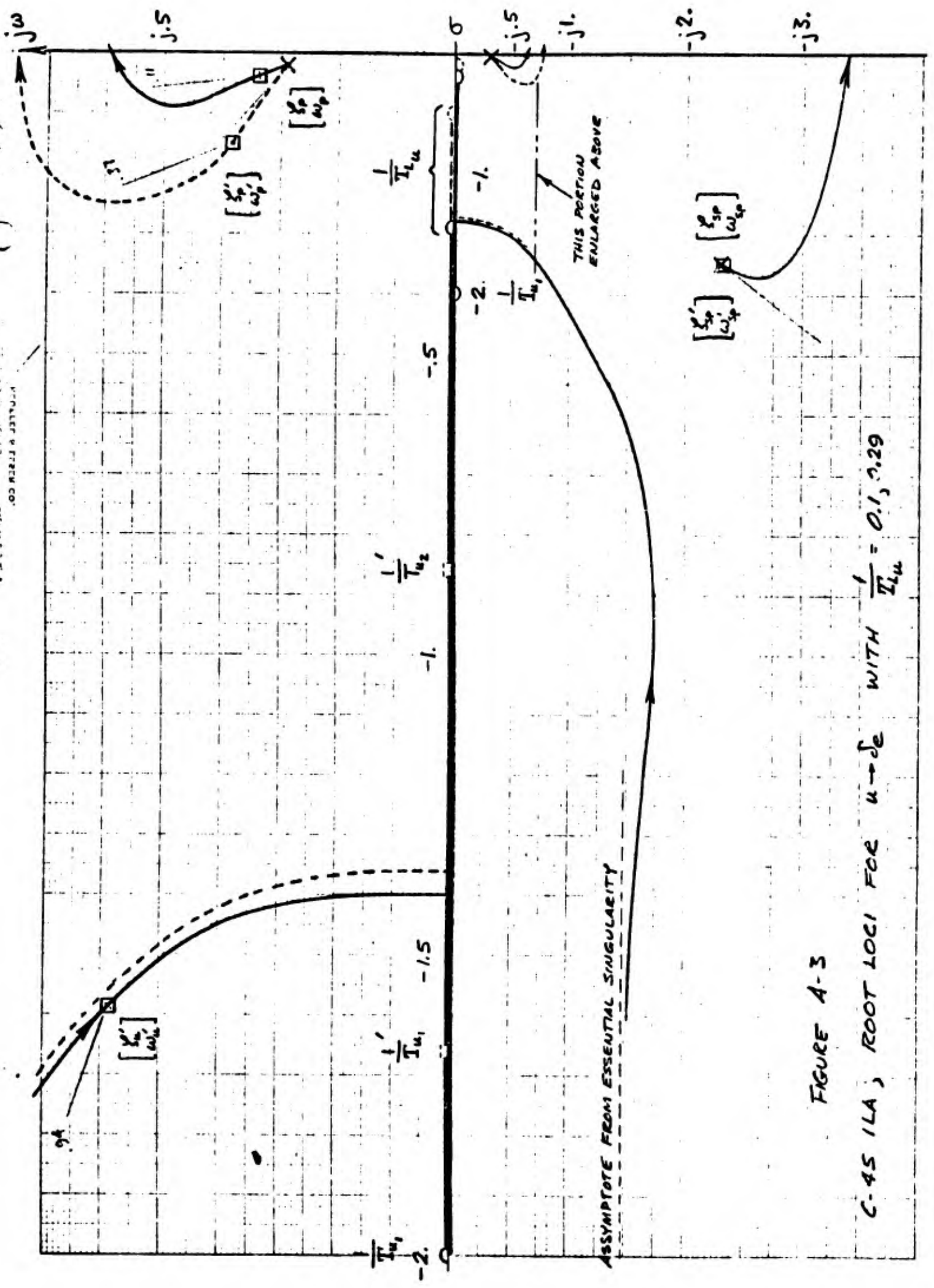


FIGURE A-3

C-45 1LA; ROOT LOCI FOR $u \rightarrow \infty$ WITH $\frac{1}{T_{Lu}} = 0.1, 0.29$

$\zeta = 1.03 + .33$
 $\tau_0 = 1.53$
 $\omega_n = 1.75$
 $\omega_c = 1.5$

$\theta = 2.5$ Ml.
Str 3

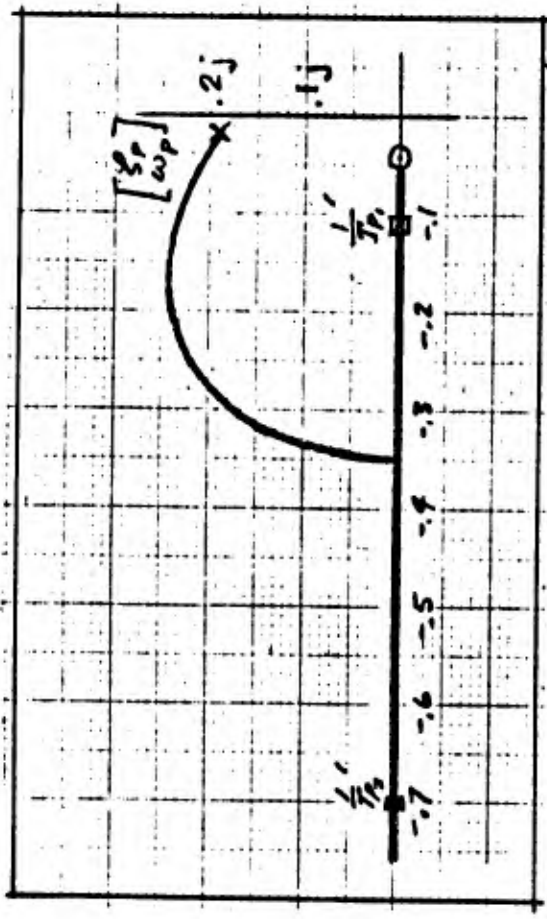
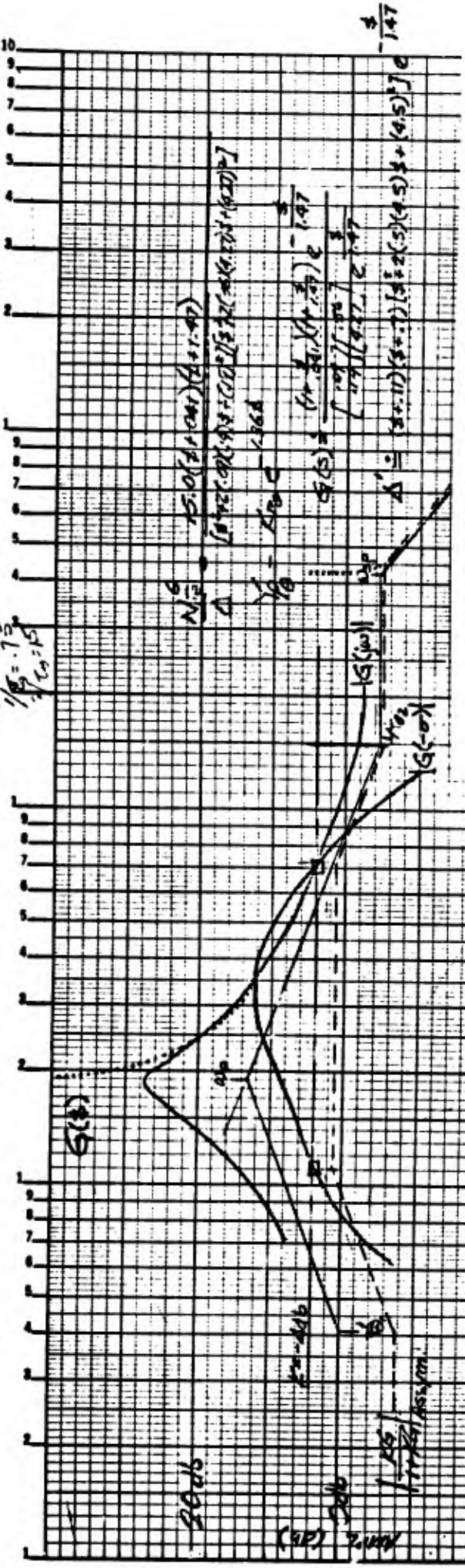
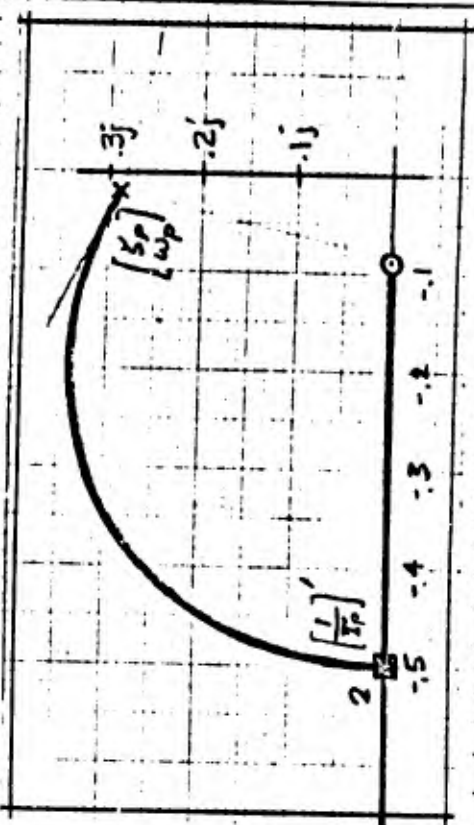
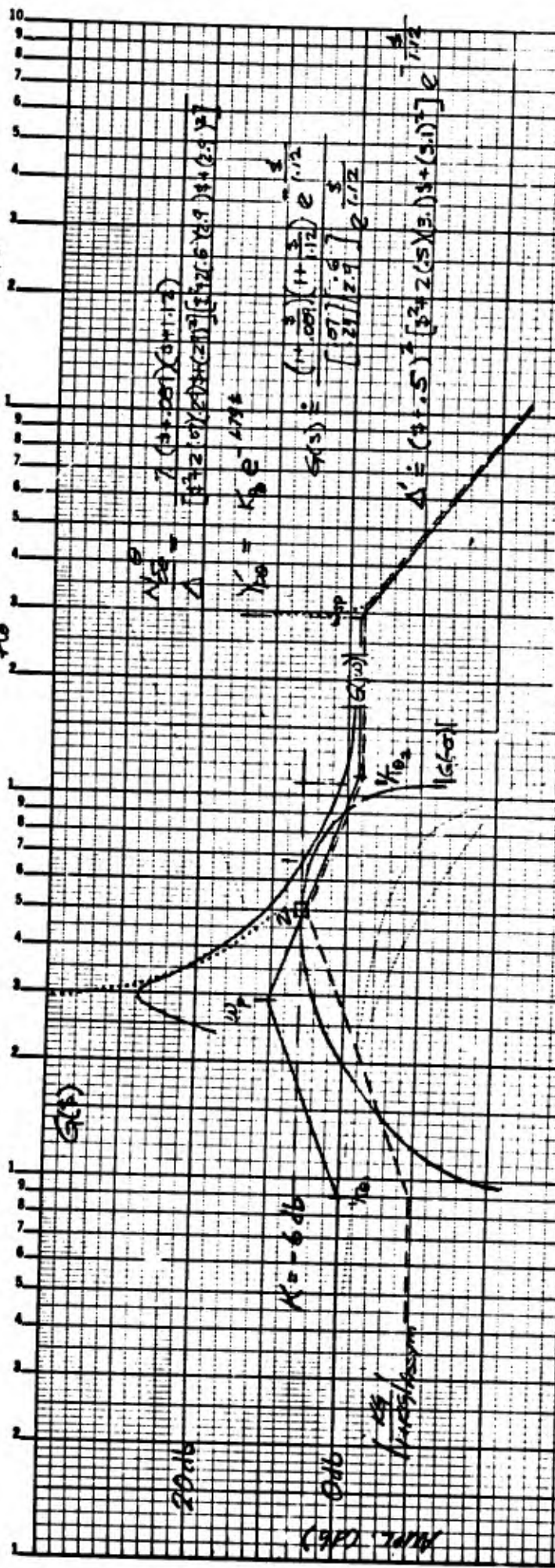


FIGURE A-4
G-95 CRUISE; BODE, SIGGY & ROOT LOCUS FOR $\theta = 2.5$

(114)
 $t_0 = 32.147$
 $t_0 = 1.79$
 $\frac{1}{\omega_0} = 0.6$



σ, ω in rad/sec.

FIGURE 1-5
 C-95.1A; BODE, SKGGY & ROOT LOCUS FOR $G \rightarrow S$

K Σ SEMI-LOGARITHMIC 46 6012
 4 CYCLES X 70 DIVISIONS MADE IN U.S.A.
 KESUPPL & ESSER CO.

TR 3 CVI
 K Σ 2 K Σ 10/0.002

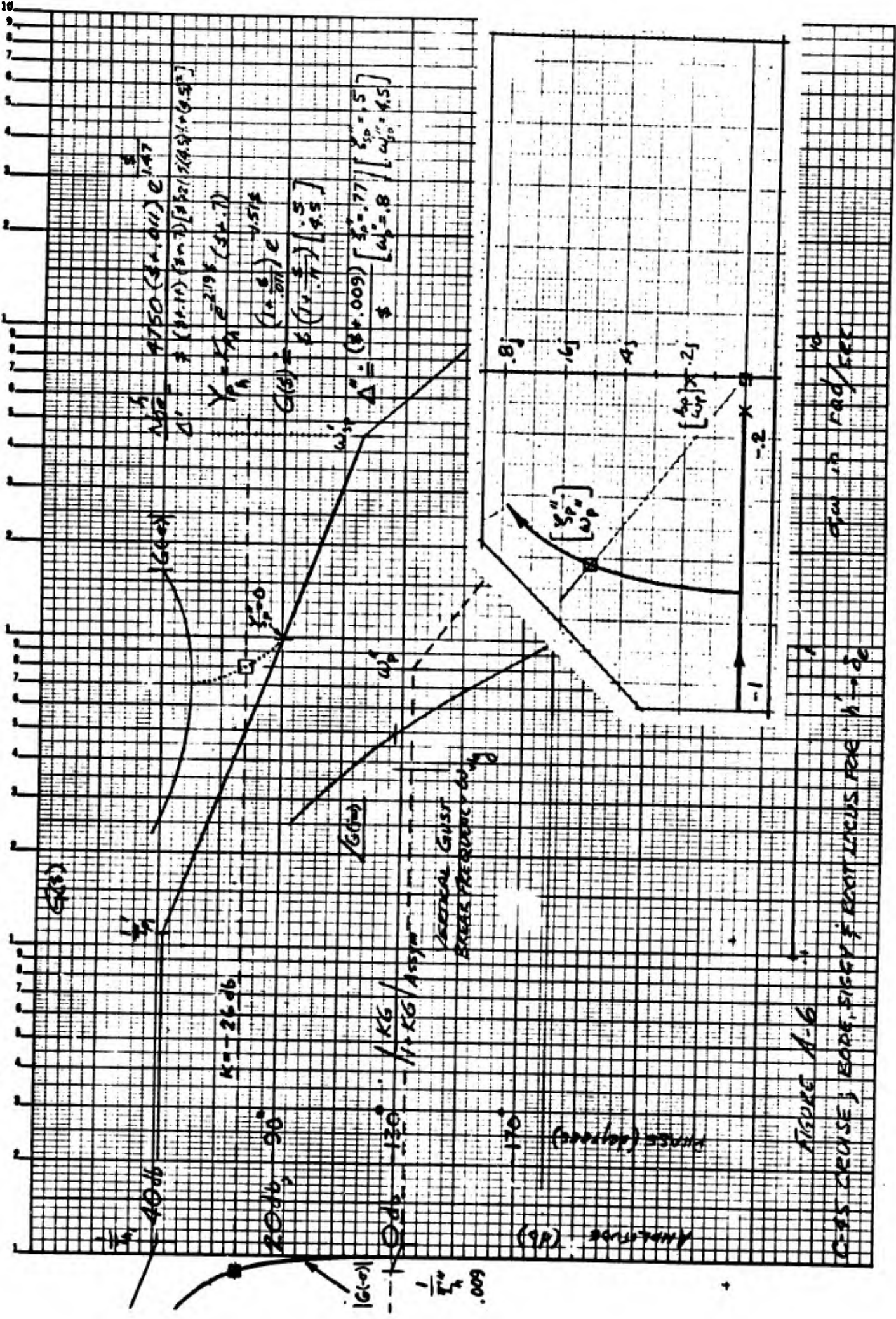


FIGURE A-6

C-15 CRUISE; EDGE-SIGHT ROLL MOTION FOR 11000

1000 RPM/SEC

(ILP)

$\zeta = 0.51$, $\omega_n = 32 = 8\sqrt{2}$
 $\zeta = 0.25$

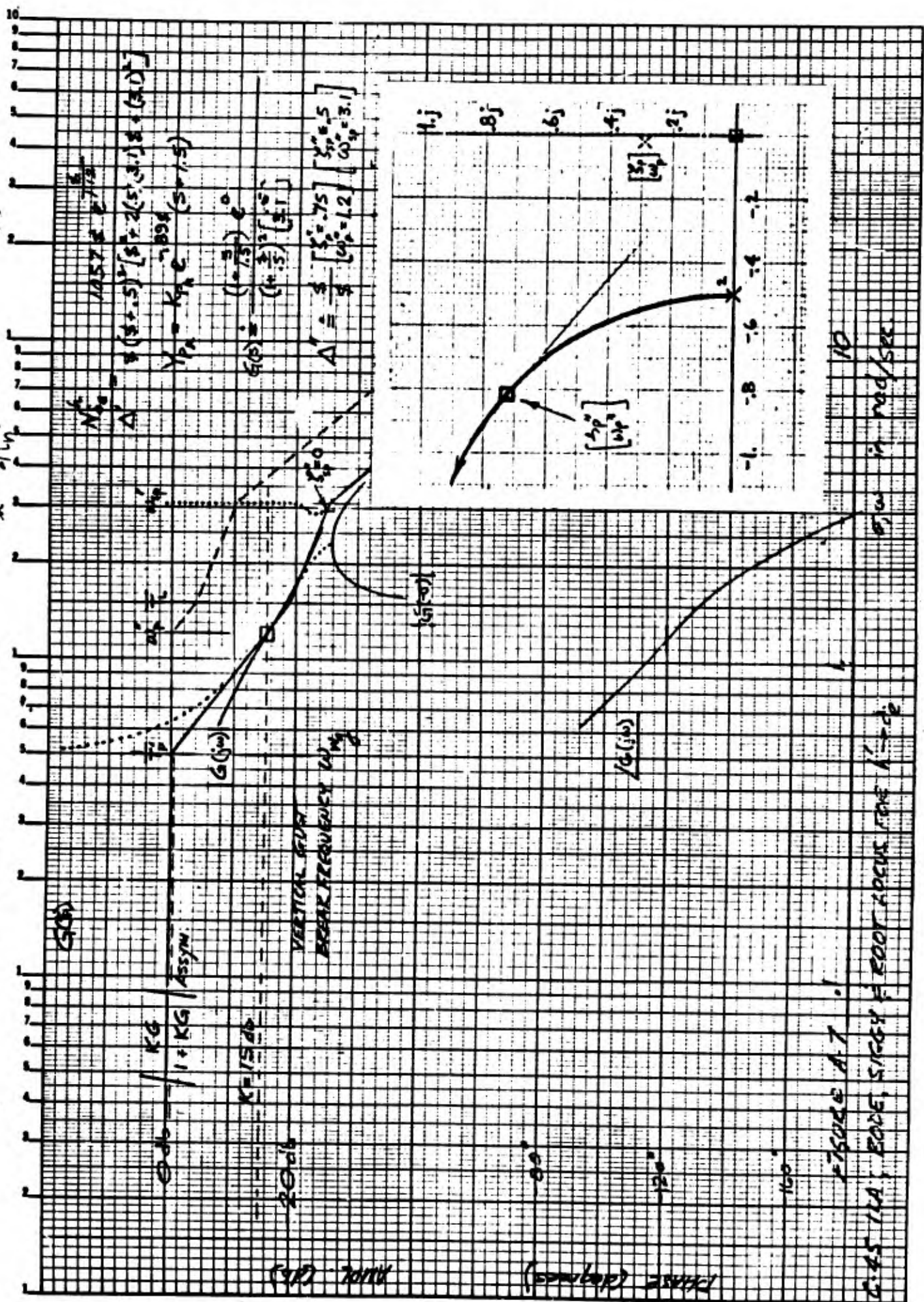
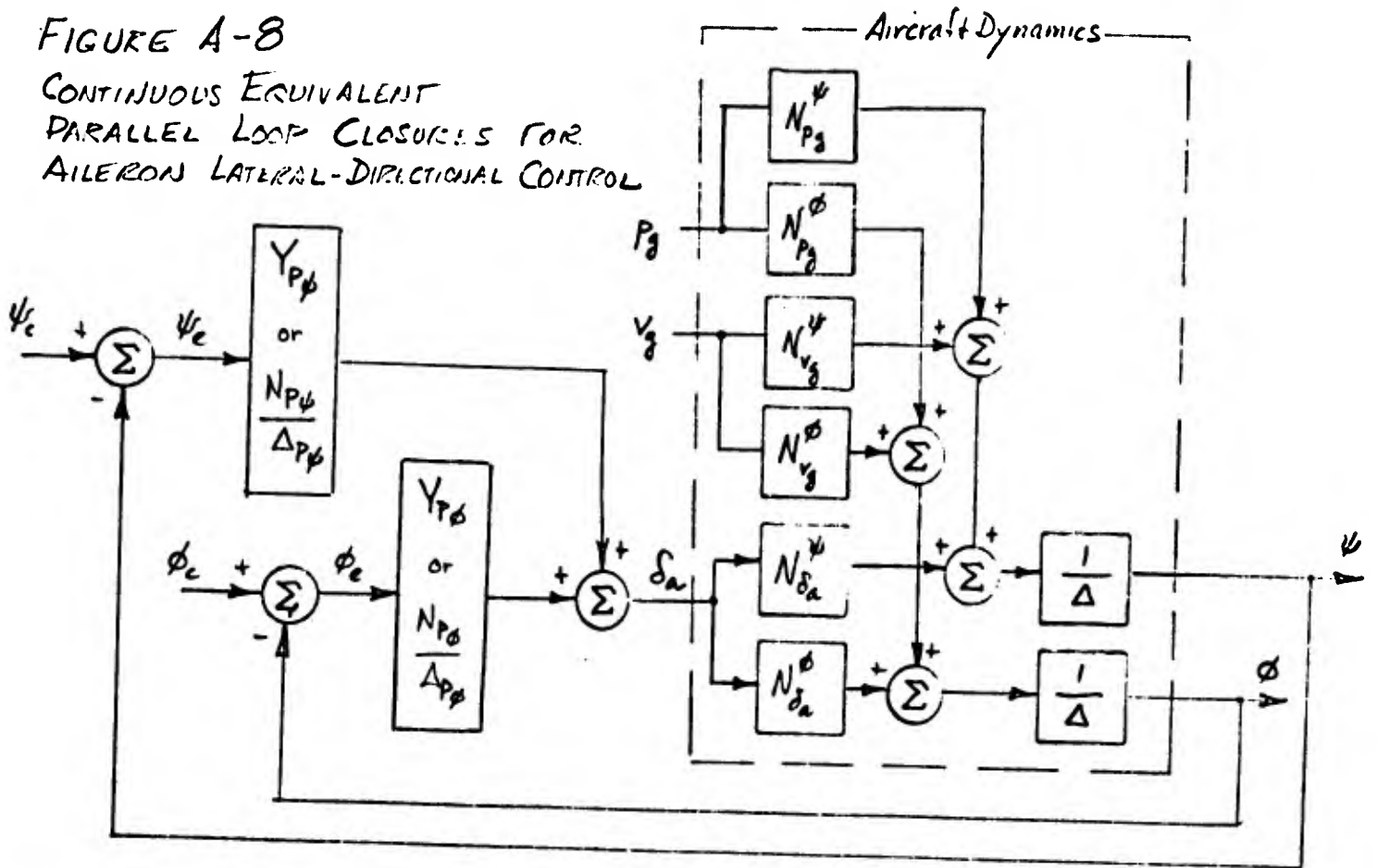


FIGURE A.1
 2.45 ILA, BODE, SIGGY = ROOT LOCUS FOR $\zeta = 0.51$

FIGURE A-8

CONTINUOUS EQUIVALENT
PARALLEL LOOP CLOSURES FOR
AILERON LATERAL-DIRECTIONAL CONTROL



$$\left[\frac{\phi_e}{\phi_c} \right] = \frac{\Delta_{P\phi} \Delta}{\Delta_{P\phi} \Delta + N_{P\phi} N_{\delta_a}^{\phi}} = \frac{\Delta}{\Delta'}$$

$$\left[\frac{\phi}{\phi_c} \right] = \frac{N_{P\phi} N_{\delta_a}^{\phi}}{\Delta_{P\phi} \Delta + N_{P\phi} N_{\delta_a}^{\phi}} = \frac{Y_{P\phi} N_{\delta_a}^{\phi}}{\Delta'}$$

$$\left[\frac{\phi}{P_{\psi}} \right] = \frac{N_{P_{\psi}}^{\phi} \Delta_{P\phi}}{\Delta_{P\phi} \Delta + N_{P\phi} N_{\delta_a}^{\phi}} = \frac{N_{P_{\psi}}^{\phi}}{\Delta'}$$

$$\left[\frac{\phi}{V_{\psi}^{\phi}} \right] = \frac{N_{V_{\psi}^{\phi}} \Delta_{P\phi}}{\Delta_{P\phi} \Delta + N_{P\phi} N_{\delta_a}^{\phi}} = \frac{N_{V_{\psi}^{\phi}}}{\Delta'}$$

$$\left[\frac{\psi_e}{\psi_c} \right] = \frac{[\Delta_{P\psi} \Delta + N_{P\psi} N_{\delta_a}^{\psi}] \Delta_{P\psi}}{\Delta_{P\psi} \Delta_{P\phi} \Delta + \Delta_{P\psi} N_{P\phi} N_{\delta_a}^{\phi} + \Delta_{P\psi} N_{P\psi} N_{\delta_a}^{\psi}} = \frac{\Delta_{P\psi} \Delta'}{[\Delta_{P\psi} \Delta' + N_{P\psi} N_{\delta_a}^{\psi}]} = \frac{\Delta'}{\Delta''}$$

$$\left[\frac{\psi}{V_{\psi}^{\psi}} \right] = \frac{N_{P_{\psi}}^{\psi} \Delta_{P\psi}}{\Delta_{P\psi} \Delta_{P\phi} \Delta + \Delta_{P\psi} N_{P\phi} N_{\delta_a}^{\phi} + \Delta_{P\psi} N_{P\psi} N_{\delta_a}^{\psi}} = \frac{N_{P_{\psi}}^{\psi} N_{\delta_a}^{\psi}}{[\Delta_{P\psi} \Delta' + N_{P\psi} N_{\delta_a}^{\psi}]} = \frac{Y_{P\psi} N_{\delta_a}^{\psi}}{\Delta''}$$

$$\left[\frac{\psi}{V_{\psi}^{\phi}} \right] = \frac{\Delta_{P\psi} \Delta_{P\phi} N_{V_{\psi}^{\phi}} + \frac{\Delta_{P\psi}}{\Delta} [N_{V_{\psi}^{\phi}} N_{\delta_a}^{\phi} - N_{\delta_a}^{\psi} N_{V_{\psi}^{\phi}}]}{\Delta_{P\psi} \Delta_{P\phi} \Delta + \Delta_{P\psi} N_{P\phi} N_{\delta_a}^{\phi} + \Delta_{P\psi} N_{P\psi} N_{\delta_a}^{\psi}} = \frac{N_{V_{\psi}^{\phi}} + \frac{Y_{P\psi}}{\Delta} [N_{V_{\psi}^{\phi}} N_{\delta_a}^{\phi} - N_{\delta_a}^{\psi} N_{V_{\psi}^{\phi}}]}{\Delta''}$$

$$\left[\frac{\psi}{P_{\psi}} \right] = \frac{\Delta_{P\psi} \Delta_{P\phi} N_{P_{\psi}}^{\psi} + \frac{\Delta_{P\psi} N_{P\phi}}{\Delta} [N_{P_{\psi}}^{\psi} N_{\delta_a}^{\phi} - N_{\delta_a}^{\psi} N_{P_{\psi}}^{\phi}]}{\Delta_{P\psi} \Delta_{P\phi} \Delta + \Delta_{P\psi} N_{P\phi} N_{\delta_a}^{\phi} + \Delta_{P\psi} N_{P\psi} N_{\delta_a}^{\psi}} = \frac{N_{P_{\psi}}^{\psi} + \frac{Y_{P\psi}}{\Delta} [N_{P_{\psi}}^{\psi} N_{\delta_a}^{\phi} - N_{\delta_a}^{\psi} N_{P_{\psi}}^{\phi}]}{\Delta''}$$

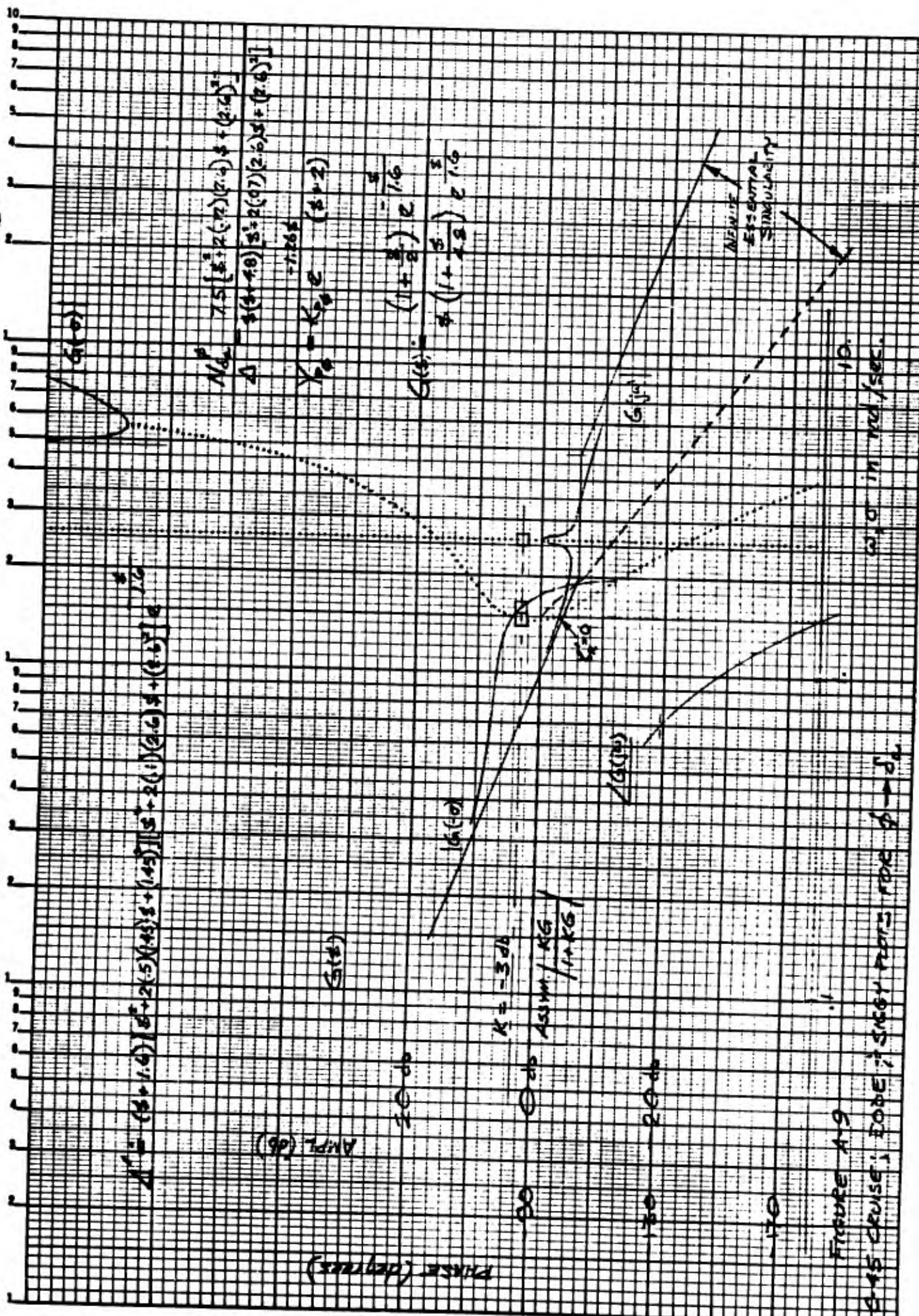


FIGURE A-9

5-15 CRUISE; EODE; SMOOT; PORS; RDE; $\delta \rightarrow \delta_d$

$\phi \rightarrow \delta$

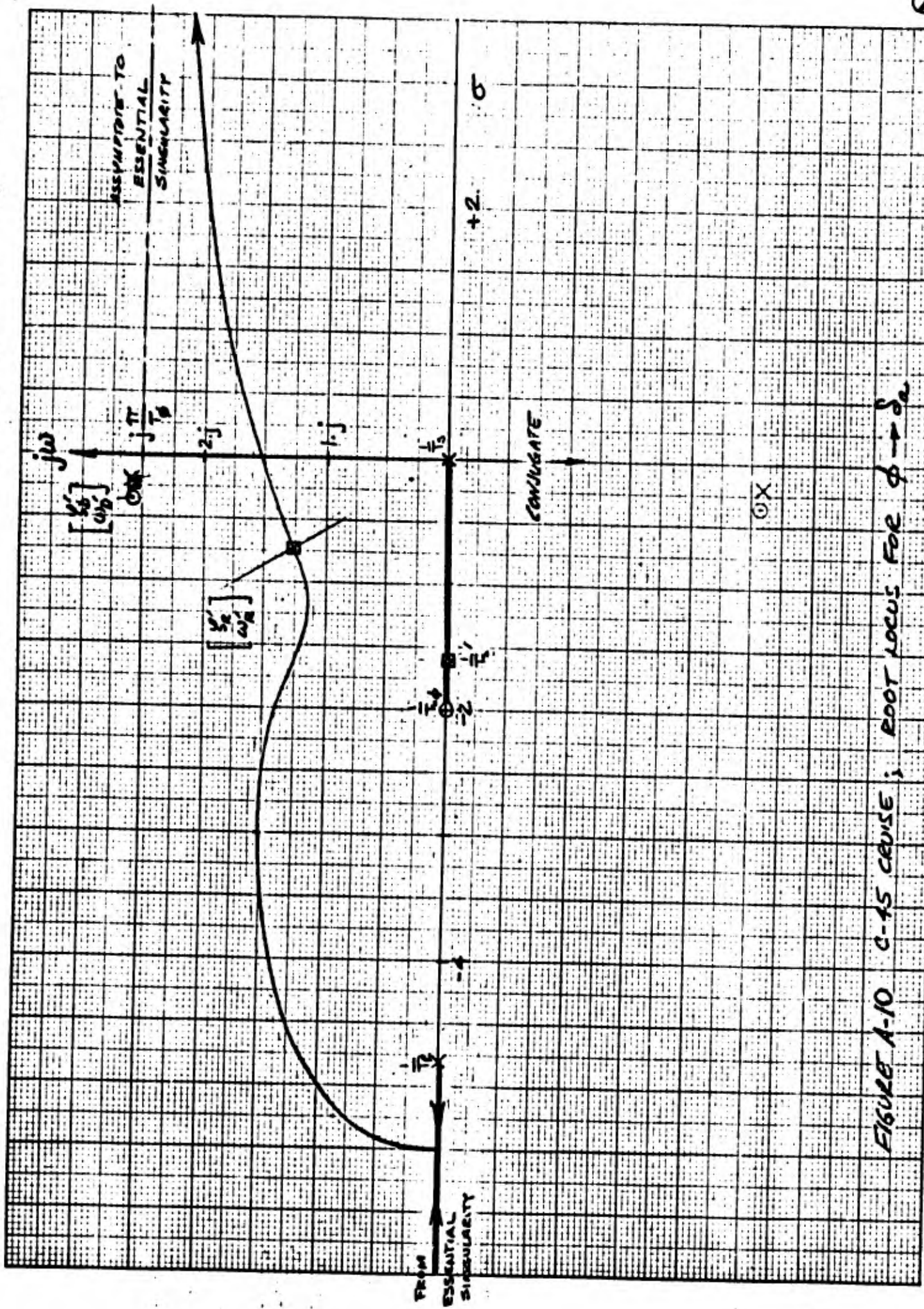


FIGURE A-10 C-15 CRUISE; ROOT LOCUS FOR $\phi \rightarrow \delta$

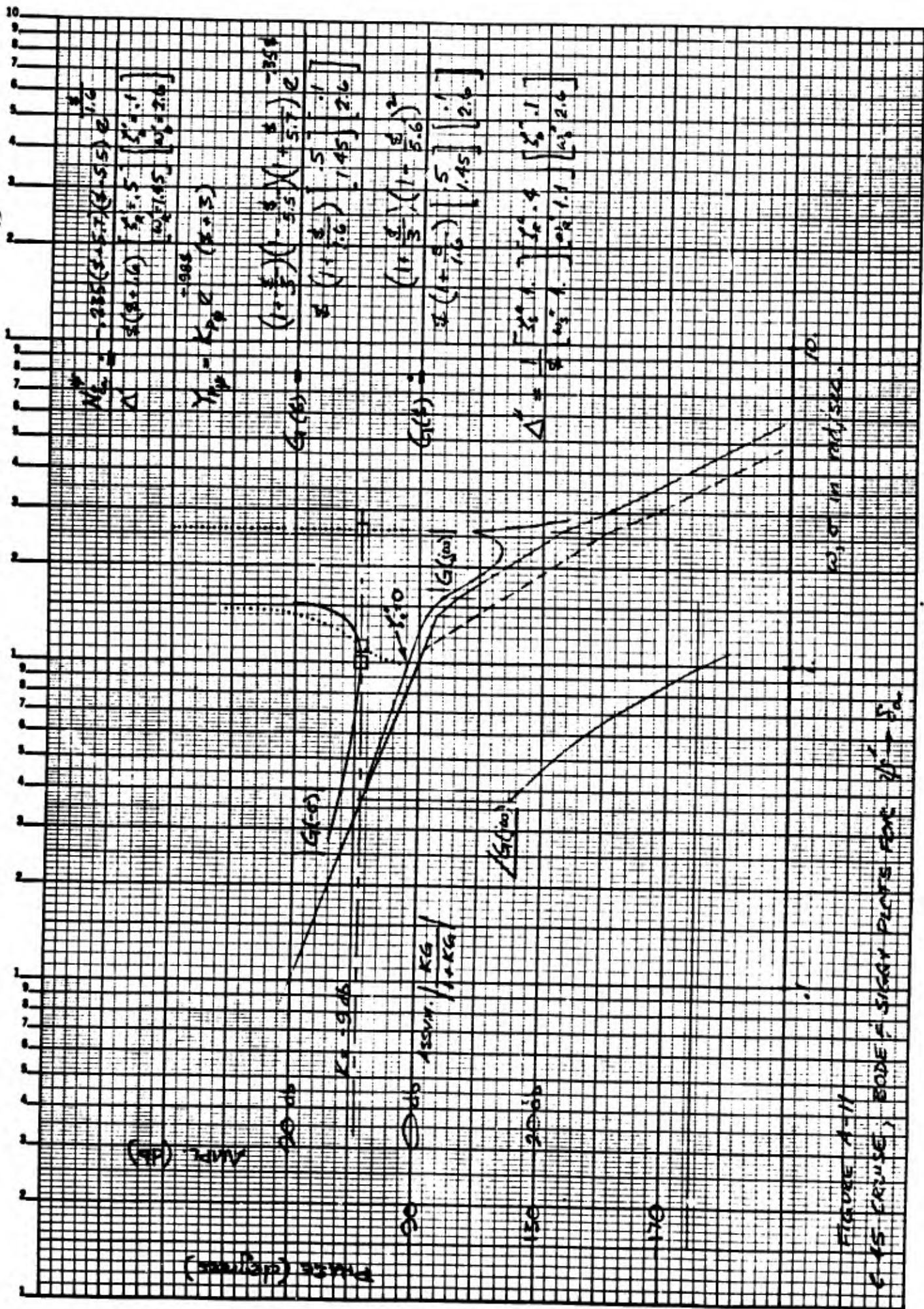


FIGURE A-11

G-K5 CRUISE, BODE PLOTS FOR $\frac{1}{s} - \frac{1}{s^2}$

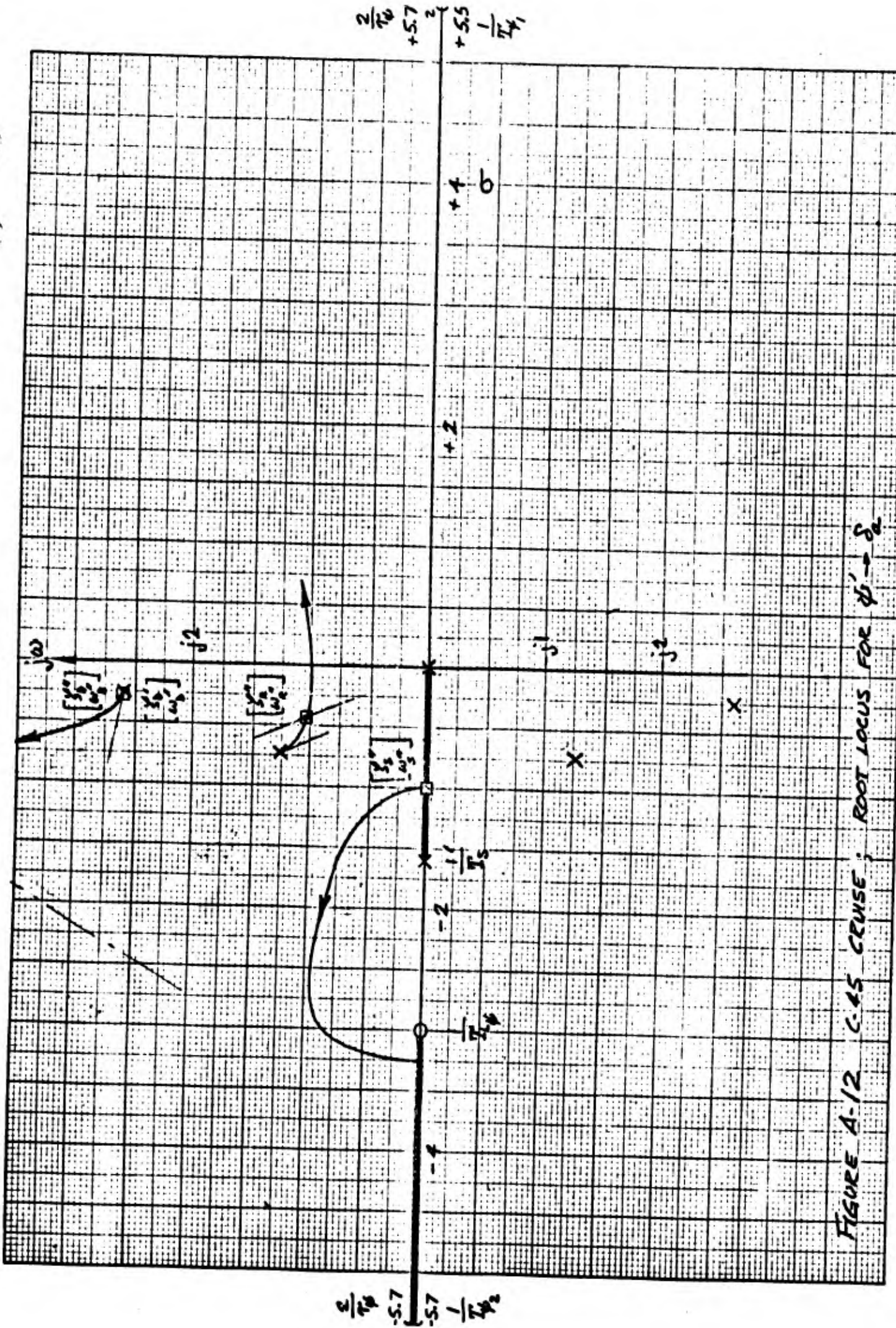
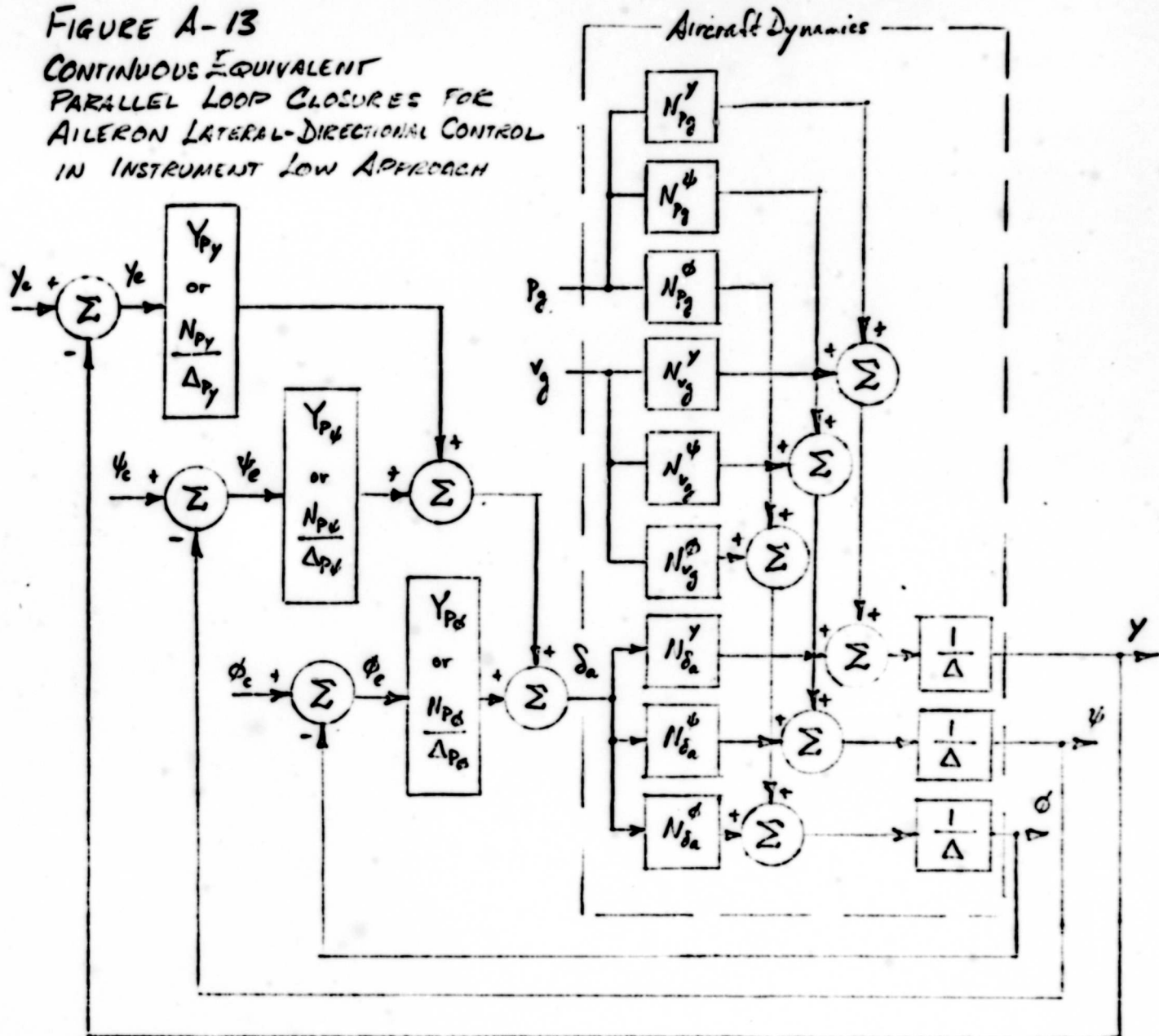


FIGURE A-12 C-45 GENSE; ROOT LOCUS FOR $\psi \rightarrow \delta$

FIGURE A-13

CONTINUOUS EQUIVALENT
PARALLEL LOOP CLOSURES FOR
AILERON LATERAL-DIRECTIONAL CONTROL
IN INSTRUMENT LOW APPROACH



FOR C-45, THIS AILERON LOOP TOPOLOGY REQUIRES YAW DAMPING
IN APPROACH FLIGHT CONDITION

THEREFORE THE FIRST LOOP CLOSURE (DENOTED BY SINGLE PRIME, ')
WILL BE ASSUMED WITHOUT ANALYSIS TO AUGMENT
DUTCH ROLL DAMPING RATIO SUCH THAT $\zeta_D' = \zeta_D$ BY
PILOT'S LOW GAIN CLOSURE $\sigma_y, r \rightarrow \delta_r$ WITH VESTIBULAR
SENSING TO INSURE SHORT TIME DELAY INSTEAD OF VERY LARGE
NEEDLE & BALL INSTRUMENT SAMPLING DELAY. AN APPROXIMATE
 $r \rightarrow \delta_r$ CLOSURE LOCUS IS SHOWN IN FIGURE A-12

FIGURE A-13 (CONTINUED)

$$\left[\frac{y_e}{y_c} \right] = \frac{[\Delta_{P\phi} \Delta_{P\psi} \Delta + \Delta_{P\psi} N_{P\phi} N_{\delta a}^{\phi} + \Delta_{P\phi} N_{P\psi} N_{\delta a}^{\psi}] \Delta_{P\gamma}}{\Delta_{P\gamma} \Delta_{P\psi} \Delta_{P\phi} \Delta + \Delta_{P\gamma} \Delta_{P\psi} N_{P\phi} N_{\delta a}^{\phi} + \Delta_{P\gamma} \Delta_{P\phi} N_{P\psi} N_{\delta a}^{\psi} + \Delta_{P\gamma} \Delta_{P\phi} N_{P\gamma} N_{\delta a}^{\gamma}}$$

$$= \frac{\Delta_{P\gamma} \Delta''}{[\Delta_{P\gamma} \Delta'' + N_{P\gamma} N_{\delta a}^{\gamma}]} = \frac{\Delta''}{\Delta'''}$$

$$\left[\frac{y}{y_c} \right] = \frac{\Delta_{P\psi} \Delta_{P\phi} N_{P\gamma} N_{\delta a}^{\gamma}}{\Delta_{P\gamma} \Delta_{P\psi} \Delta_{P\phi} \Delta + \Delta_{P\gamma} \Delta_{P\psi} N_{P\phi} N_{\delta a}^{\phi} + \Delta_{P\gamma} \Delta_{P\phi} N_{P\psi} N_{\delta a}^{\psi} + \Delta_{P\psi} \Delta_{P\phi} N_{P\gamma} N_{\delta a}^{\gamma}}$$

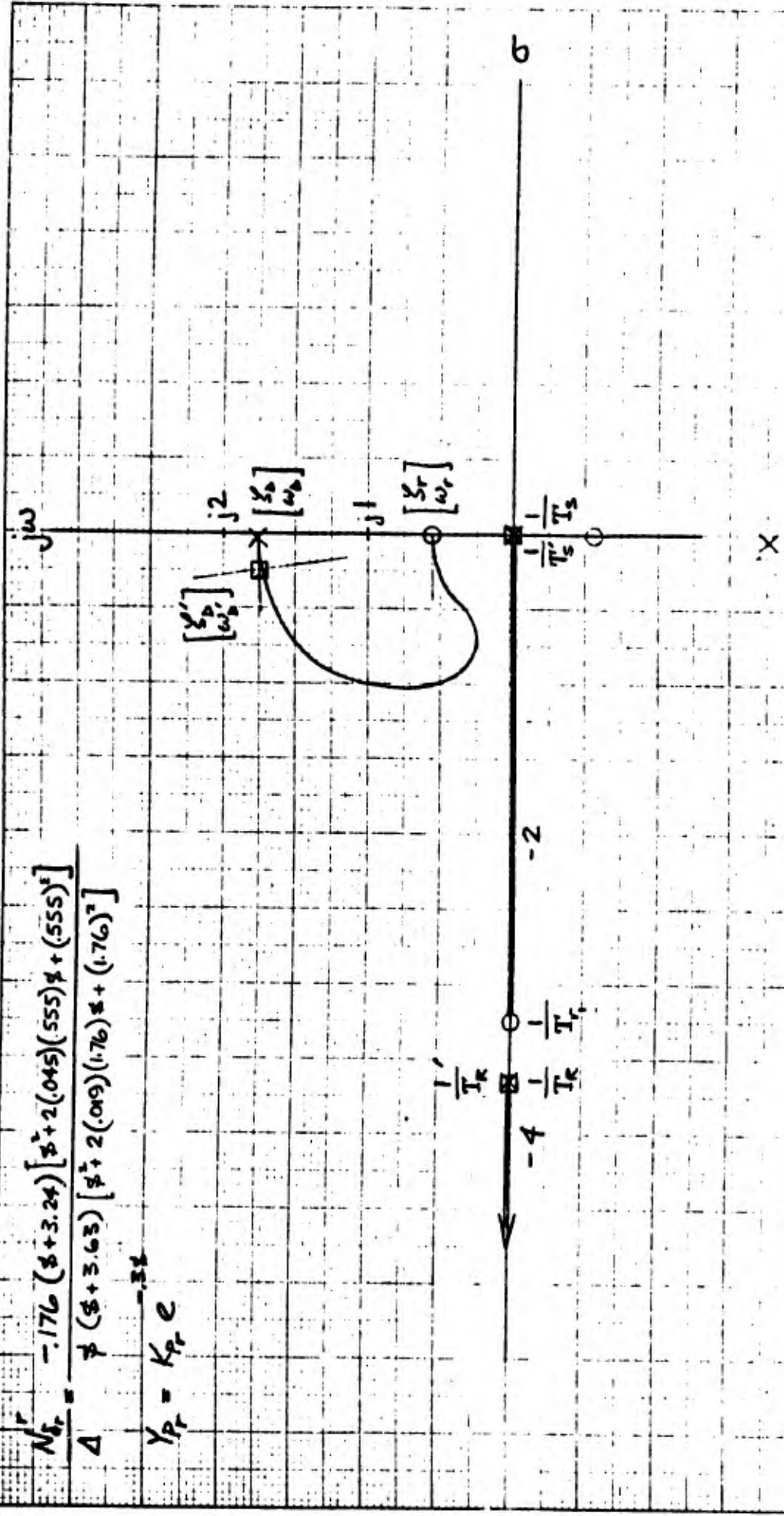
$$= \frac{N_{P\gamma} N_{\delta a}^{\gamma}}{[\Delta_{P\gamma} \Delta'' + N_{P\gamma} N_{\delta a}^{\gamma}]} \cdot \frac{Y_{P\gamma} N_{\delta a}^{\gamma}}{\Delta'''}$$

$$\left[\frac{y}{v_g} \right] = \frac{N_{v_g}^{\gamma} + \frac{Y_{P\phi}}{\Delta} [N_{v_g}^{\gamma} N_{\delta a}^{\phi} - N_{v_g}^{\phi} N_{\delta a}^{\gamma}]}{\Delta'''} + \frac{Y_{P\psi}}{\Delta} [N_{v_g}^{\gamma} N_{\delta a}^{\psi} - N_{v_g}^{\psi} N_{\delta a}^{\gamma}]$$

$$\left[\frac{y}{P_g} \right] = \frac{N_{P_g}^{\gamma} + \frac{Y_{P\phi}}{\Delta} [N_{P_g}^{\gamma} N_{\delta a}^{\phi} - N_{P_g}^{\phi} N_{\delta a}^{\gamma}]}{\Delta'''} + \frac{Y_{P\psi}}{\Delta} [N_{P_g}^{\gamma} N_{\delta a}^{\psi} - N_{P_g}^{\psi} N_{\delta a}^{\gamma}]$$

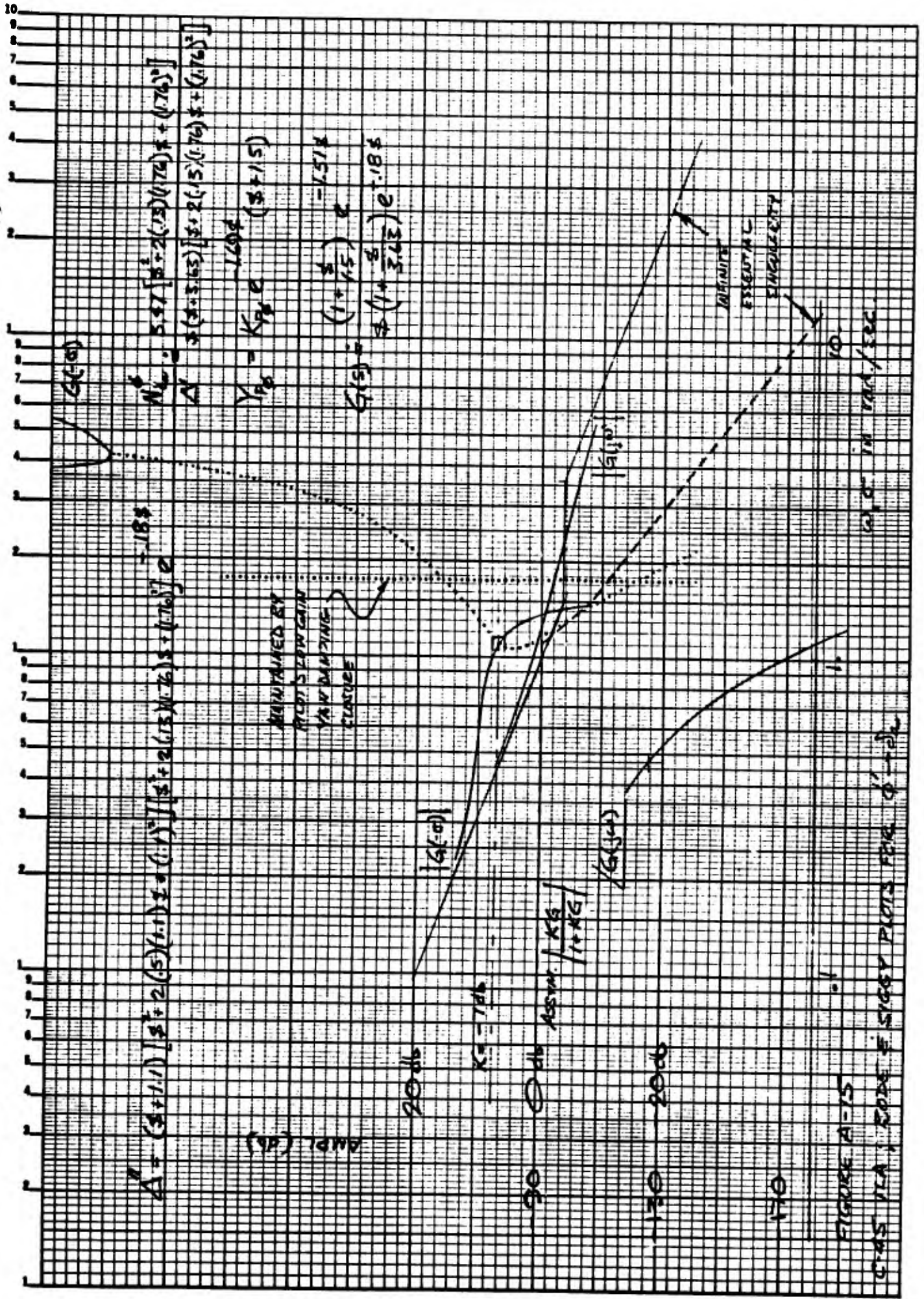
$$\frac{N_{T_r}}{\Delta} = \frac{-176 (s+3.24) [s^2 + 2(0.45)(555)s + (555)^2]}{s (s+3.63) [s^2 + 2(0.09)(1.76)s + (1.76)^2]}$$

$$Y_{T_r} = K_{T_r} e^{-3t}$$



$$\Delta' = s (s+3.63) [s^2 + 2(0.15)(1.76)s + (1.76)^2]$$

FIGURE A-14 C-45 1LA; APPROXIMATE LOCUS FOR $r \rightarrow \delta_r$



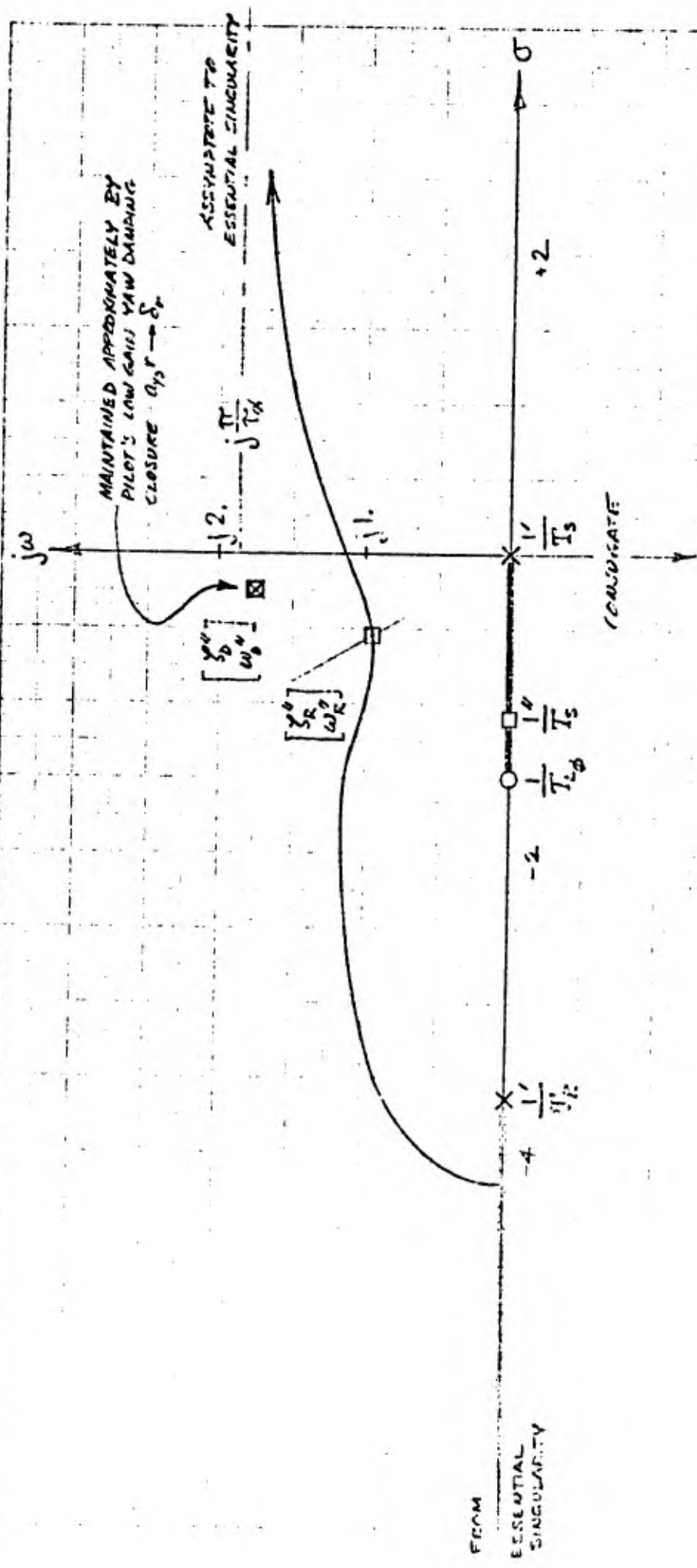


FIGURE 1-16 C-45 1/A; ROOT LOCUS FOR $\phi \rightarrow \delta_r$

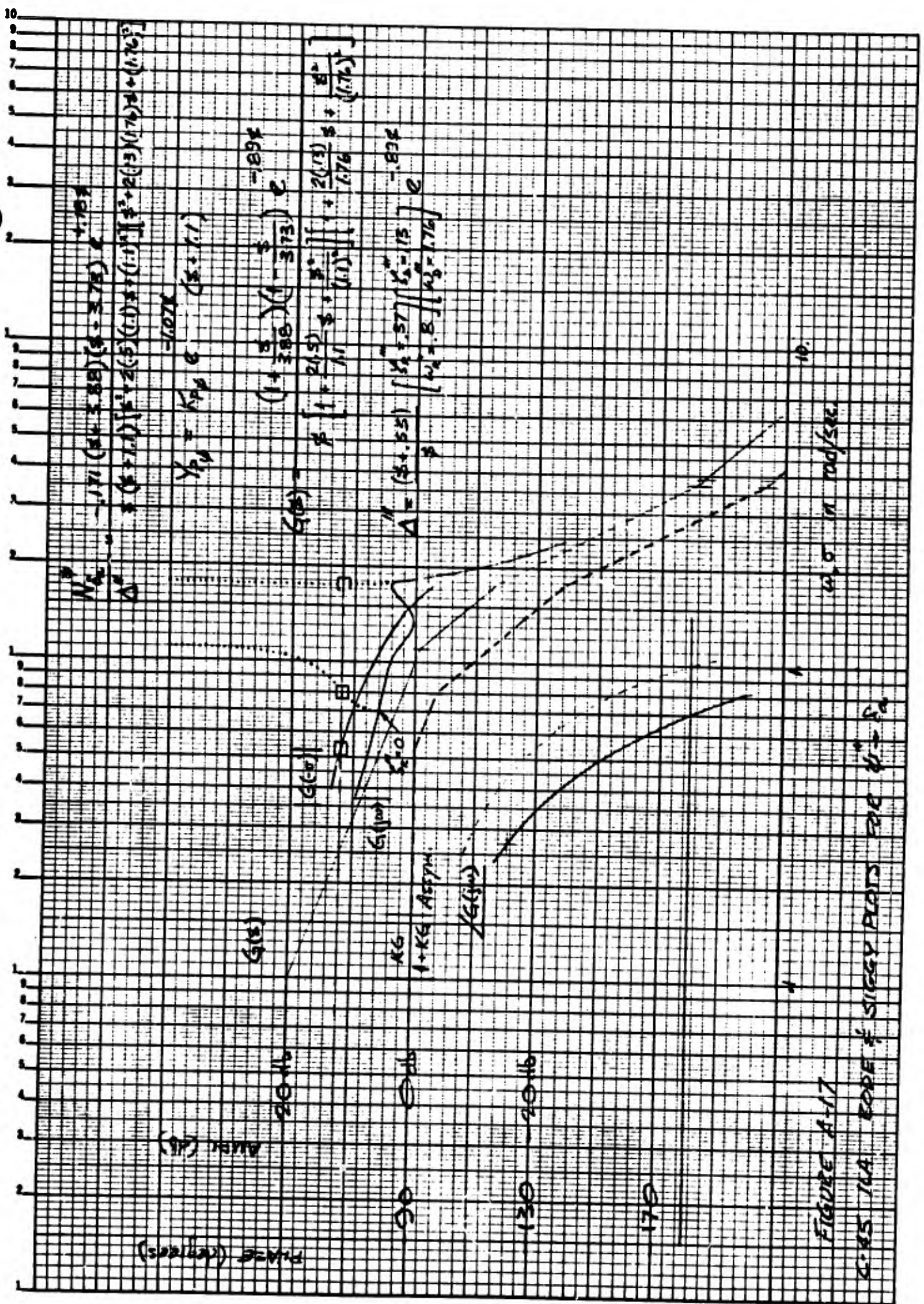


FIGURE A-17

C-85 10A RODE & SIGGY PLOTS FOR $\omega = \sigma_0$

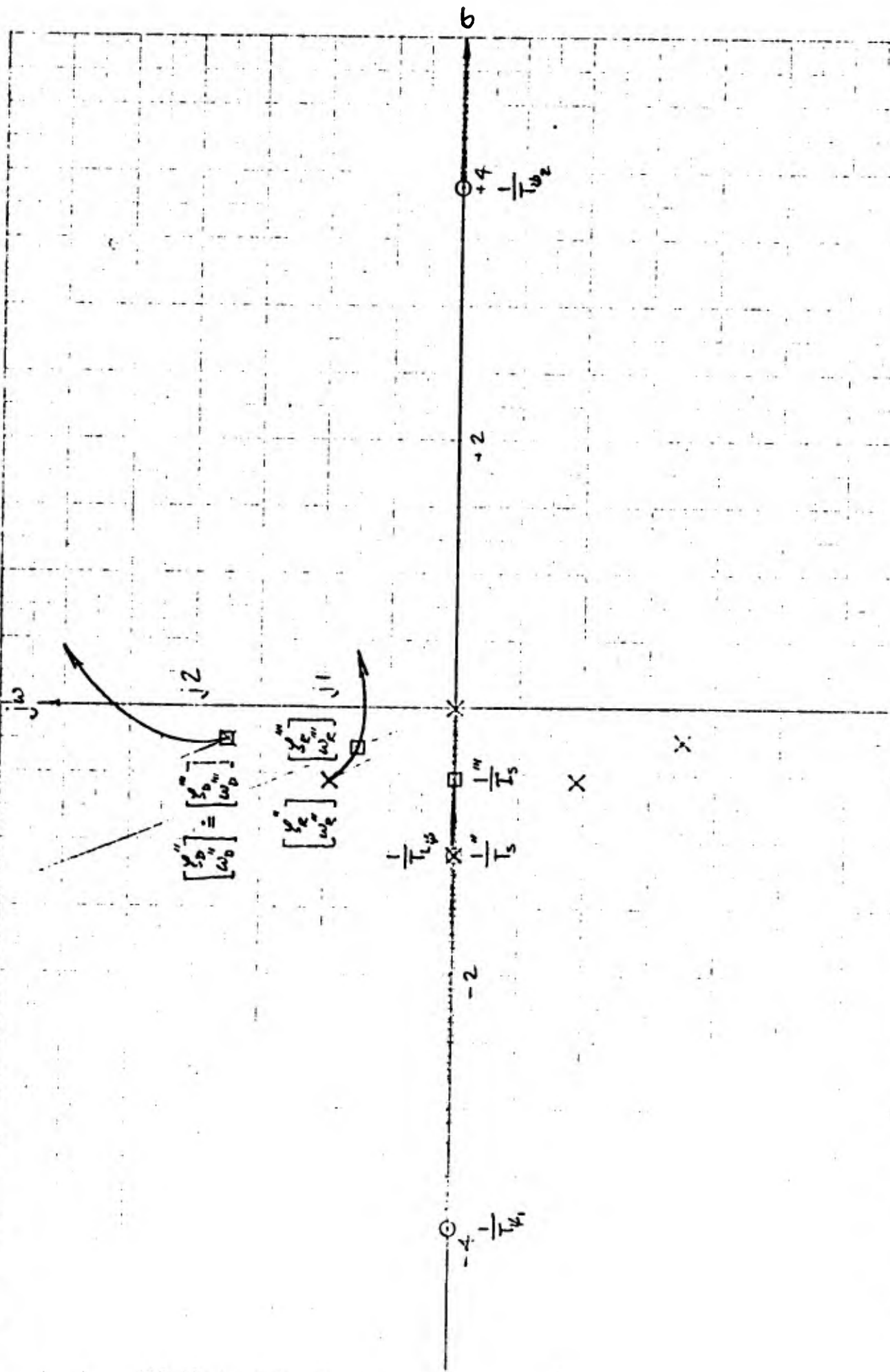


FIGURE A-18 C-45 1/4 Root locus for $\psi'' - \dots$

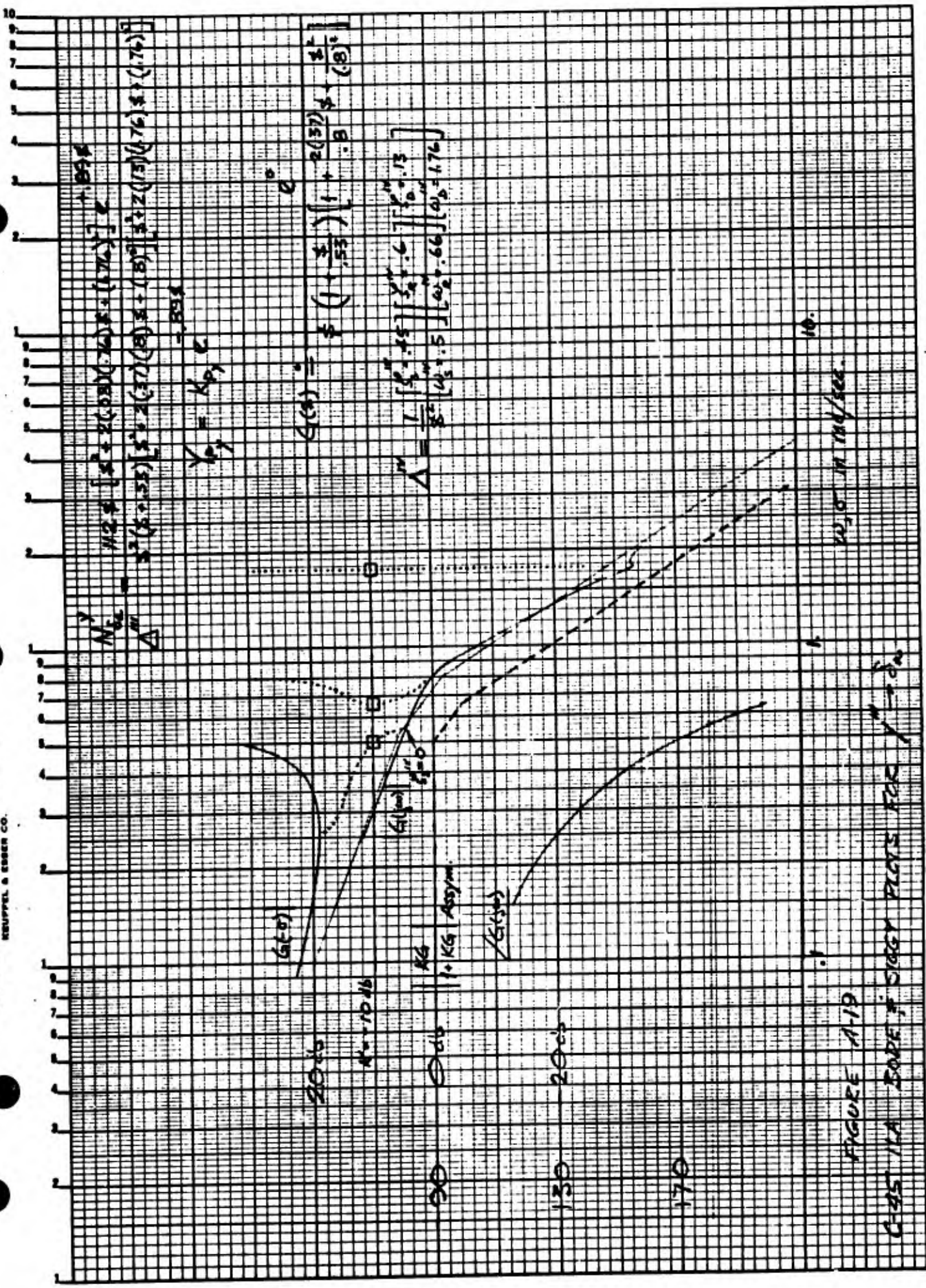


FIGURE A-19
 C-95 1/A BODE & SIGGY PLOTS FOR $\frac{1}{s^2 + 0.6s + 1.76}$

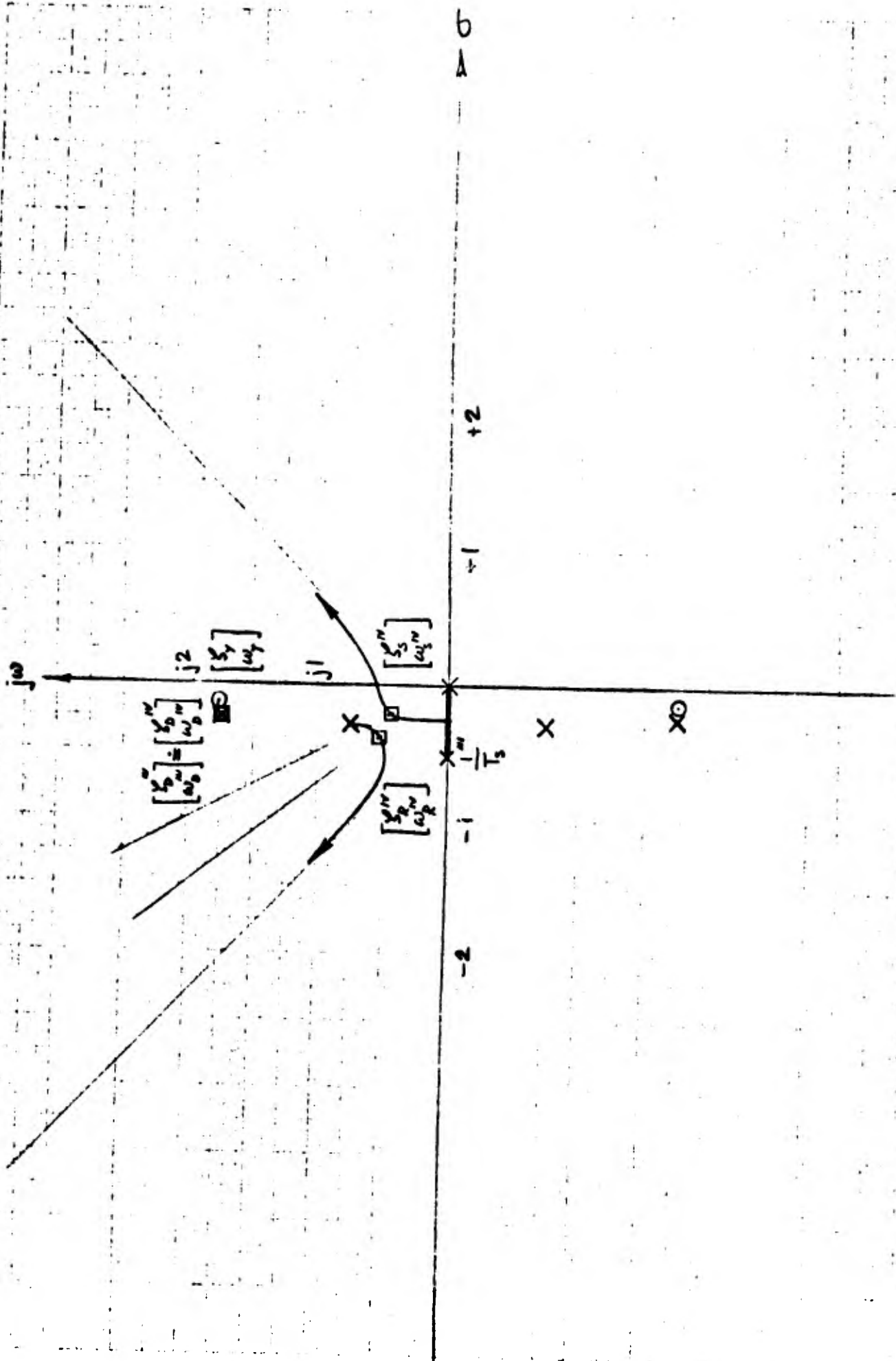
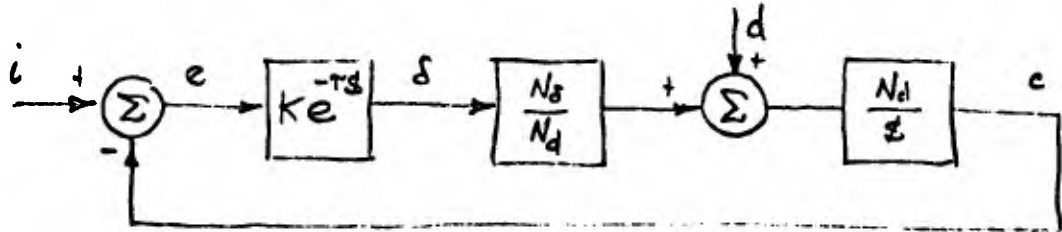


FIGURE A-20 C-45 1LA ROOT LOCUS FOR $y^M - s_a$

FIGURE A-21

SINGLE LOOP CROSSOVER MODEL ILLUSTRATING AIR TURBULENCE [BANDWIDTH] DISTURBANCE SUPPRESSION

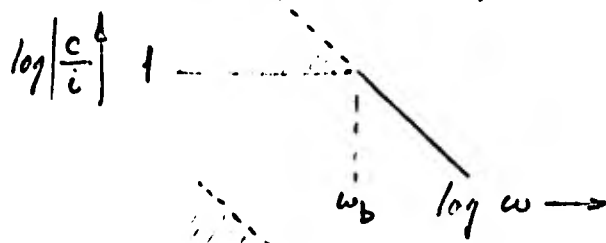
INSTRUMENT REFERENCE, i	CONTROLLED VARIABLE, c	AIR TURBULENCE DISTURBANCE, d
PITCH OR ROLL	ATTITUDE ANGLE	ANGULAR VELOCITY
ALTITUDE OR VERTICAL OR LATERAL DEVIATION	POSITION	TRANSLATIONAL VELOCITY



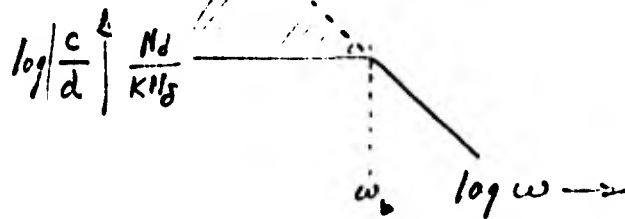
$$\frac{e}{i} = \frac{\phi}{\phi + Ke^{-Ts} N_s}$$



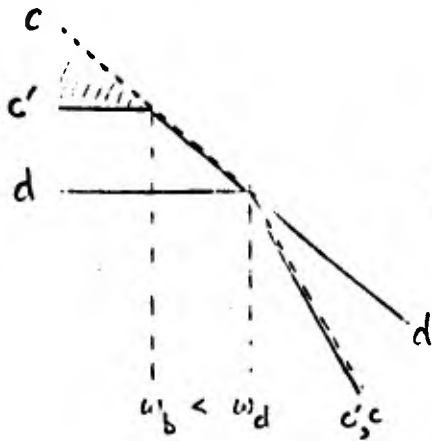
$$\frac{c}{i} = \frac{Ke^{-Ts} N_s}{\phi + Ke^{-Ts} N_s}$$



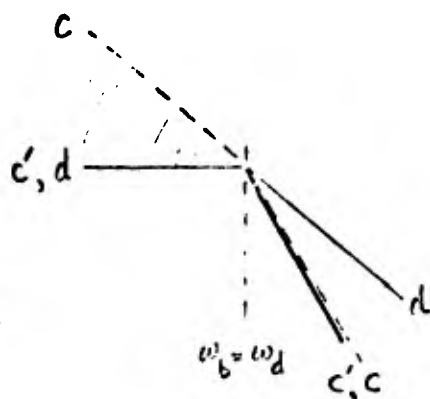
$$-\frac{e}{d} = \frac{c}{d} = \frac{N_d}{\phi + Ke^{-Ts} N_s}$$



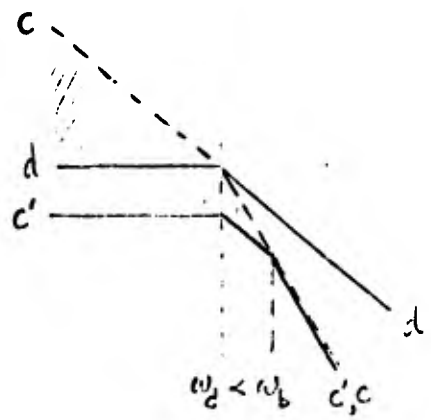
THREE CASES OF DISTURBANCE SUPPRESSION FOR ISOTROPIC TURBULENCE, d



CASE (1)
INSUFFICIENT SUPPRESSION
BANDWIDTH



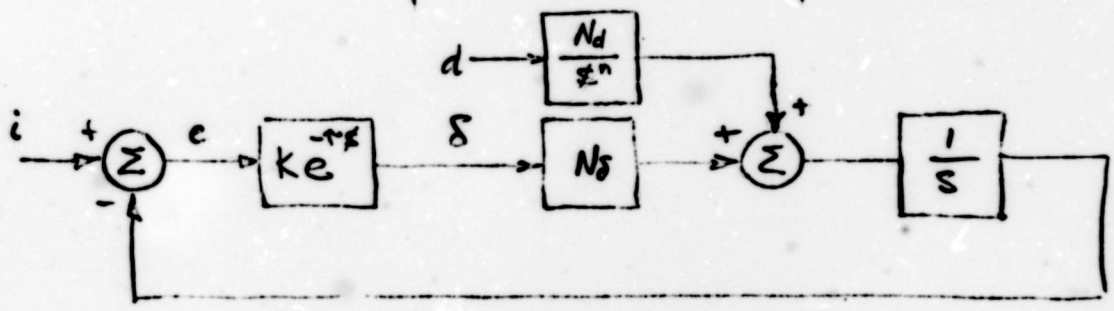
CASE (2)
MATCHED BANDWIDTH



CASE (3)
EXCESSIVE SUPPRESSION
WITH DIMINISHING RETURNS

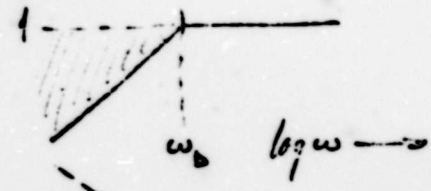
FIGURE A-22 ROLLING TURBULENCE BANDWIDTH DISTURBANCE SUPPRESSION

INSTRUMENT REFERENCE, i	CONTROLLED VARIABLE, c	AIR TURBULENCE DISTURBANCE, d	INTEGER n
HEADING	ANGLE	ROLLING VELOCITY	1
LATERAL DEVIATION	POSITION	ROLLING VELOCITY	2



$$\frac{e}{i} = \frac{\phi}{\phi + Ke^{-\tau s} N_s}$$

$$\log \left| \frac{e}{i} \right|$$



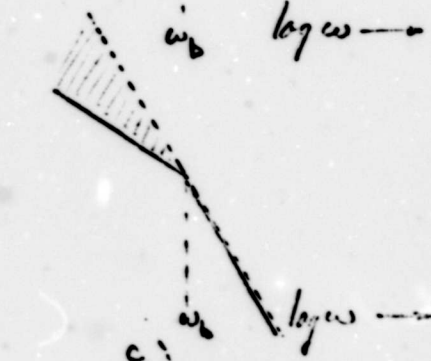
$$\frac{c}{i} = \frac{Ke^{-\tau s} N_s}{\phi + Ke^{-\tau s} N_s}$$

$$\log \left| \frac{c}{i} \right|$$



$$-\frac{e}{d} = \frac{c}{d} = \frac{N_d}{\phi(\phi + Ke^{-\tau s} N_s)}$$

$$\log \left| \frac{c}{d} \right|$$



THREE CASES OF DISTURBANCE SUPPRESSION FOR ISOTROPIC TURBULENCE, d

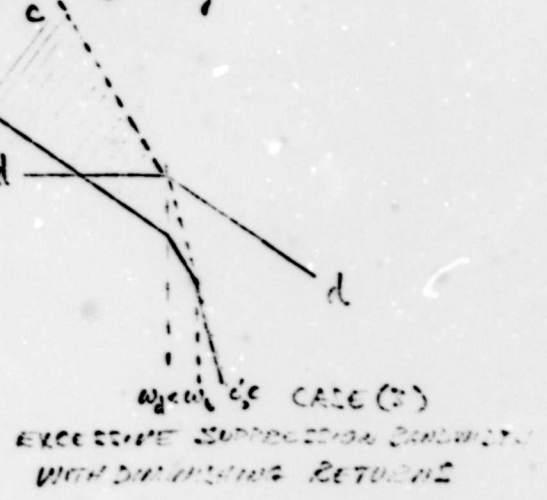
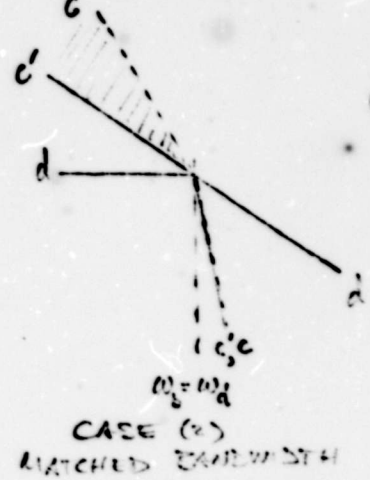
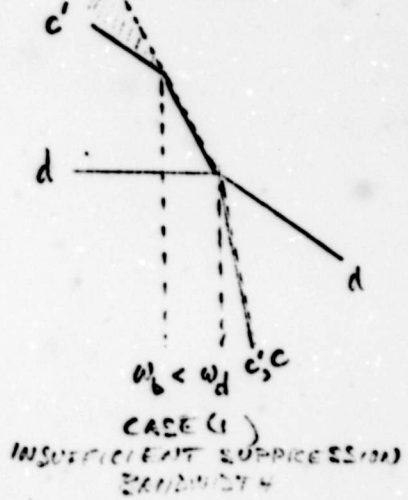
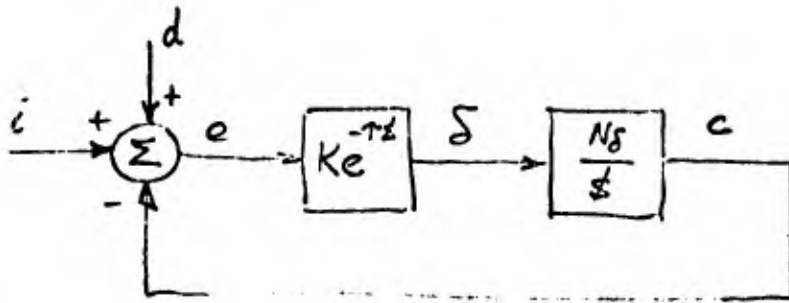


FIGURE A-23

ILS RADIO [BANDWIDTH

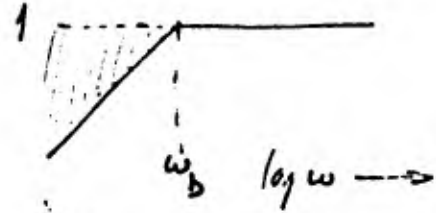
SINGLE LOOP CROSSOVER MODEL ILLUSTRATING DISTURBANCE SUPPRESSION

INSTRUMENT REFERENCE, i	CONTROLLED VARIABLE, c	RADIO DISTURBANCE, d
VERTICAL OR LATERAL DEVIATION	POSITION	POSITION



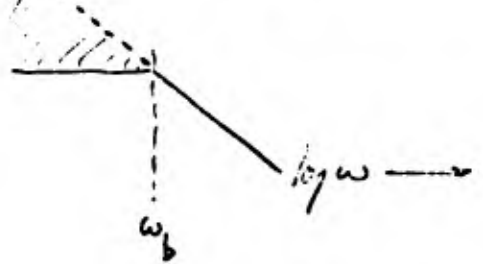
$$\frac{e}{d} = \frac{e}{i} = \frac{s}{s + Ke^{-Tz} N_s}$$

$$\log \left| \frac{e}{d} \right|$$

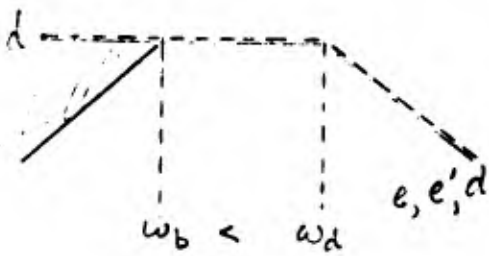


$$\frac{c}{d} = \frac{c}{i} = \frac{Ke^{-Tz} N_s}{s + Ke^{-Tz} N_s}$$

$$\log \left| \frac{c}{i} \right|$$

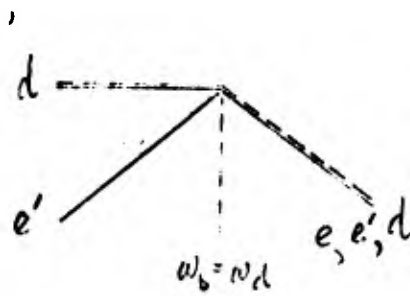


THREE CASES OF DISTURBANCE SUPPRESSION FOR RADIO NOISE, d



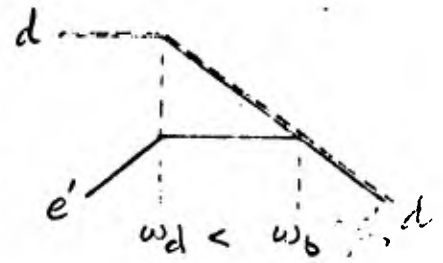
CASE (1)

UNDERMATCHED SUPPRESSION BANDWIDTH



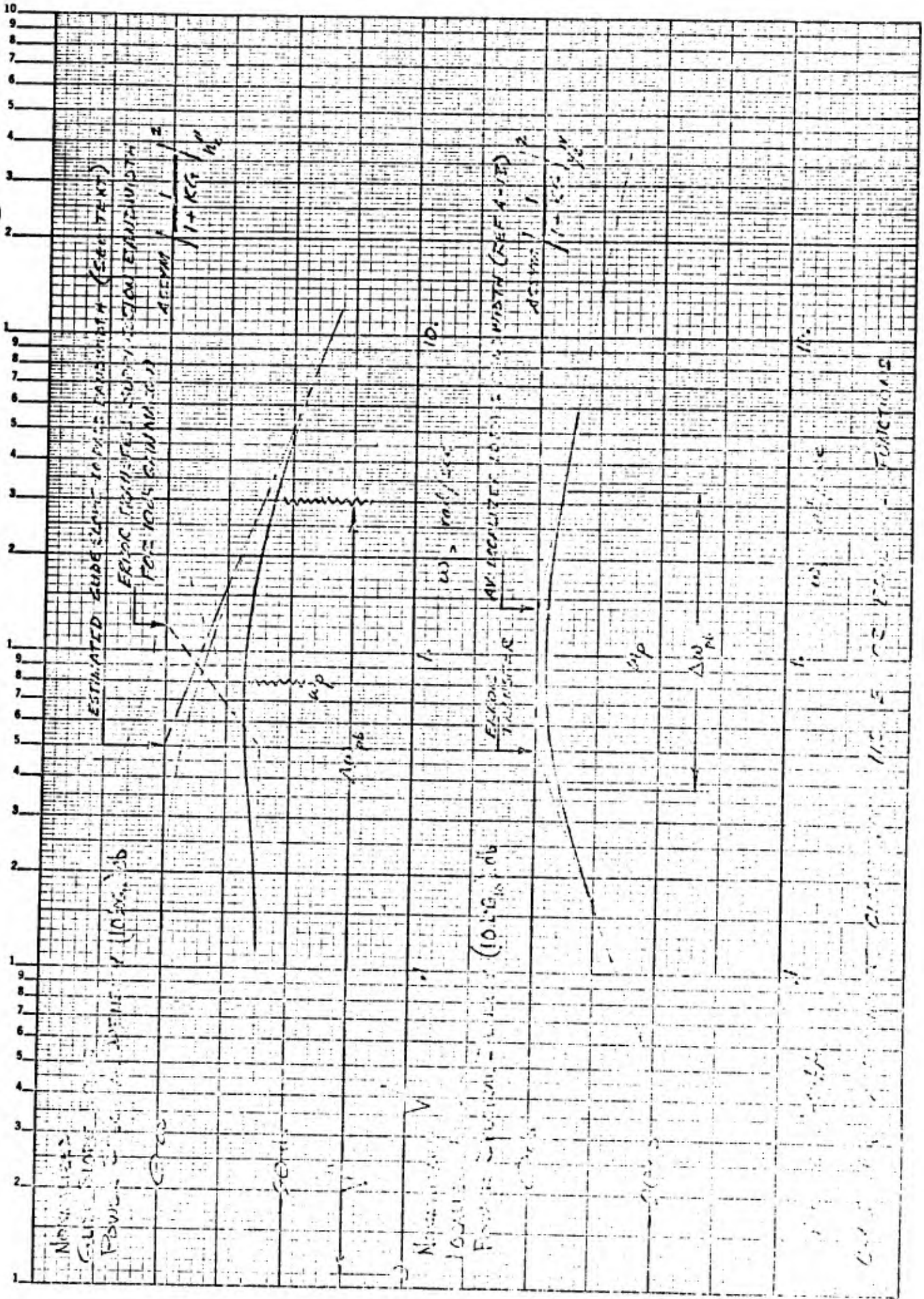
CASE (2)

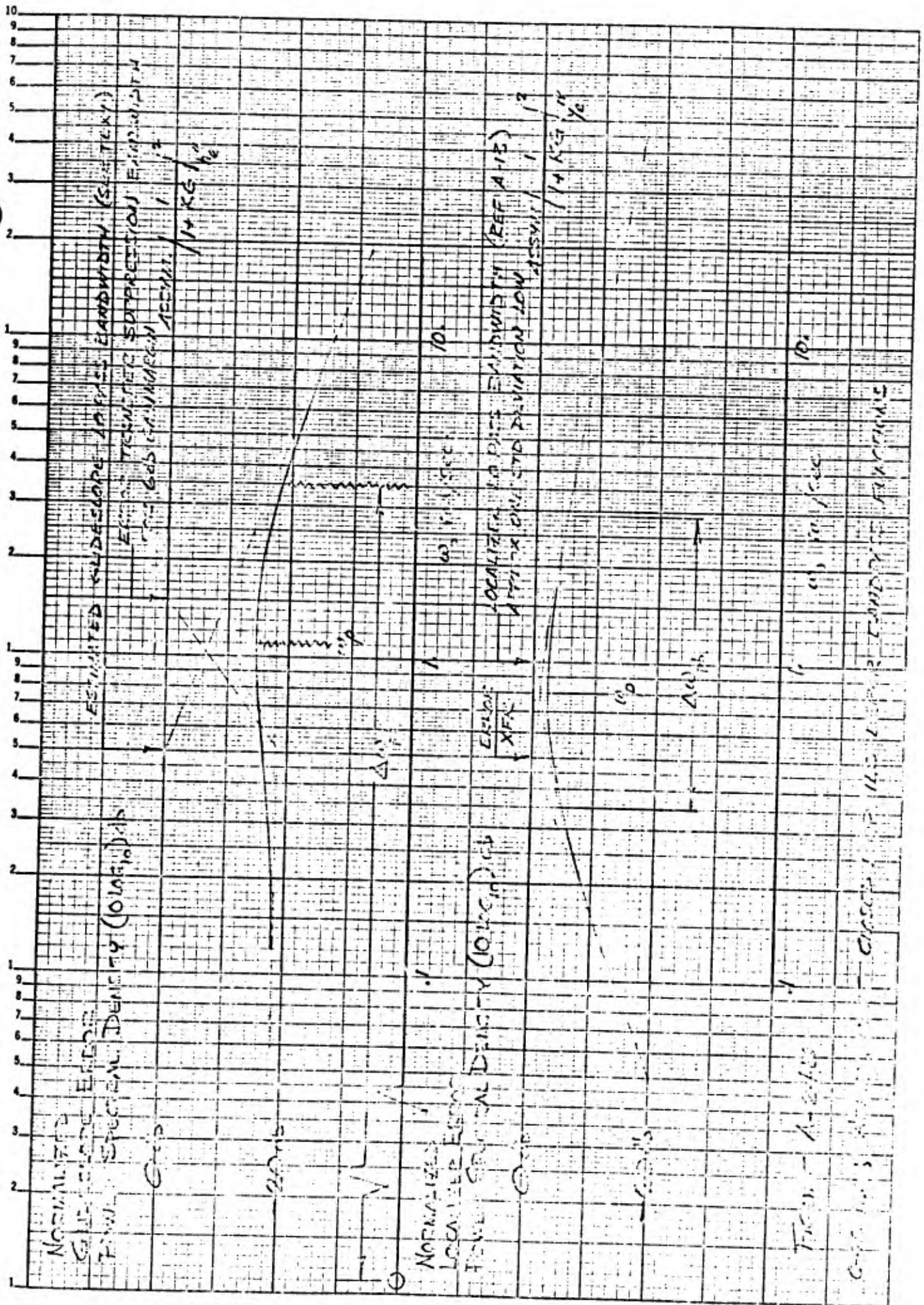
MATCHED SUPPRESSION BANDWIDTH



CASE (3)

OVERMATCHED SUPPRESSION BANDWIDTH





APPENDIX B

CALCULATION OF EYE MOVEMENT LINK VALUES BETWEEN AIRCRAFT INSTRUMENTS BY SENDERS' APPROXIMATE METHOD [47, 48]

Eye movement link values between each pair of instruments give the relative frequency of eye movements between the stated pair referred to all eye movements. [18, 20] Observed mean fixation frequencies and mean fixation dwell times for each instrument will be taken from [18, 20] for the instrument low approach with standard Air Force panel arrangement in a C-45 aircraft.

Flight Instr.	Mean Fixation Frequency	$\frac{FF_i}{\sum_i FF_i}$	Mean Dwell Time	$\pi_i \bar{T}_{d_i}$	$\frac{\pi_i \bar{T}_{d_i}}{\sum_i \pi_i \bar{T}_{d_i}}$	Estimator of P_i Probability of Fixation on i^{th} Instrument	
	Cycles/Minute	FF_i	Seconds	\bar{T}_{d_i}	ϕ_i	(OBS) [18] P_i	ϕ_i^2
XPT	29.6	.279	0.86	.240	.41	.41	.17
AS	16.0	.151	.38	.057	.10	.10	.01
DG	28.0	.264	.56	.148	.25	.25	.0625
GH	16.9	.159	.54	.086	.15	.15	.0225
ALT	2.7	.026	.38	.010	.017	.02	.0003
TB	0.9	.008	.34	.003	.005	.01	.000025
VS	3.5	.033	.39	.013	.022	.02	.0005
ENG	1.7	.016	.71	.011	.019	.02	.0004
MISC.	(NA)	.063 (est)	.19	.012 (est)	.02	(NA)	.0004
Σ	106.0 [†]	1.0 [†]		.58	.993	.98	.2666

† includes eye blinks and wanderings around cockpit

(OBS) .59[†] [18, 20]

$$[1 - \sum \phi_i^2] = +.7334$$

1. —

Fitts, Jones & Milton
 Eye Movements of Pilots (ILAS)
 AER 9:2 1949 cont'd

24 Oct 66

JFM
 (2)


ILAS

Calculated common instrument link values

Instr Pair	$\phi_i \phi_j$	$2\phi_i \phi_j$	$\delta_{ij} + \delta_{ji} = \frac{2\phi_i \phi_j}{1 - \sum \phi_k^2}$	observed [18] link values
XPT-AS	(.41)(.10)	.082	.11	.16
XPT-DG	(.21)(.25)	.205	.28	.29
XPT-GH	(.11)(.14)	.115	.15	.10
AS-DG	(.10)(.25)	.05	.07	.11
AS-GH	(.10)(.15)	.03	.04	.04
DG-GH	(.25)(.15)	.075	.10	.15
GH-ALT	(.15)(.017)	.0051	.007	(11)
GH-VS	(.15)(.022)	.0066	.009	.03

These values are plotted
 in Figure 14.

APPENDIX C


 3 Dec 66
 Rev. 21 Feb 67

Calculation of Eye Movement Link Values for C-45 Instrument Low Approach (ILAS) based on preliminary scanning model hypotheses

Flight Instrument ILAS	Mean Fixation Frequency Hypothesis	Display-Control Frequency Bandwidth (ω_b)	Mean Fixation Frequency (RAD/SEC) FF_i	$\frac{FF_i}{\sum_i FF_i}$ π_i	Mean Dwell Time (SEC) \bar{I}_{d_i}	$\pi_i \bar{I}_{d_i}$	$\frac{\pi_i \bar{I}_{d_i}}{\sum_i \pi_i \bar{I}_{d_i}}$ ϕ_i	Estimator of Probability of Fixation, P_i ϕ_i^2
XPT	$3\omega_b$	1.4	4.2	.385	.8	.308	.51	.26
AS	$3\omega_b$	0.5	1.5	.138	.5	.069	.114	.013
IG	$4\omega_b$	0.5	2.0	.184	.5	.092	.152	.0231
GH	$4\omega_b$	0.5	2.0	.183	.5	.091	.15	.0225
ALT	ω_b	0.5	0.5	.046	.4	.018	.03	.0009
TB	0	0.5	0	0	.4	0	0	0
VS	ω_b	0.5	0.5	.046	.4	.018	.03	.0009
ENG	—	—	0.1 (EST)	.009	.8	.007	.012	.0001
MISC	—	—	0.1 (EST)	.009	.2	.002	.003	0
Σ			10.9	1. —		.605	1. —	.3205
								.6795

P_i , Probability of Fixation, observed [36], [37] in flight

XPT	.41	.45	.56
AS	.10	.07	.08
IG	.25	.20	.18
GH	.15	.11	.06
ALT	.02	.02	.02
TB	.01	0	0
VS	.02	.05	.05
ENG	.02	.04	.02

Apdx C. Calculation of Eye Movement Link Values for C-45 ILAS
based on preliminary scanning model hypotheses

JL
5 Dec 66
Rev 21 Feb 67

Flight
Instrument Pair

	$\phi_i \phi_j$	$2\phi_i \phi_j$	$\frac{2\phi_i \phi_j}{1 - \sum_k \phi_k^2} = \beta_{ij} + \beta_{ji} = \text{link value}$	[36] (obs)	[39] (DAY)	[39] (NITE)
XPT-AS	(.51)(.114)	.116	.17	.16	.10	.17
XPT-DG	(.51)(.152)	.155	.23	.29	.31	.32
XPT-GH	(.51)(.15)	.153	.225	.10	.22	.17
XPT-ALT	(.51)(.03)	.030	.044	<.02	.02	.02
XPT-VS	(.51)(.03)	.030	.044	<.02	.04	.06
XPT-ENG	(.51)(.012)	.012	.018	<.02	.02	.02
AS-DG	(.114)(.152)	.035	.052	.11	.02	.03
AS-GH	(.114)(.15)	.034	.05	.04	.02	.02
AS-ALT	(.114)(.03)	.007	.01	<.02	.02	.02
DG-GH	(.152)(.15)	.046	.068	.15	.06	.04
DG-ALT	(.152)(.03)	.009	.013	<.02	.02	.02
DG-VS	(.152)(.03)	.009	.013	<.02	.05	.04
GH-ALT	(.15)(.03)	.009	.013	<.02	<.02	<.02
GH-VS	(.15)(.03)	.009	.013	.03	.05	.04

These values are plotted in
Figure 17

APPENDIX D

Modified AS & DG hypotheses in

JHE
5 Dec 66
REV 21 Feb 67

Calculation of Eye Movement Link Values

for C-45 Instrument Low Approach (ILAS)

based on preliminary scanning model hypotheses

Flight Instrument	Mean Fixation Frequency Hypothesis	Display-Control Frequency Bandwidth (RAD/SEC)	Mean Fixation Frequency (RAD/SEC)	$\frac{FF_i}{\sum_i FF_i}$	Mean Dwell Time (SEC)	$\frac{\pi_i \bar{T}_{d_i}}{\sum_i \pi_i \bar{T}_{d_i}}$	Estimator of Probability of Fixation, P_i	
ILAS		ω_b	FF_i	π_i	\bar{T}_{d_i}	$\pi_i \bar{T}_{d_i}$	ϕ_i	
							ϕ_i^2	
XPT			4.2	.379	.8	.303	.50	.25
AS	$2.4\omega_b$	0.5	1.2	.108	.5	.054	.089	.0079
DG	$5\omega_b$	0.5	2.5	.225	.5	.113	.187	.035
GH			2.0	.18	.5	.09	.149	.0222
ALT			0.5	.045	.4	.018	.03	.0009
TB			0	0	.4	0	0	0
VS			0.5	.045	.4	.018	.03	.0009
ENG			0.1 (EST)	.009	.8	.007	.012	.0001
Misc			0.1 (EST)	.009	.2	.002	.003	0
Σ			11.1	1. —		.605	1. —	.317
								+ .683
								1. —

D Calculation of Eye Movement Link Values for C-45 ILAS
 based on preliminary scanning model
 with modified DG hypothesis

JAC
 5 Dec 66
 Rev 21 Feb 67

Flight

Instrument Pair

Instrument Pair	$\phi_i \phi_j$	$2\phi_i \phi_j$	$\frac{2\phi_i \phi_j}{1 - \sum_k \phi_k^2} = \beta_{ij} + \beta_{ji} = \text{link value}$
XPT-AS	(.50)(.089)	.089	.13
XPT-DG	(.50)(.187)	.187	.274
XPT-GH	(.50)(.149)	.149	.218
XPT-ALT	(.50)(.03)	.03	.044
XPT-VS	(.50)(.03)	.03	.044
XPT-ENG	(.50)(.012)	.012	.018
AS-DG	(.089)(.187)	.033	.048
AS-GH	(.089)(.149)	.027	.039
AS-ALT	(.089)(.03)	.005	.007
DG-GH	(.187)(.149)	.056	.082
DG-ALT	(.187)(.03)	.011	.016
DG-VS	(.187)(.03)	.011	.016
GH-ALT	(.149)(.03)	.009	.013
GH-VS	(.149)(.03)	.009	.013

These values are plotted in
 Figure 18

Unclassified

Security Classification

DOCUMENT CONTROL DATA - R&D

(Security classification of title, body of abstract and indexing annotation must be entered when the overall report is classified)

1 ORIGINATING ACTIVITY (Corporate author) Systems Technology, Inc. 13766 South Hawthorne Boulevard Hawthorne, California 90250	2a REPORT SECURITY CLASSIFICATION Unclassified
	2b GROUP N/A

3 REPORT TITLE
A Reexamination of Eye Movement Data

4 DESCRIPTIVE NOTES (Type of report and inclusive dates)
Technical Memorandum

5 AUTHOR(S) (Last name, first name, initial)
Clement, Warren F.
Graham, Dunstan
Best, John J.

6 REPORT DATE 28 February 1967	7a TOTAL NO. OF PAGES 113	7b NO. OF REFS 81
-----------------------------------	------------------------------	----------------------

8a CONTRACT OR GRANT NO. N00014-66-C0072 b. PROJECT NO. NR 213-044 c. d.	9a ORIGINATOR'S REPORT NUMBER(S) STI TM 163-A
	9b OTHER REPORT NO(S) (Any other numbers that may be assigned this report) None

10 AVAILABILITY/LIMITATION NOTICES
Qualified requesters may obtain copies of this report from DDC.

11 SUPPLEMENTARY NOTES None	12 SPONSORING MILITARY ACTIVITY Office of Naval Research Air Programs Naval Applications Group Washington, D. C.
--------------------------------	--

13 ABSTRACT
This technical memorandum contains an analysis of aircraft pilot eye movement data obtained in the past by other investigators from piloted flight tests. This includes a comprehensive account and reanalysis of the data contained in several reports, by different investigators, and it suggests some features of a useful systems model which should be compatible with (i.e., "explain") all, or nearly all, of these data.

The second Section of the memo presents a review of key contributions to the literature, primarily of Fitts' and Senders' work. Pilots' eye fixation frequency measurements are first discussed with respect to four possible variables on which they may depend: display-control closed-loop bandwidth, flight maneuvers, instrument arrangement, and the redundancy of information. Pilots' eye fixation dwell times are then discussed with respect to a quantized time interval which appears in certain experiments, and the purpose for and type of sampled signal reconstruction which may be performed by the pilot. Finally, an approximate method suggested by Senders for calculating paired-display fixation link values is applied to one of the extant cases not investigated by him.

The third Section suggests some experiments to resolve questions, validate models and fill voids in existing results.

A series of Appendices presents the analytical details used in Section II of the text.

Unclassified

Security Classification

Security Classification

14. KEY WORDS	LINK A		LINK B		LINK C	
	ROLE	WT	ROLE	WT	ROLE	WT
Control (Displays) Display Systems Flight Instruments Sensory Mechanisms Vision Adaptation (Physiology) Tracking Human Engineering						

INSTRUCTIONS

1. **ORIGINATING ACTIVITY:** Enter the name and address of the contractor, subcontractor, grantee, Department of Defense activity or other organization (*corporate author*) issuing the report.

2a. **REPORT SECURITY CLASSIFICATION:** Enter the overall security classification of the report. Indicate whether "Restricted Data" is included. Marking is to be in accordance with appropriate security regulations.

2b. **GROUP:** Automatic downgrading is specified in DoD Directive 5200.10 and Armed Forces Industrial Manual. Enter the group number. Also, when applicable, show that optional markings have been used for Group 3 and Group 4 as authorized.

3. **REPORT TITLE:** Enter the complete report title in all capital letters. Titles in all cases should be classified. If a meaningful title cannot be selected, the classification, show title classification in all caps in parentheses immediately following the title.

4. **DESCRIPTIVE NOTES:** If appropriate, state the type of report, e.g., interim, progress, summary, annual, or final. Give the inclusive dates when a specific reporting period is covered.

5. **AUTHOR(S):** Enter the name(s) of author(s) as shown on or in the report. Enter last name, first name, middle initial. If military, show rank and branch of service. The name of the principal author is an absolute minimum requirement.

6. **REPORT DATE:** Enter the date of the report as day, month, year, or month, year. If more than one date appears on the report, use date of publication.

7a. **TOTAL NUMBER OF PAGES:** The total page count should follow normal pagination procedures, i.e., enter the number of pages containing information.

7b. **NUMBER OF REFERENCES:** Enter the total number of references cited in the report.

8a. **CONTRACT OR GRANT NUMBER:** If appropriate, enter the applicable number of the contract or grant under which the report was written.

8b, 8c, & 8d. **PROJECT NUMBER:** Enter the appropriate military department identification, such as project number, subproject number, system numbers, task number, etc.

9a. **ORIGINATOR'S REPORT NUMBER(S):** Enter the official report number by which the document will be identified and controlled by the originating activity. This number must be unique to this report.

9b. **OTHER REPORT NUMBER(S):** If the report has been assigned any other report numbers (*either by the originator or by the sponsor*), also enter this number(s).

10. **AVAILABILITY/LIMITATION NOTICES:** Enter any limitations on further dissemination of the report, other than those

imposed by security classification, using standard statements such as:

- (1) "Qualified requesters may obtain copies of this report from DDC."
- (2) "Foreign announcement and dissemination of this report by DDC is not authorized."
- (3) "U. S. Government agencies may obtain copies of this report directly from DDC. Other qualified DDC users shall request through _____."
- (4) "U. S. military agencies may obtain copies of this report directly from DDC. Other qualified users shall request through _____."
- (5) "All distribution of this report is controlled. Qualified DDC users shall request through _____."

If the report has been furnished to the Office of Technical Services, Department of Commerce, for sale to the public, indicate this fact and enter the price, if known.

11. **SUPPLEMENTARY NOTES:** Use for additional explanatory notes.

12. **SPONSORING MILITARY ACTIVITY:** Enter the name of the departmental project office or laboratory sponsoring (*paying for*) the research and development. Include address.

13. **ABSTRACT:** Enter an abstract giving a brief and factual summary of the document indicative of the report, even though it may also appear elsewhere in the body of the technical report. If additional space is required, a continuation sheet shall be attached.

It is highly desirable that the abstract of classified reports be unclassified. Each paragraph of the abstract shall end with an indication of the military security classification of the information in the paragraph, represented as (TS), (S), (C), or (U).

There is no limitation on the length of the abstract. However, the suggested length is from 150 to 225 words.

14. **KEY WORDS:** Key words are technically meaningful terms or short phrases that characterize a report and may be used as index entries for cataloging the report. Key words must be selected so that no security classification is required. Identifiers, such as equipment model designation, trade name, military project code name, geographic location, may be used as key words but will be followed by an indication of technical context. The assignment of links, rules, and weights is optional.